UNIVERSITÀ
DEGLI STUDI
DI PADOVA

Sede Amministrativa: Università degli Studi di Padova

Dipartimento di GEOSCIENZE

SCUOLA DI DOTTORATO DI RICERCA IN SCIENZE DELLA TERRA
CICLO XXIII

THE MIDDLE – LATE TRIASSIC $\delta^{13}C_{plant}$ TREND AND THE CARNIAN PLUVIAL EVENT C-ISOTOPE SIGNATURE

Direttore della Scuola : Ch.mo Prof. Gilberto Artioli
Supervisore :Ch.mo Prof. Paolo Mietto
Co-supervisori: Dr. Nereo Preto, Dr. Guido Roghi

Dottorando : Jacopo Dal Corso

THE MIDDLE – LATE TRIASSIC $\partial^{13}C_{plant}$ TREND AND THE CARNIAN PLUVIAL EVENT C-ISOTOPE SIGNATURE

Jacopo Dal Corso

to Carmelo

Acknowledgements

The author would like to thank Franz Seraph von Pfistermeister

and all who helped him during his PhD years.

CONTENTS

I. Contents **I**

II. Extended Abstract – Riassunto **V**

1. Introduction **1**

1.1 Problem: The Carnian Pluvial Event

1.2 Searching for the CPE $\partial^{13}C$ signature and a little deviation to the Cretaceous

2. The C-isotope variability of Triassic and Cretaceous fossil plants remains **9**

2.1 The C-isotope signature of fossil plants remains

2.2 Set of samples

2.2.1 First set

2.2.1.1 Triassic material

2.2.1.2 Cretaceous amber

2.3 Methods

2.4 Results

2.4.1 First set: Triassic Amber, Wood and Leaves

2.4.2 First set: Cretaceous Amber – San Just Deposit

2.4.3 First set: Crataceous Amber - all other localities

2.4.4 Second set: Triassic Wood

2.5 Discussion

2.5.1 C-isotope variability of amber, wood and leaves

2.5.2 The Middle – early Late Triassic $\partial^{13}C_{plant}$ trend

2.5.3 $\partial^{13}C_{amber}$ trends in the Cretaceous

2.6 Conclusions

3. Biomarker analyses **39**

3.1 The $\partial^{13}C$ of plant-derived n-alkanes

3.2 Sampled Sections

3.3 Methods

3.3.1 Samples preparation

3.3.2 Maturity parameters

3.4 Results and discussion

3.4.1 GC-MS and diagnostic biomarker and non-biomarker ratios

3.4.2 $\partial^{13}C_{n\text{-alkanes}}$

3.4.3 $\partial^{13}C$ of other compounds

3.5 An early Carnian molecular $\partial^{13}C$ curve

3.6 Conclusions

4. The C-isotope signature of the Carnian Pluvial Event (CPE) 53

4.1 Abstract

4.2 Introduction

4.3 Materials and Methods

4.4 Results

4.5 Discussion

4.6 Conclusions I - The CPE C-isotope signature.

4.7 Conclusions. II - A possible mechanism for massive resin exudation?

5. Conclusions 61

References 63

Supplement

II. EXTENDED ABSTRACT

The Middle-Late Triassic $\partial^{13}C_{org}$ trend and the Carnian Pluvial Event C-isotope signature

After the Permian/Triassic mass extinction, the Early – lowermost Middle Triassic carbon cycle was extremely unstable (see Figure I for a Triassic Time Scale). The global $\partial^{13}C_{carb}$ curve (e.g. Korte et al., 2005) shows a series of large short-term excursions, tentatively associated to a limited biological recovery that characterized this time interval. Carbonate carbon isotopic values seem to stabilize during the Anisian (Middle Triassic), when a Middle – early Late Triassic positive secular trend of 3-4 ‰ begins. This $\partial^{13}C$ rise has been linked to the re-establishment of carbon burial and the re-emergence of coal-swamps (Korte et al., 2005). However, a deeper comprehension of this great $\partial^{13}C$ rise is still necessary: the available data come from carbonates, that reflect the complex marine environment and are very dispersed, then the shape of the curve is not clear. Many questions are open: is the trend really a slow long $\partial^{13}C$ rise or does it rather take place by steps, in one or few short time intervals? If so, which are the causes of these putative steps? Can we observe the same positive shift also in the atmospheric $\partial^{13}C$?

By the end of the Early Carnian (Julian), the $\partial^{13}C$ of carbonates reached already its maximum values of ca. 3.5 ‰ (Korte et al., 2005). However, a short-term climatic episode of late Julian age is documented worldwide at least at tropical latitudes (e.g., Rigo et al., 2007). This episode, known as "Carnian Pluvial Event" or CPE, is characterized by the demise of rimmed carbonate platforms, an increase of coarse terrigenous input, paleosols indicative of a relatively humid climate and a rise of the Carbonate Compensation Depth in the deep Tethys sea. Such characteristics are similar to those of Jurassic and Cretaceous Oceanic Anoxic Events (OAE), that are characterized by significant perturbations of the carbon cycle (Rigo et al., 2007).

This work aimed at building a Middle – early Late Triassic $\partial^{13}C$ curve based on terrestrial organic matter (wood, leaves and biomarkers) and testing whether a carbon isotope shift is associated with the CPE.

In recent years, researchers have performed C-isotopic analyses of many types of specific structures and compounds exclusively associated with terrestrial land plants, including wood (e.g., Hesselbo et al., 2007), cuticles (e.g., Arens and Jahren, 2000) and pollen (e.g., Jahren, 2004). Plant $\partial^{13}C$ is the result of three fractionation processes of the atmospheric C: 1) fractionation during the photosynthesis, 2) post-photosynthetic fractionation, 3) diagenetic fractionation. Following the Farquhar model (Farquhar et al., 1989), three important factors influence the carbon isotope composition of C_3 vascular plant during photosynthesis: 1) physical and biochemical fractionation occurring before and during carboxylation; 2) ecological factors such as water stress (3-6‰ positive shift), nutrients shortage (4‰ negative), light limitation (5-6‰ negative) and temperature (3‰ negative) (Arens et al., 2000); 3) the carbon isotope composition of the atmosphere ($\partial^{13}C_{atm}$). The interplay of these factors produces highly variable carbon-isotope signatures in modern C_3 plants and their component parts (wood, cuticles, resin, etc.), with $\partial^{13}C$ values varying from -19‰ to -35‰ (Tipple

and Pagani, 2007). Similar variability is to be expected in the fossil record, potentially compromising palaeoclimatic reconstructions based on organic $\partial^{13}C$. Despite these limitations, Jahren et al.'s (2008) experiments on living plants demonstrate a good correlation in $\partial^{13}C_{atm}$ and $\partial^{13}C_{plant}$, and this suggests that carbon isotope values from fossil plants can be used as a proxy for $\partial^{13}C_{atm}$ across a range of pCO_2 levels.

The study of molecular fossils (biomarkers) is a relatively new frontier for palaeoecology and palaeoclimatology. N-alkanes (normal alkanes; straight-chain saturated hydrocarbons) with chain lengths of C_{25} - C_{35} and odd-over-even carbon-number distribution derive from epicuticular waxes of terrestrial higher plants (Peters et al., 2005). These lipids are common in both marine and continental sediments and very resistant to diagenesis. Their C isotope signature has been successfully used to study $\partial^{13}C$ shifts associated with major events such as the P/T mass extinction (Xie et al., 2007) or the Paleocene/Eocene Thermal Maximum (Pagani et al., 2006); to determine the advent of the C_4 photosynthetic pathway (Tipple and Pagani, 2007); or to study the relative proportions of C_3 and C_4 plant material in sediments (Pancost and Boot, 2004, and references therein). $\partial^{13}C$ analysis of n-alkanes partially overcomes issues associate with the large $\partial^{13}C$ range in plants (see above), as they pool together the contribution of numerous individual plants, and thus have maximum statistical significance.

We collected wood, leaves and amber from a number of stratigraphic beds of the Middle - lower Upper Triassic of the Southern Alps (Italy), very rich of plant remains. Wood, leaves and amber were hand picked from disgregated or undisturbed rock, powdered and treated with HCl in order to remove carbonates and pyrite; weighted aliquots of material were analysed for the $\partial^{13}C_{org}$. The carbon isotope signatures of separated wood and leaves fragments from the same layers lie in a range of 3-4‰ that is narrower than that expected for modern wood and leaves values (cf. Cernusak et al., 2009), probably due to the loss of some compounds during the diagenesis. Carbon-isotope values of amber vary by 4–5‰, comparable to the range recorded in modern and Cretaceous resins (cf. Stern et al., 2008; Mckellar et al., 2008). Amber seems to better retain the original C-isotope signature (Dal Corso et al., accepted; Roghi et al., in prep.).

Moreover, Middle Triassic wood and leaves are offset by ca. 3‰ with respect to Late Triassic ones: Anisian and Ladinian values vary from -27‰ to -23,5‰ ca., instead the Carnian ones show more positive values, from -24‰ to -19,5‰ ca. These data confirm that a ca. 3‰ $\partial^{13}C_{carb}$ excursion from Middle to early Late Triassic (Korte et al., 2005) is recorded also by terrestrial organic matter (Dal Corso et al., accepted).

Here the first report is presented of a sharp negative $\partial^{13}C_{org}$ excursion at the onset of the CPE. A ~-4‰ abrupt C isotope excursion is registered by leaf waxes n-alkanes, whereas total organic carbon (TOC) shows a ~-2‰ shift. This shift testifies a rapid injection of CO_2 with a light C-isotope composition into the atmosphere. This new dataset confirm the hypothesis that the CPE was a global event. We propose that the C isotope negative shift was triggered by the eruption of the coeval Wrangellia flood basalts with strong consequences for the environments and biosphere (e.g.: demise of carbonate platforms, extinctions and radiations of some of the most important Mesozoic groups).

Il Trend isotopico del Carbonio nel Triassico Medio-Superiore e la firma isotopica del "Carnian Pluvial Event"

Dopo l'estinzione di massa al limite Permo-Triassico il ciclo del carbonio durante il Triassico Inferiore e il primo Triassico Medio è stato estremamente instabile (vedere figura I per una scala del tempo triassica). La curva del $\partial^{13}C_{carb}$ globale (e.g. Korte et al., 2005) mostra una serie di ampie e rapide escursioni dei valori isotopici, probabilmente legate ad un limitato "recovery" biologico. I valori isotopici del carbonio dei carbonati sembra stabilizzarsi durante l'Anisico (Triassico Medio), ove ha inizio un trend secolare positivo del $\partial^{13}C$ pari a circa + 3-4 ‰ che si conclude alla base del Triassico Superiore (Carnico). Questa crescita del $\partial^{13}C$ è stata spiegata con l'aumento del seppellimento di grandi quantità di carbonio organico e il ripristino della deposizione di carbone (Korte

et al., 2005). Tuttavia, una maggiore comprensione di questo trend isotopico Anisico-Carnico è ancora necessaria: gli isotopiche del carbonio sono stati misurati su carbonati che riflettono un ambiente marino molto complesso e la forma della curva del $\partial^{13}C$ non è chiara poiché i dati sono alquanto dispersi. Molte domande sono ancora aperte: il trend è veramente una lenta e graduale salita dei valori isotopici oppure l'escursione isotopica avviene a gradini, in pochi eventi di breve durata? Possiamo osservare lo stesso trend isotopico in atmosfera?

Alla fine del Carnico inferiore il $\partial^{13}C$ dei carbonati raggiunge il suo valore massimo (circa 3.5 ‰, Korte et al., 2005). In questo periodo è stato scoperto un evento climatico, chiamato "Carnian Pluvial Event" (CPE), le cui espressioni biologiche e sedimentologiche sono state documentate globalmente, almeno a paleolatitudini tropicali. Questo episodio è caratterizzato dalla morte delle piattaforme carbonati che orlate nella Tetide Occidentale, l'improvviso ed ingente aumento dell'apporto terrigeno, paleosuoli indicativi di clima relativamente umido e dalla risalita della CCD (Carbonate Compensation Depth) nei bacini profondi della Tetide. Questi connotati rendono il CPE simile agli Eventi Anossici Oceanici (OAE) (Rigo et al., 2007), eventi climatici a scala globale caratterizzati inoltre da una perturbazione del ciclo del carbonio. Questo lavoro ha avuto la finalità di costruire una curva del $\partial^{13}C$ per il Triassico Medio-Superiore basata su analisi di resti fossili vegetali (legni, foglie e biomarker molecolari) e di verificare se una perturbazione del ciclo del carbonio è associata o meno al CPE.

Negli ultimi anni l'uso di tessuti fossili di piante superiori, quali legni (e.g. Hesselbo et al., 2007), cuticole (e.g. Arens and Jahren, 2000) a pollini (e..g. Jahren 2004), per misure isotopiche del C organico ha preso via via sempre più piede. La composizione isotopica del carbonio delle piante superiori fossili è il risultato di tre processi di frazionamento a partire dal $\partial^{13}C$ del C atmosferico originale: 1) frazionamento durante la fotosintesi, 2) frazionamento post-fotosintetico, 3) frazionamento "diagenetico". Secondo il modello di Farquhar (1989), sono tre i fattori principali che controllano il $\partial^{13}C$ delle piante superiori C_3 durante la fotosintesi: 1) frazionamento fisico e biochimico prima e durante la carbossilazione; 2) fattori ecologici quali lo stress idrico (che causa uno shift positivo fino al 3-4 ‰), la mancanza di nutrienti (-4 ‰), la limitata esposizione alla luce solare (- 5-6 ‰), la temperatura (- 3 ‰) (Arens et al, 2000); 3) il $\partial^{13}C$ atmosferico. L'interazione di questi fattori ha come conseguenza la grande variabilità di valori che il $\partial^{13}C$ di tessuti di piante superiori attuali C_3 (legno, foglie, resine, etc...) può assumere, da -19‰ a -35‰ circa (Tipple e Pagani, 2007). In materiale vegetale fossile una simile variabilità può compromettere e falsare profondamente ricostruzioni paleoclimatiche basate su analisi del $\partial^{13}C$. Nonostante queste limitazioni, Jahren et al. (2008) hanno dimostrato, con esperimenti in laboratorio ad atmosfera controllata, che esiste un'ottima correlazione tra il $\partial^{13}C$ delle piante a il $\partial^{13}C$ dell'atmosfera in cui queste piante vivono, risultato che rende i resti vegetali fossili potenzialmente degli ottimi proxy per la ricostruzione del $\partial^{13}C$ atmosferico.

Lo studio di molecole fossili (biomarker) è relativamente una nuova frontiera nelle paleoecologia e paleoclimatologia. N-alcani (normal-alcani, idrocarburi saturi a catena dritta) con lunghezze comprese fra C_{25} e C_{35} a una predominanza di omologhi dispari su pari, derivano dalle cere epicuticolari di piante superiori terrestri (Peters et al., 2005). Questi lipidi sono molto resistenti ai processi diagenetici e molto comuni sia in sedimenti marini che terrestri. Il loro $\partial^{13}C$ è stato usato con successo per studiare perturbazioni isotopiche associate a grandi eventi climatico-biologici del passato, come l'estinzione di massa al limite Permo/Triassico (Xie et al., 2007) o il massimo termico al limite Paleocene/Eocene (Pagani et al., 2006), per definire l'avvento delle piante con via metabolica di tipo C_4 (Tipple and Pagani, 2007); o per studiare la proporzione relative di piante C3 e C4 nel passato (Pancost and Boot, 2004). Analisi del $\partial^{13}C$ di n-alcani associati a piante superiori permettono di superare i problemi legati all'alta variabilità del $\partial^{13}C$ di singoli tessuti vegetali poiché le molecole fossili disperse nei sedimenti rappresentano una larga comunità floristica, specialmente se si analizzano sedimenti marini, ed il loro $\partial^{13}C$ costituisce dunque un valore medio che ha un alto valore statistico.

Per questa ricerca sono stati campionati legni, foglie e ambre da numerosi livelli del Triassico Medio-Superiore delle Albi Meridionali (Italia), molto ricchi in resti vegetali. Legni, foglie e ambre sono stati saparati manualmente da campioni di roccia integri o sedimenti

sciolti, polverizzati e trattati con HCl per rimuovere eventuali tracce di carbonati e pirite; piccole quantità di materiale così trattato sono state dunque analizzate per il $\partial^{13}C$ organico. Il $\partial^{13}C$ di legni e foglie mostra range isotopici tra 3 ‰ e 4 ‰ in ogni singolo livello stratigrafico campionato. Tale range è più limitato rispetto a quanto osservato in legni e foglie recenti (cf. Cernusak et al., 2009), probabilmente perchè durante la diagenesi alcuni composti che costituiscono il legno (cellulosa ed emicellulosa in particolare) vengono rimossi. I valori isotopici dell'ambra, al contrario, variano in un range del 4 ‰, molto simile a quanto misurato in resine recenti e cretaciche (Stern et al., 2008; McKellar et al., 2008). L'ambra dunque sembra conservare meglio l'originale composizione isotopica rispetto ad altri tessuti vegetali fossili (Dal Corso et al., accepted; Roghi et al., in prep.).

Legni e foglie del Triassico Medio presentano valori isotopici più negativi di circa il 3 ‰ rispetto al materiale del Carnico (Triassico Superiore): i valori dell'Anisico e del Ladinico variano tra -27 ‰ e -23,5 ‰, mentre quelli del Carnico tra -24 ‰ e -19,5 ‰. Questi dati confermano che l'escursione isotopica secolare, pari a +3 ‰, registrata in carbonati marini e brachiopodi, è stata registrata anche dalle piante superiori terrestri e dunque lo shift isotopico secolare ha interessato il sistema oceani-atmosfera (Dal Corso et al., accepted).

Misure del $\partial^{13}C$ della sostanza organica totale (TOC) dei sedimenti, associate ad analisi isotopiche di n-alcani di piante superiori terrestri hanno permesso di scoprire una rapida4 escursione isotopica negativa associata al Carnian Pluvial Event. In particolare gli n-alcani dispari a catena lunga mostrano uno uno shift del -4 ‰, mentre il TOC uno shift del -2 ‰ circa. Questi dati sono la testimonianza di una rapida iniezione di CO_2 con una composizione isotopica "leggera" nell'atmosfera carnica e confermano la natura globale del CPE. Lo scenario che qui si propone per l'interpretazione di questo evento lega indissolubilmente il CPE alla coeva (Furin et al., 2006) eruzione della provincia magmatica di Wrangellia con grandi conseguenze per il clima e la vita (e.g. la morte delle piattaforme carbonatiche e l'estinzioni e la radiazioni di alcuni dei gruppi più importanti nella storia della vita sulla terra).

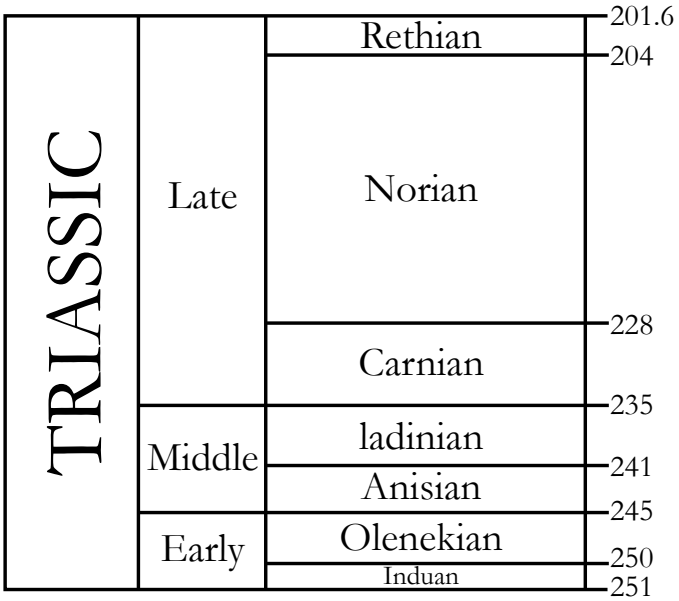

Fig. I: Triassic Time Scale. Modified after Walker and Geissman, 2009.

1. INTRODUCTION

1.1 Problem: The Carnian Pluvial Event

During the early Late Triassic a major climatic and biotic turnover have been recognized, namely the Carnian Pluvial Event (CPE) (Simms and Ruffel, 1989). This event has been very well dated to a short stratigraphic interval about the uppermost Julian – lowermost Tuvalian (Carnian, Late Triassic; Fig 1.1) by ammonoids, palynomorphs and conodonts, and its minimum U/Pb absolute age was given by Furin et al. (2006) to be 230.91±0.33 Ma.

The sedimentological and palaeontological features that mark the CPE have been attributed to a shift from the general arid climate of the Late Triassic to more humid conditions (Schlager and Schöllnberger, 1974; Simms and Ruffel, 1989; Roghi 2004; Breda et al., 2009; Preto et al., 2010; Stefani et al., 2010; Roghi et al., 2010). At least three (Breda et al., 2009; Stefani et al., 2010) to four (Roghi et al., 2010) distinct humid pulses have been recognized so far to constitute the CPE, which is thus a complex episode. Increasing pluvial conditions enhanced the run-off and

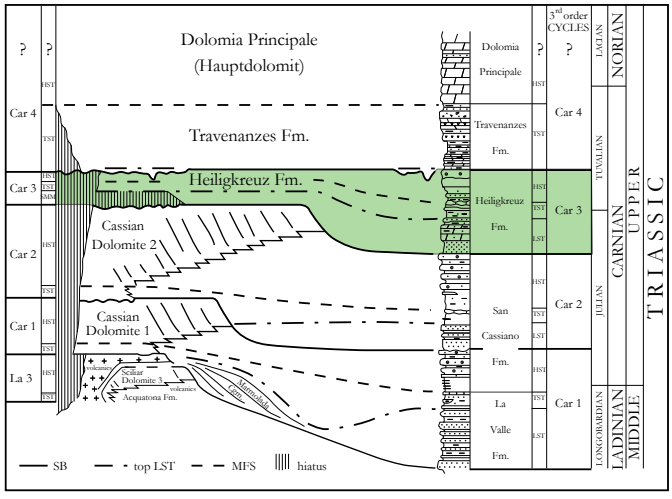

Fig 1.1: Carnian stratigraphy of the Dolomites after De Zanche et al. (1993) and Breda et al. (2009). In green: highlight of the Heiligkreutz Fm. corresponding to the silicoclastic input that characterize the Carnian Pluvial Event.

the accumulation of coarse siliciclastics in marginal marine successions of the Southern Alps (Heiligkreuz Fm., Fig. 1.1), while the carbonate platforms (Cassian Dolomite, Fig 1.1) stopped their growth and experienced karstification, such as the development of dolines and caves filled by terrigenous sediments and breccias (Stefani et al., 2010). An halt of the carbonate sedimentation has been observed during the CPE also in deep water successions of the Southern Apennines (Southern Italy) (Rigo et al., 2007). A rise of the Carbonate Compensation Depth (CCD) has been invoked to explain the dissolution of carbonates in deep marine settings (Rigo et al., 2007).

In the continental Germanic Basin the CPE is marked by the deposition of a large amount of fluvial sandstones (Schilfsandstein Fm.) and in the Northern Calcareous Alps coal seams formed locally.

In the Dolomites (Southern Alps), palaoesols within the Heiligkreuz Fm. (Fig. 1.1) show very well developed histic and spodic horizons that today form in tropical humid climates with a positive water budget throughout the year (Preto and Hinnov, 2003; Breda et al., 2009). Palaeosols within the overlying Travenanzes Fm. have in contrast features typical of calcic vertisols, i.e. soils that develop today in arid to semiarid climates in tropical belts. Similarly, coeval palaeosols from the lower Chinle Fm. in Utah (USA) registered also increasing rainfalls with respect to the Middle Triassic paleosols below and the Carnian-Norian ones above (Prochnow et al., 2006).

A biological turnover has been recognized both in terrestrial and marine realms. A clear shift from xerophytic to hygrophytic palynological assemblages, i.e. from assemblages reflecting a vegetation growing under arid and humid conditions respectively, has been recognized during the CPE. At the

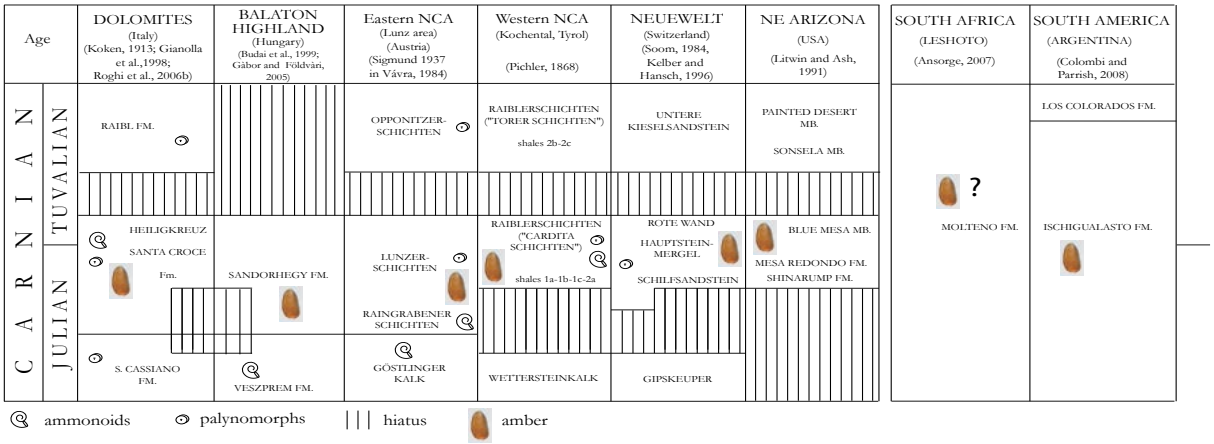

Fig 1.2: correlation of Carnian amber deposits discovered so far.

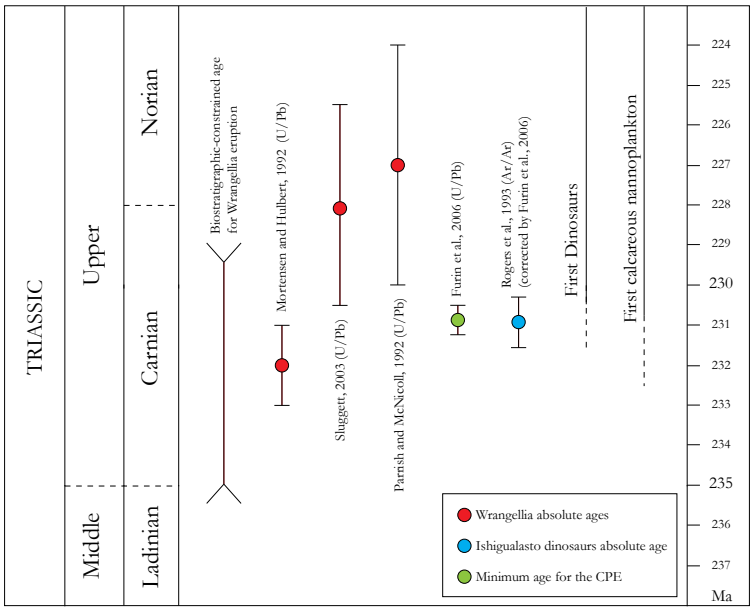

Fig 1.3: U/Pb absolute ages available for the Wrangellia LIP, U/Pb minimum absolute age for the CPE, Ar/Ar absolute age of the first dinosaurs and the emergence of calcareous nannoplankton.

Julian/Tuvalian boundary an increase of pollen and spores with an equisetophytic, pteridophytic and cycadophytic botanical affinity have been observed in the Julian Alps (Roghi, 2004) and in the Northern Calcareous Alps (Roghi et al., 2010), associated to a decrease of forms attributed to plants living in more arid environments (mostly conifers). This "humid" floral peak can be recognized also in Central and North Europe, Barents Sea, Svalbard and northern Iraq Carnian successions, indicating a widespread vegetational shift in the Boreal and Tethyan realms at least (Hochuli and Vigran, 2010; Roghi et al., 2010 and references therein). Associated to this floral change a lot of amber (fossil resin) has been found in Carnian deposits of Europe (Southern Alps, Itay; Northern Calcareous Alps (NCA), Austria; Balaton Highland, Hungary); Arizona, North America; Argentina, South America and Leshoto, South Africa (Fig. 1.2) (Gianolla et al., 1998; Roghi et al., 2006).

The CPE is marked also by high extinction rates among ammonoids, crinoid, briozoa (Simms and Ruffel 1989, 1990; Simms et al., 1995) and conodonts (Simms and Ruffel, 1989; Rigo et al., 2007). The magnitude of the extinction is minor when compared to the biggest mass extinctions during the Phanerozoic (Rohde & Muller 2005), but the CPE may have had a key role in the origin and/or radiation of some of the most important groups in Mesozoic ecosystems. The first known dinosaurs occur in the Carnian of the Ishigualasto Fm. (Argentina) (Martinez et al., 2011) and have an absolute age (Fig 1.3) very similar to that of the CPE (Rogers et al., 1993; Furin et al., 2006).

The first calcareous nannoplankton also dates back to the Carnian (Erba, 2006) (Fig 1.3) and the radiation of modern-like conifers occurs during the Late Triassic (Taylor et al, 2009). The Carnian seems to have been also crucial for the evolution of scleractinian corals that started to be important constituents of the reefs (Stanley, 1988, 2003).

The question is: what triggered this major climatic and biological turnover during the Carnian?

Among the explanations that have been suggested there are an increase in rainfall and modified atmospheric circulation in the Tethyan realm driven by the uplift of the Cimmerian orogen (Hornung and Brandner, 2005), and a maximum of expansion and intensity of Pangean mega-monsoon corresponding to the maximum aggregation of continents (Parrish, 1993). These hypotheses cannot explain the whole suite of sedimentological , environmental and biotic changes that define the CPE, in particular the extinctions/radiations and the dissolution of carbonates in deep sea basins. Rigo et al. (2007) highlighted that the CPE show similarities with some perturbations of the C-cycle, expecially the early Aptian Event. The whole suite of palaeoclimatic and biological changes associated to these events have been attributed to a rise of the pCO_2 levels. Some characteristics of the CPE can be explained by increasing pCO_2 levels (Rigo et al., 2007), such the rise of the CCD. However, no data exist to support this hypothesis so far and the question remains still open: where the excess of CO_2 come from? It has been pointed out that the CPE has an absolute age similar to that of the Wrangellia Large Igneous Province (LIP) outcropping in north eastern North America (Fig 1.3) (Furin et al., 2006). A huge volcanic activity could have provided the amount of greenhouse gases to trigger an ocean acidification episode and a global climate change with strong consequences on environments and biota, as observed for others great climatic/biological perturbations in the Earth history (e.g. the Permian/Triassic and Triassic/Jurassic mass extinctions). However, nothing but age similarity links the CPE to the eruption of Wrangellia flood basalts so far.

1.2 Searching for the CPE $\partial^{13}C$ signature and a little deviation to the Cretaceous

The aim of this study is to explore whether a $\partial^{13}C$ excursion is associated to the CPE. It has been pointed out that major climatic crises and biological turnovers are associated with C-isotope

excursions (CIE). As previously said, environmental and biotic changes linked to the CPE show patterns similar to those associated to OAEs and the absolute age of the CPE agrees with that of the eruption of the Wrangellia LIP. OAEs are characterized by a global positive $\partial^{13}C$ shift and sometimes also a pronounced negative CIE (e.g. early Aptian, early Albian and Toarcian OAEs) (Jenkyns 2010 and references therein). Major climatic and biological crises linked to LIPs, including some OEAs, are associated to a sharp global negative CIE (Courtillot & Renne, 2003; Rampino, 2010). Thus, the study of the CPE C-isotope signature is crucial to deeply understand it and its causes.

However, a C-isotope study of the CPE can be very tricky because of both intrinsic and methodological problems linked to the subject of isotope analyses. The question is: what can we analyze for $\partial^{13}C$ safely? On the one hand Tethyan successions encompassing the CPE lack carbonates in basinal environments (Rigo et al., 2007) to perform classical inorganic marine bulk carbonates $\partial^{13}C$ analyses and the $\partial^{13}C$ of shallow water carbonates could be hard to interpret. On the other hand bulk organic matter (OM) $\partial^{13}C$ data can be of difficult interpretation when the composition of OM is unknown and could be changing through time (e.g. van de Schootbrugge et al. 2008), especially when samples come from marine successions that contain a mixture of terrestrial and marine OM.

A possible solution is the C-isotope analysis of fossil plant materials, both macroscopic and microscopic (i.e. fossil molecules) remains, as plants during the photosynthesis take CO_2 directly from the atmosphere and changes of their C-isotope composition must reflect $\partial^{13}C$ changes in the atmosphere, one of the most important C reservoirs. Unfortunately, plants fractionate C isotope both during (Farquhar et al., 1989) and after photosynthesis (Badeck et al., 2005; Cernusak et al., 2009). This C-isotope fractionation is regulated by environmental and biochemical processes resulting in highly variable plant $\partial^{13}C$ values within and between plant communities (see chapter 2 for a comprehensive description of C_3 plants C-isotope fractionation). Moreover, 230 Myrs old fossil plant remains, as those coming from the CPE, have experienced a long diagenetic history that could have changed their original C-isotope composition (van Bergen and Poole 2002; Poole et al., 2006). A study of $\partial^{13}C$ variability of plant remains within single stratigraphic levels (i.e. sampling fossil plants with the same age) is thus necessary to understand their ability to faithfully record

atmospheric C-isotope changes. The first part of the project was thus devoted to the study of the $\partial^{13}C$ variability of separated anatomical plant parts, namely wood and leaves, collected from three sections of the Middle-Late Triassic of the Southern Alps. $\partial^{13}C_{plant}$ data have been also compared to existing $\partial^{13}C_{inorg}$ curve for the same time interval in order to understand if wood and leaves registered the secular trend of bulk marine carbonates and brachiopod calcitic shells. It has been also possible to perform $\partial^{13}C$ analyses of Triassic amber from the Dibona section (Dolomites, Southern Alps), the oldest rich amber-bearing deposit. Amber C-isotope composition has been poorly explored so far but it has been pointed out that it can be a useful tool for palaeoclimatic/palaeoecological studies (e.g.: Nissenbaum and Yakir, 1995). As Dibona amber is restricted to few stratigraphic beds within the Heiligkreutz Formation and it is easily collectible only from one paleosol, it wasn't possible to build a $\partial^{13}C_{amber}$ curve. For this purpose several C-isotope analyses of different Cretaceous amber drops from Spain and France were performed.

The isotope analysis of single compounds (compound specific isotope analysis, CSIA) can obviously help overcoming problems linked to the inter- and intra-specific variability of plant $\partial^{13}C$, as plant-related molecules extracted from sediments represent a mixture of a number of individuals from a large catchment area, and thus their $\partial^{13}C$ value is a mean value that is statistically significant to infer the C-isotope composition of the atmosphere. However, the CSIA of lipids extracted from very old sediments could be sometimes impossible because of diagenesis and degradation of OM, the low concentration of specific compounds or the lack of plant-related biomarkers. Two sections of the Dolomites have been selected for lipid extraction to encompass most of the Carnian stage and because of their supposed low diagenetic overprint (Milieres-Dibona and Prati di Stuores/Stuores-Wiesen section).

The schedule and strategic planning of my PhD years are summarized in Tab. 1.1. I first studied the C-isotope variability of selected Middle – early Late Triassic plant remains, namely wood, leaves and amber (chapter 2), and Cretaceous amber from several deposits of Spain and France in collaboration with Hugh Jenkyns (Oxford University, UK), Xavier Delclos (Universitat de Barcelona, Spain) and Carmen Soriano (European Synchrotron Radiation Facilities, France). Then,

CSIA of samples collected from two key section of the Carnian of the Dolomites (Southern Alps) have been performed at the School of Chemistry of Bristol University (UK) in collaboration with Richard Pancost (chapter 3). Finally, more $\partial^{13}C$ data of newly sampled wood and bulk OM have been collected at the School of Earth and Environments (Leeds University, UK) in collaboration with Robert Newton and Paul Wignall (chapter 2 & 4).

	I year				II year				III year			
Bibliographic survey												
Sampling												
Samples preparation												
Analyses (Oxford)												
Sampling II												
Samples preparation												
CSIA analyses (Bristol)												
Analyses (Leeds)												
Writing papers and thesis												

Tab 1.1: schedule of the PhD project.

2. THE C-ISOTOPE VARIABILITY OF TRIASSIC AND CRETACEOUS FOSSIL PLANTS REMAINS

2.1 The C-isotope signature of fossil plants remains

The carbon-isotope composition of terrestrial fossil plant-derived material is widely used in geochemical and chemostratigraphic studies. Separated fossil land plant tissues, such as wood (Gröcke et al., 1999; van Bergen and Poole, 2002; Gröcke 2002; Hesselbo et al., 2003; Robinson and Hesselbo, 2004; Poole et al., 2006; Hesselbo et al., 2007; Bechtel et al., 2008; Whiteside et al., 2010; Yans et al., 2010), cuticle (Arens and Jahren, 2000; Jahren et al., 2001, 2005, 2009; Retallack and Jahren, 2008; Jahren and Arens, 2009), pollen (Beerling and Jolley, 1998; Loader and Hemming 2004), and bulk terrestrial organic matter (e.g.: Barclay et al., 2010) have been analyzed to reconstruct $\partial^{13}C_{org}$ trends, infer carbon-cycle perturbations and evaluate the carbon-isotope composition of atmospheric CO_2 in the past. Additionally, few papers have explored the carbon-isotope signature of amber, pointing out that such analysis of fossil resin could be a useful tool for palaeobotanical, palaeoclimatic and palaeoenvironmental purposes: existing data show that amber has $\partial^{13}C$ values similar to those expected for C_3 plants and seems to retain its original carbon-isotope signature (Murray et al., 1994; Nissenbaum and Yakir, 1995; Murray et al., 1998; McKellar et al., 2008; Stern et al., 2008).

The $\partial^{13}C$ of plant-derived material could be difficult to interpret in deep-time geological records, due to the natural high variability of isotope signatures in plant carbon and the absence of adequate palaeoenvironmental and/or palaeoecological information. The carbon-isotope composition of plants depends upon the composition of the carbon source used for photosynthesis, the photosynthetic pathway (C_3, C_4 and CAM) and a number of environmental and ecological factors. C_3 plants are the predominant and ubiquitous metabolic group since the Devonian Period, as

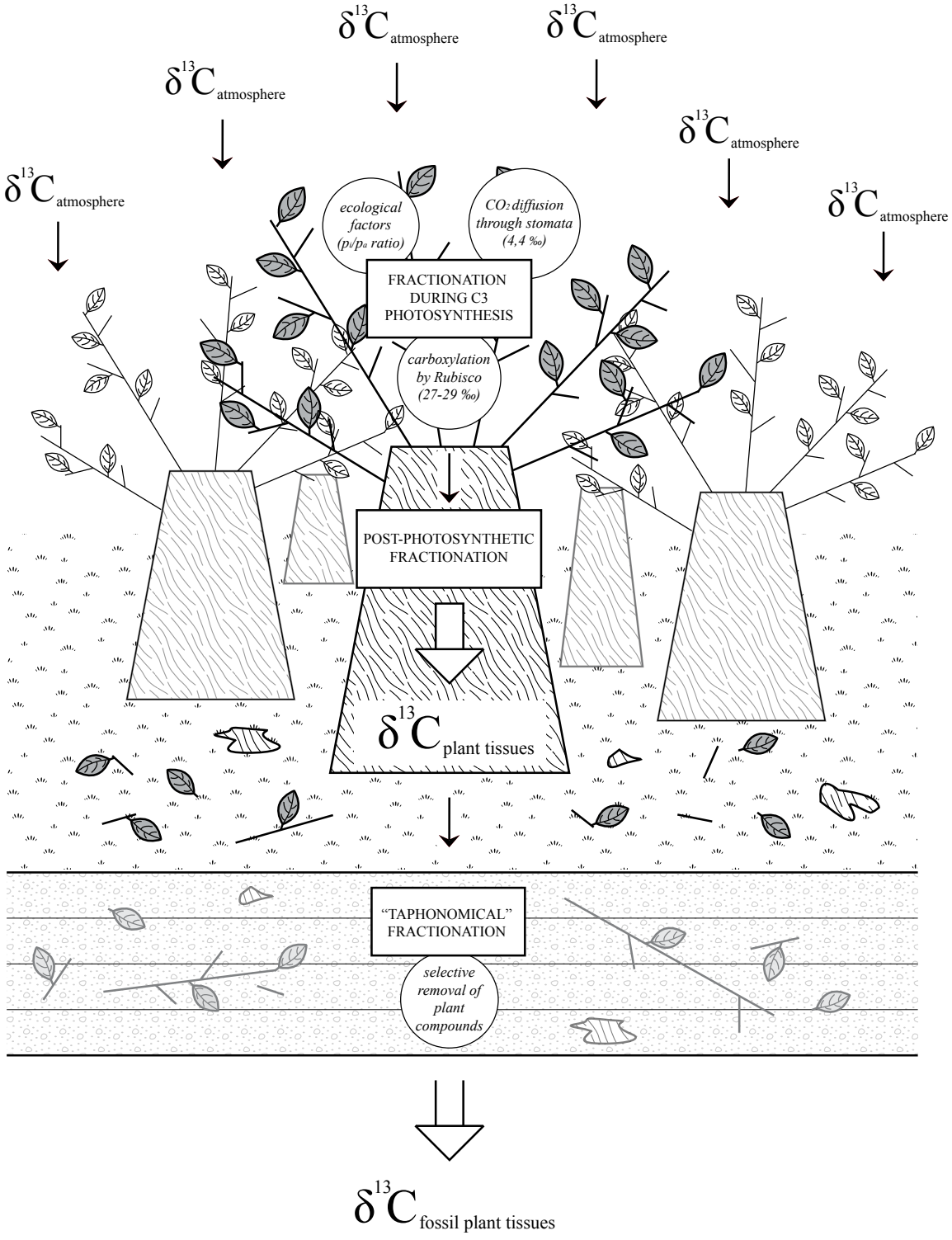

Fig 2.1: schematic representation of the C fractionation processes during and post the photosynthesis and "taphonomical" fractionation during the burial of plant remains into the sediments.

opposed to the C_4 plants that became common only from the Late Miocene (Tipple and Pagani, 2007).

The C-isotope signature of fossil plant remains is the result of multiple C fractionation of the initial captured atmospheric C, by biochemical and taphonomic processes. These processes can be summarized in three distinct steps: 1) fractionation during C3 photosynthesis, 2) post-photosynthetic fractionation during the biosynthesis of plant components and tissues, 3) taphonomical fractionation (Fig. 2.1).

Carbon isotope discrimination during C_3 photosynthesis is described by the following equation (Farquhar et al., 1989):

$$\partial^{13}C_{plant} = \partial^{13}C_{atm} - a - (b - a) * p_i / p_a \qquad \text{[eq. 2.1]}$$

On the basis of this model, four factors influence the carbon-isotope composition of C_3 plants: (1) the carbon-isotope composition of atmospheric CO_2 ($\partial^{13}C_{atm}$); (2) *a*, the physical fractionation during diffusion of CO_2 from the atmosphere into leaves (4,4‰); (3) *b*, the biochemical fractionation during the carboxylation by Rubisco, a key enzyme of photosynthesis (27-29‰); (4) the ratio between intercellular (p_i) and ambient (p_a) CO_2 partial pressures. The p_i/p_a ratio is regulated by stomatal conductance and enzymatic activity that depend upon the ecological conditions in which the plant grows. These ecological factors could strongly affect the plant carbon-isotope signature (Tab 2.1): e.g., plants subject to water shortage show $\partial^{13}C$ values enriched in ^{13}C of about 3-6‰, due to the closure of stomata to limit water loss and consequent decrease of internal pCO_2 (p_i in eq.1);

Ecological factor	$\partial^{13}C$ shift direction	Range
Altitude	+	3-7 ‰
Increasing temperature	+	?
Decreasing temperature	-	3 ‰
Low light	-	5-6 ‰
Low nutrients	-	4 ‰
Recicled CO_2	-	1-5 ‰
Sun – shade leaves	-	1-3 ‰
Water stress	+	3-6 ‰

Tab. 2.1: ecological factors affecting the $\partial^{13}C$ of living plant during the photosynthesis. After Arens et al. (2000) and Gröcke (1998).

$\partial^{13}C_{plant}$ values become more positive (3-7‰) with increasing altitude due to the decrease of pCO_2 and p_i/p_a ratio; conversely the $\partial^{13}C_{plant}$ decreases with nutrient shortage (4‰), light limitation (5-6‰), decreasing temperatures (3‰) and recycling of CO_2 under forest canopies (1-5‰) (Gröcke, 1998; Arens et al., 2000; Dawson et al., 2002 and references therein). However, recent controlled-growth experiments have demonstrated that plant $\partial^{13}C$ values reflect linearly the atmospheric $\partial^{13}C$ in the absence of environmental stresses, across a wide range of pCO_2 levels (Jahren et al., 2008).

After photosynthesis, carbon isotopes are further fractionated during the biosynthesis of different plant components and tissues, causing a different isotope signature among plant organs and compounds ("post-photosynthetic fractionation", Badeck et al., 2005). In general, non-photosynthetic, or heterotrophic, organs (wood, roots, etc.) are enriched in ^{13}C by 1-3‰ compared with photosynthetic tissues (leaves), for a number of reasons as yet unclear (see review by Cernusak et al., 2009). At the molecular level, significant differences exist between plant compounds. Polysaccharides (cellulose, hemicellulose), lignin and lipids, the major components of plant tissues, all have different carbon-isotope signatures: e.g., holocellulose has $\partial^{13}C$ values more enriched than bulk leaf tissue by ~ 2-4‰, and lignin has $\partial^{13}C$ values depleted by ~ 2-6‰ relative to bulk leaf tissue (Benner et al., 1987; Rundgren et al., 2003). Modern and sub-fossil oak wood shows $\partial^{13}C$ values of lignin more depleted than cellulose with an offset of ~ 3‰ (Loader et al., 2003). Differences exist also between the same component isolated from different tissues: cellulose in leaves was found to be depleted in ^{13}C by ~ 2‰ with respect to cellulose extracted from wood of the same tree (Leavitt and Long, 1982; Guehl et al., 1998).

The $\partial^{13}C$ of C_3 plants living under the same atmospheric carbon-isotope composition, measured on different species coming from a variety of environments, and on different plant organs and components (i.e., the mixture of land plant parts that is usually found in sediments deriving from a catchment area of even small dimensions), should exhibit a large range of carbon-isotope values, within ~ -19‰ to ~ -35‰.

To this high ecological and biochemical variability in the $\partial^{13}C$ of living plants we should add a diagenetic overprint whenever fossil material is analyzed for its $\partial^{13}C$ value. Taphonomical processes can remove certain compounds and change the $\partial^{13}C$ value of each plant tissue: e.g., the polysaccharides constituting wood, hemicellulose and cellulose are preferentially removed during

diagenesis, whereas lignin is more resistant (van Bergen and Poole, 2002). Because lignin has lower $\partial^{13}C$ values in comparison with those of polysaccharides, this process causes relatively depleted bulk $\partial^{13}C_{wood}$ values (van Bergen and Poole 2002; Poole et al., 2006).

It is clear that the $\partial^{13}C$ measured on fossil terrestrial plant remains reflects a combination of all carbon fractionation processes that it has experienced during and after a plant's life after the initial fixation of atmospheric CO_2 during photosynthesis. All these factors, potentially affecting the fossil plant carbon-isotope signature, could severely hamper geochemical and chemostratigraphic analyses in deep time based on fossil plant material, since they could modify or even obliterate short-time shifts and secular $\partial^{13}C_{org}$ trends. It has been suggested that a rock sample comprising a number of individual plants of different species could be a very good substrate to reconstruct the $\partial^{13}C$ of the atmosphere (Arens et al., 2000; Jahren et al., 2008; Jahren and Arens, 2009). Unfortunately such substrate is often very difficult to reproduce in older sedimentary rocks, as a statistically significant number of plant macroremains is often lacking or too difficult to sample. Moreover, when working on marine sections, the OM is a mixture of both terrestrial and marine elements, and thus the $\partial^{13}C_{org}$ signal of bulk OM doesn't reflect the C-isotope composition of the atmosphere. Palynological analyses coupled with ∂^{13}Corg measurements of the bulk OM show that variations in the proportion of marine versus terrestrial elements and/or between different taxonomical plant groups could explain the negative and positive shifts in the bulk organic carbon-isotope signature at the Triassic/Jurassic boundary (van de Schootbrugge et al. 2008).

Because of the listed factors affecting the C-isotope signature of living and fossil plant material, it is necessary to understand how fossil plant remains retain their original carbon isotope signature and to define the $\partial^{13}C$ variability of samples coming from the same stratigraphic level, i.e. with the same age, before attempting to use them for any chemostratigraphic – palaeoclimatic – geochemical purpose. Thus, I first studied the spread in carbon-isotope values of well-preserved material, by isolating Triassic tissues (leaves and wood) of terrestrial plants and Triassic and Cretaceous amber. Then, I tried to build a Middle-Late Triassic C-isotope curve based on wood and leaves in order to evaluate their $\partial^{13}C$ variability and their potential in reproducing the $\partial^{13}C$ trend identified in Middle – early Late Triassic marine carbonates (Korte et al., 2005), and an amber-based Cretaceous $\partial^{13}C$ curve.

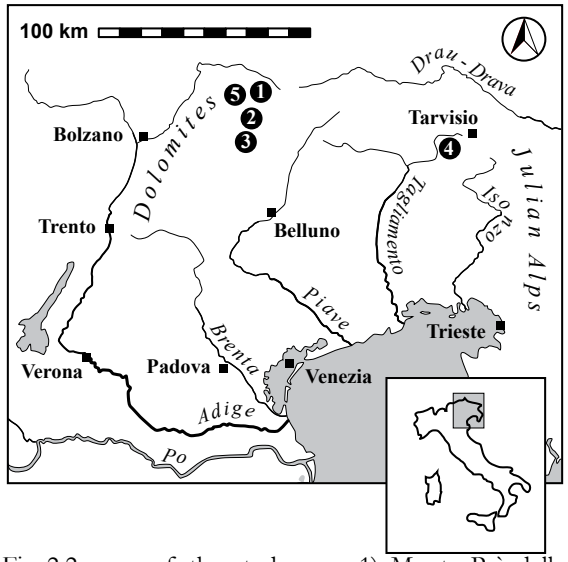

Fig 2.2: map of the study area. 1) Monte Prà della Vacca section, 2) Rifugio Dibona section, 3) Savinér section, 4) Dogna section, 5) Stuores Wiesen section.

2.2 Set of samples

Two sets of samples were analyzed in two different laboratories. The first one was analyzed at Oxford University and includes wood, leaves and amber form the Middle – Upper Triassic of Southern Alps and Cretaceous amber drops from several deposits in Spain, Canada and France. The second set was analyzed at Leeds University and includes wood from two selected sections of the Carnian (Late Triassic) of the Dolomites. In the following paragraphs the two sets will be described separately.

2.2.1 First set

2.2.1.1 Triassic material

The first analyzed Triassic samples were collected in four different localities of the Southern Alps characterized by abundant plant remains with good preservation (Fig. 2.2). Four localities exposing Triassic sediments (Fig. 1.1) were selected with ages ranging from the Anisian to the Carnian.

A succession of hemipelagic limestones and marls (Dont Formation) containing ammonoids and other marine fossils along with plant remains, is exposed at Monte Prà della Vacca /Kühwiesenkopf in the north-eastern Dolomites. Samples of plant tissue analyzed in this study derive from a horizon containing both marine and terrestrial fossils, dated to the middle-late Pelsonian (Anisian) by ammonoid and palynomorph biostratigraphy (Broglio Loriga et al., 2002; Kustatscher et al.,

2006).

A newly investigated outcrop of upper Ladinian deep-water volcaniclastic siltites and arenites (Wengen Formation) in the central Dolomites, near the village of Caprile in the Cordevole Valley, is identified here as "locality Savinér". Abundant plant remains were found in the outcrop and as debris in this locality.

A third set of samples was collected in shallow-water limestones and marls of the Rio del Lago Formation near Dogna, in the Dogna Valley of eastern Southern Alps. This formation represents the middle portion of a mixed carbonate-siliciclastic ramp of early Carnian age (Preto et al., 2005). Abundant plant remains (Fig. 2.3) were collected in a fine marly limestone bed at the base of the formation.

Samples of wood, leaves and amber were collected also at Rifugio Dibona (Tofane mountains) near Cortina d'Ampezzo in the central Dolomites. This section consists of carbonates, shales and arenites (Heiligkreuz Fm., formerly Dürrenstein Fm.) deposited in a marginal marine setting between the end of the early Carnian and the beginning of the late Carnian (Preto and Hinnov, 2003). The section includes several hydromorphic paleosols, i.e. soils developed under conditions of water saturation, formed in marginal marine swamps below the water table, which yielded abundant plant remains and amber droplets (Fig. 2.4). Former physico-chemical analyses, such as infrared spectrophotometry (FTIR), pyrolysis-gas-chromatography/mass-spectrometry (pyr-GC/MS), nuclear magnetic resonance (NMR), thermo-gravimetry and differential thermogravimetry, were performed on the same Rif. Dibona amber analyzed in this paper and showed that it has unique physico-chemical fingerprints (Roghi et al., 2006). In particular, pyr-GC-MS analyses show that Triassic amber can be ascribed to the Class II resins proposed by Anderson et al. (1992) but have also some elements typical of Class I resins (Roghi et al., 2006). These analyses, coupled with palaeobotanical and palynological studies, suggest that Rif. Dibona amber was exuded by plants belonging to the Cheirolepidiaceae conifer family (Gianolla et al., 1998; Ragazzi et al., 2003; Roghi et al., 2006; Breda et al., 2009). Organic-rich histic soil horizons were sampled from three of these paleosols, whose age is close to the early-late Carnian boundary.

Leaf fragments from Monte Prà della Vacca (Anisian) and Dogna (Carnian) and wood from the Dibona section (Carnian) were sampled from identified, well-preserved coalified fossil plant

Fig 2.3: fossil plants from Dogna section (CHIUT level): 1) undetermined Seed Fern, 2) undetermined Conifer, 3) undetermined Seed Fern, 4) undetermined Conifer.

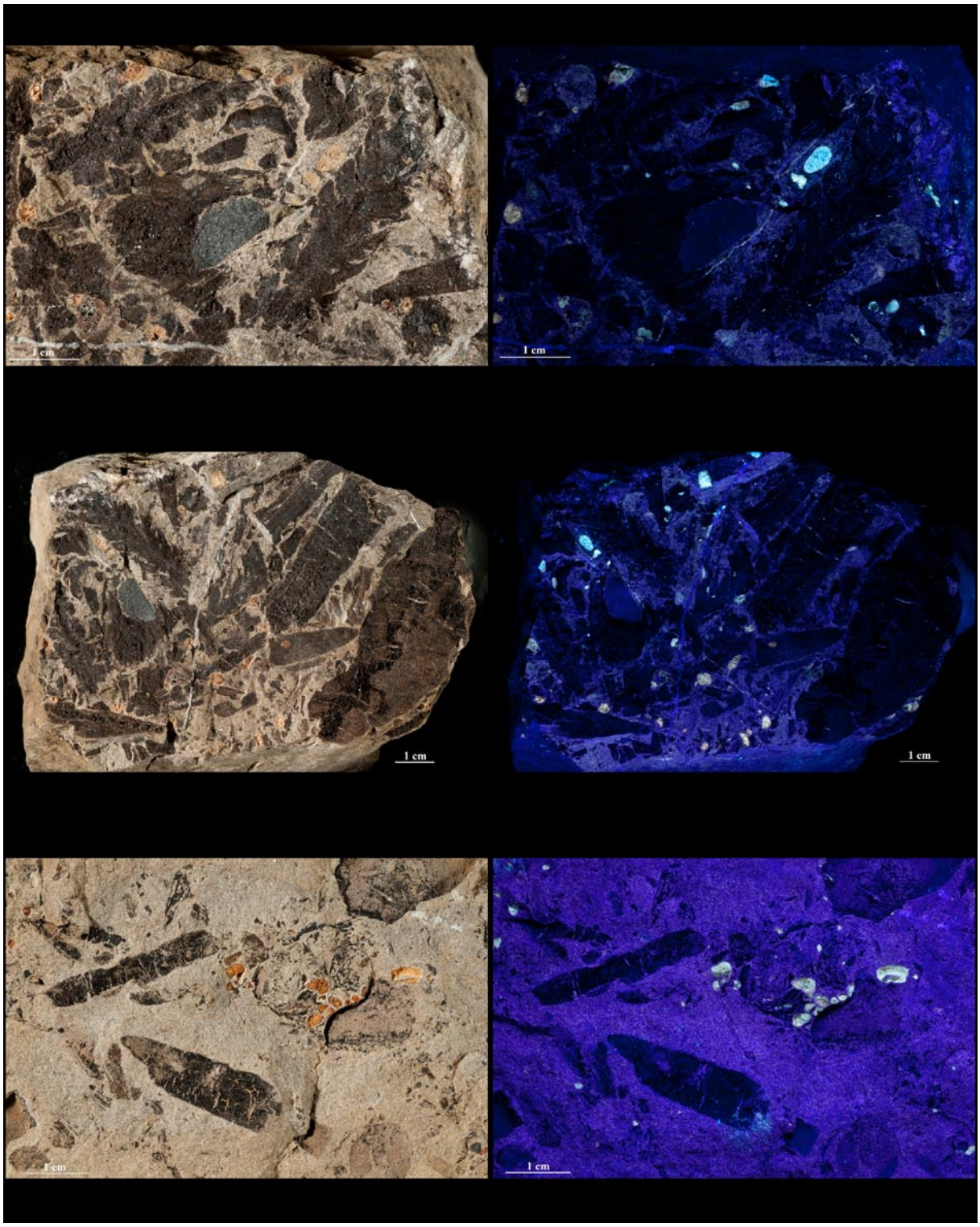

Fig 2.4: some examples of amber-bearing rock samples coming from the NRE103 stratigraphic bed at Dibona section. Note the presence of several amber drops mixed to a number of plant fragments. On the right: samples under UV light reflected by amber.

remains. Coalified wood fragments from the NRE101-2 and NRE109 Carnian levels at the Dibona section were hand-picked from soft sediment as dispersed material that could not be classified more specifically. Leaves and wood from the Savinér section (Ladinian), preserved as coalified fragments, were hand-picked and were not classified. Amber was sampled as individual drops dispersed into the sediment of level NRE103 at Dibona section (Carnian).

2.2.1.2 Cretaceous Amber

Cretaceous Amber samples come from several sections in Spain and France, and from the Grassy Lake deposit in Canada. Their origin and age are summarized in Tab 2.2.

Ten Late Albian – Santonian amber drops from France were provided by D. Néraudeau (Université Rennes) and V. Perrichot (University of Kansas). These fossil resins were very well dated with dinoflagellates, foraminifers and ostracods (Ragazzi et al., 2009 and references therein).

Grassy Lake amber was collected by A. Wolfe (University of Alberta) and was attributed to a Campanian age according to McKellar et al. (2008).

Spanish San Just amber was collected by G. Roghi (CNR Padova) at San Just deposit, an outcrop near the Escucha village (Teruel, Spain). The seven analyzed ambers come from an organic-rich level within the Regachuelo Member of the Escucha Formation (Peñalver et al., 2007) and were found associated with abundant plant remains, mainly belonging to the Cheirolepidiaceae family

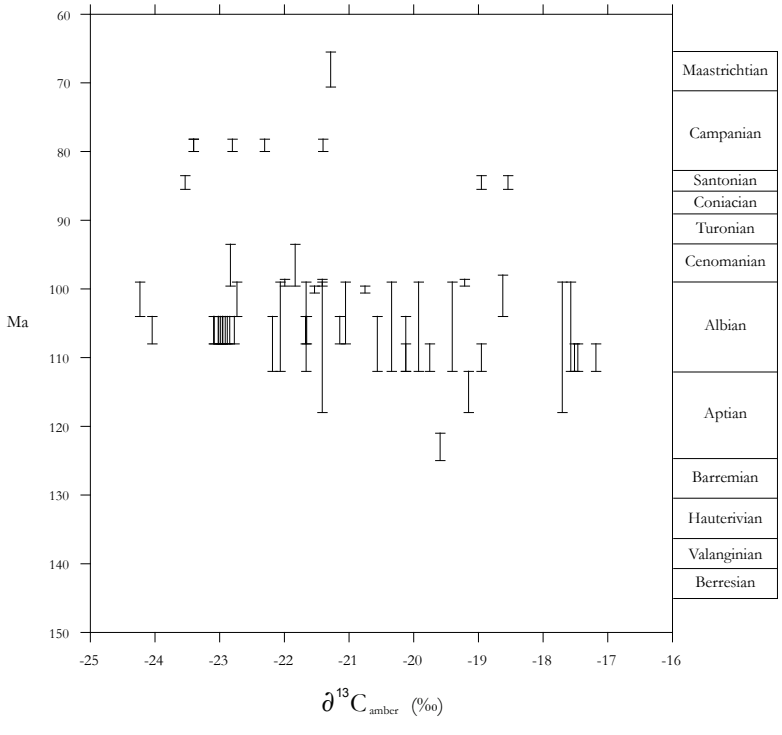

Fig 2.5: age uncertainties of cretaceous amber drops from Spain and France.

Sample	*Deposit*	*Geological Age*	*Age (Ma)*	*$\partial^{13}C$ (‰)*	*Colour*	*Preservation*
SPAG 2	Camijanes	Early Albian	108 – 112	-19.75	Y	NA
SPAG 4	Arroyo de la Pascueta	Early Albian	108 – 112	-18.95	DY	NA + A
SPAG 6	La Hoya	Early Albian	108 – 112	-17.18	R	NA
SPAG 11	Puente "el Arrudo"	Early Albian	108 – 112	-17.46	Y - R	NA
SPAG 33	Cabo Quintre	Early Albian	108 – 112	-17.51	Y	NA
SPAG 27	Peñacerrada	Early Albian	108 – 112	-20.12	DY	NA
SJU 5.1	San Just	Early – Middle Albian	104 – 108	-22.88	DY	NA
SJU 5.2	San Just	Early – Middle Albian	104 – 108	-23.09	DY	NA
SJU 5.3	San Just	Early – Middle Albian	104 – 108	-23.02	DY	NA
SJU 6.1	San Just	Early – Middle Albian	104 – 108	-22.91	DY	NA
SJU 6.2	San Just	Early – Middle Albian	104 – 108	-22.95	DY	NA
SJU 6.3	San Just	Early – Middle Albian	104 – 108	-23.01	DY	NA
SJU 6.4	San Just	Early – Middle Albian	104 – 108	-23.08	R - Y	A
SJU 6.5	San Just	Early – Middle Albian	104 – 108	-22.95	DY	NA
SJU 6.6	San Just	Early – Middle Albian	104 – 108	-22.98	DY	NA
SJU 7	San Just	Early – Middle Albian	104 – 108	-21.14	R - Y	A
SJU 8.2G	San Just	Early – Middle Albian	104 – 108	-22.77	DY	NA
SJU 8.3A	San Just	Early – Middle Albian	104 – 108	-22.84	DY	A
SJU 9A	San Just	Early – Middle Albian	104 – 108	-21.67	DY - R	NA
SJU 10	San Just	Early – Middle Albian	104 – 108	-24.04	DY	NA
SJU 11	San Just	Early – Middle Albian	104 – 108	-21.65	DY	NA
SPAG 12	Arroyo de la Pascueta	Early – Middle Albian	104 – 112	-20.56	R	A
SPAG 17	Minas de Val de la Piedra	Early – Middle Albian	104 – 112	-22.18	Y	A
SPAG 28	Peñacerrada II	Early – Middle Albian	104 – 112	-20.12	DY	NA
SPAG 7	Villel	Albian	99 – 112	-20.34	R	NA
SPAG 13	Maliaño	Albian	99 – 112	-22.06	R - Y	NA
SPAG 21	Reocín	Albian	99 – 112	-19,40	DY	NA
SPAG36	Zubielki	Albian	99 – 112	-17.57	Y	NA
SPAG 37 (I)	Suances	Albian	99 – 112	-21.66	R	NA
SPAG 37 (II)	Suances	Albian	99 – 112	-19.92	R	NA
SPAG 15	Faro de Ajo	Late Aptian - Albian	99 – 118	-17,70	R - Y	NA
SPAG 18	Cuchía	Late Aptian - Albian	99 – 118	-21.41	DY	NA
SPAG 26	El Caleyo	Late Albian	99 – 104	-22.73	Y	NA
SPAG 30	Páramo de la Lora	Late Albian	99 – 104	-24.23	R - Y	NA
SPAG 32	Cabo Quintre	Late Albian – Early Cenomanian	98 – 104	-18.62	R - Y	NA

SPAG 23	Salinillas de Buradón	Middle – Late Albian	99 – 108	-21.05	DY	NA
SPAG 5	Oruña	Late Aptian	112 – 118	-19.15	Y - R	NA
SPAG 3	Mas de la Parreta	Early Aptian	121 – 125	-19.59	Y - DY	NA
SPAG 31	Puerto Vicuña	Maastrichtian	65.5 – 70.6	-21.28	R - Y	NA
SPAG 35	Alloz	Middle Cretaceous	89 – 125	-21.19	DY	NA
F 1	Archingeay	Late Albian	99.6 – 100.6	-20.75	DY	NA
F 2	Cadeuil	Late Albian	99.6 – 100.6	-21.53	DY	NA
F 3	Fouras	Early Cenomanian	98.6 – 99.6	-21.41	Y	NA
F 4	Ile d'Aix	Early Cenomanian	98.6 – 99.6	-21.99	Y	NA
F 5	La Buzinie	Early Cenomanian	98.6 – 99.6	-19.21	DY - R	NA
F 6	Fourtou	Cenomanian	93.5 – 99.6	-21.83	DY - R	NA
F 7	Salignac	Cenomanian	93.5 – 99.6	-22.83	DY - R	NA
F 8	Piolenc	Santonian	83.5 – 85.5	-23.53	Y	NA
F 9	Belcodène	Santonian	83.5 – 85.5	-18.54	Y	NA
F 10	Ensuès-la-Redonne	Santonian	83.5 – 85.5	-18.95	DY	NA
CA 1	Grassy Lake	Campanian	78.2 – 79	-22,80	Y	NA
CA 2	Grassy Lake	Campanian	78.2 – 79	-23,40	Y	NA
CA 3	Grassy Lake	Campanian	78.2 – 79	-23,40	Y	NA
CA 4	Grassy Lake	Campanian	78.2 – 79	-21,40	Y	NA
CA 5	Grassy Lake	Campanian	78.2 – 79	-22.30	Y	NA

Tab. 2.2: Cretaceous amber from Spain, France and Canada analyzed for the $\partial^{13}C$. Absolute ages after Walker & Geissman, 2009. (Y = yellow, DY = dark yellow, R = red, A = altered, NA = non altered).

(*Frenelopsis* sp.).

Other Spanish amber drops (25 specimens) were provided by X. Delclòs (Universitat de Barcelona). They come from several Cretaceous (Aptian to Maastrichtian in age) deposits of the Asturian, Cantabrian and Maestrat basins in the Iberian Peninsula. The age of these deposits, mainly constrained by pollen and spores, is often very uncertain (see Tab 2.2 and Fig 2.5) (Delclòs et al., 2007; X. Delclòs personal communication).

2.2.2 Second set

The second set of plant fragments includes wood coming from two different sections of the Carnian (Late Triassic) of the Dolomites (Fig 2.2). Stuores Wiesen is the type section for the base of the Carnian (Mietto et al., 2007) and encompasses a series of hemipelagites and thin turbidite beds deposited in a rapidly infilling basin under some hundreds of meter of water depth belonging to the San Cassiano Formation. Milieres-Dibona section lies within the *Austrotrachyceras austriacum* ammonoid zone (uppermost lower Carnian) (Bizzarini & Gnoli 1991) and encompasses a succession of marls, limestone and sandstone deposited in a prodelta - coastal to paralic environment, belonging to the Heiligkreuz Fm., formerly Dürrenstein Fm. Coalified/Charcoalified wood were hand-picked from soft sediment as dispersed material or isolated from rock samples with a cesel. It was not possible to classify at any taxonomic level collected wood macroscopically.

2.3 Methods

As already said, C-isotope analyses have been performed in two laboratories and samples were prepared following two similar standard methods described below.

Oxford laboratory: all samples were first crushed with an agate mortar. The obtained powder was placed in a polypropylene tube and treated with HCl 3M for 3 hours at 70 °C in a water bath to remove carbonates and pyritic compounds. Samples were rinsed with deionized water and centrifuged until neutrality was reached. All the procedure was repeated until the HCl solution, after the 3 h treatment, became transparent. Samples were then oven-dried at 50 °C. An aliquot of 1.5 mg of sample was weighed, embedded in tin capsules and analyzed at the Research Laboratory for Archaeology and the History of Art (University of Oxford) with a Carlo Erba NA 1108 elemental

analyser coupled to a SERCON Geo 20/20 IRMS running in continuous flow mode with a He carrier gas (flow rate 100 ml per min) using an alanine in-house standard routinely checked against international standards IAEA-CH-6 and IAEA-CH-7 and traceable back to the VPDB standard. All results are accurate to better than ±0.15‰ (1σ).

Leeds laboratory: all wood fragments were first crushed with an agate mortar. The obtained powder was placed in a glass jar and acid-washed with HCl 3M overnight to remove carbonates. Samples were rinsed with deionized water until neutrality was reached. Samples were then oven-dried at 50°C. An aliquot of 0.01-0.1 mg of powdered wood was weighed, embedded in tin capsules and analyzed at the stable isotopes Laboratory of the Earth and Environment Department (University of Leeds) with a Micromass Isoprime continous flow mass spectrometer coupled to a Eurovector Elemental Analyser. Results were calibrated using international ANU-sucrose standard and IAEA-CH7 (polyethylene film) to the Vienna-Pee Dee Belemnite (V-PDB) scale in per mil notation (‰). The analytical precision for this analysis is ±0.24‰ (1σ).

2.4 Results

2.4.1 A) First set: Triassic Amber, Wood and Leaves

All the results are shown if Fig. 2.6 and Tab. 2.3. Thirty-nine Julian/Tuvalian (Carnian) amber drops coming from layer NRE103 of Dibona section gave $\partial^{13}C$ values that varied by up to 5.43‰, with a mean $\partial^{13}C$ value of -20.03‰ and a standard deviation of 1.26‰. Amber $\partial^{13}C$ is 2.14‰ heavier on average with respect to wood $\partial^{13}C$ coming from the same stratigraphic layer.

All $\partial^{13}C_{wood}$ values are in the range expected for living C_3 plants. Analyzed wood samples show $\partial^{13}C$ values within any single stratigraphic layer that vary in a range of 1.63‰ (Ladinian SAVI samples) to 2.44‰ (Carnian NRE101-2 samples) and the standard deviations are very similar for all the sampled levels (0.54-0.63‰). Carnian carbon-isotope values of wood are more enriched in ^{13}C compared with those of the Ladinian. Carnian NRE109 wood samples are the heaviest, with a mean $\partial^{13}C_{wood}$ 5.36‰ higher than the Ladinian mean $\partial^{13}C_{wood}$.

As is the case with wood, leaves values lie in the range of living C_3 plants, but show slightly larger $\partial^{13}C$ variability than does wood (ranges of 2.58-2.82‰). The three leaves from Saviner constituted a sample too small to be included in this calculation. Anisian and Carnian $\partial^{13}C_{leaf}$ show

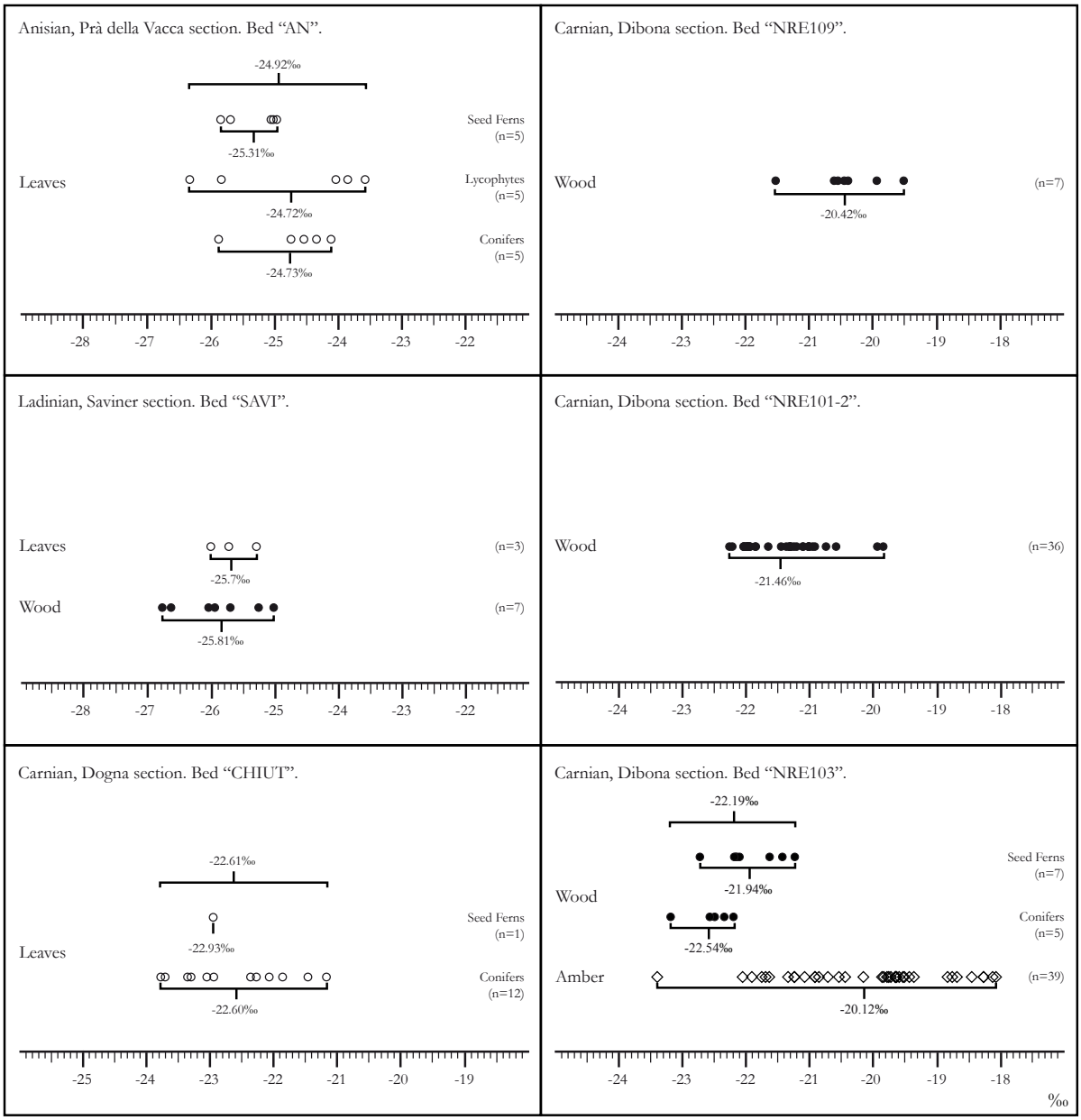

Fig 2.6: stable carbon isotope values, mean values and number of analyzed amber, wood and leaves for each sampled Middle-early Late Triassic stratigraphic bed.

the same standard deviation (0.84-0.85‰), that is larger than that of wood. Ladinian leaves from Saviner show $\partial^{13}C$ values comparable to those of wood in the same bed. Julian (Carnian, lower Upper Triassic) leaves (13 specimens) show higher $\partial^{13}C$ values than the Middle Triassic material: considering mean values, Julian leaves are enriched by 2.31‰ and 3.09‰ with respect to Anisian and Ladinian leaves, respectively.

The $\partial^{13}C$ values of different taxonomic groups are statistically indistinguishable within the same sample.

2.4.2 B) First set: Cretaceous Amber – San Just Deposit

Seven bulk amber samples from San Just were analyzed for their $\partial^{13}C$. This amber show $\partial^{13}C$ values ranging from -21.14‰ to -24.04‰ (Tab 2.2), with a mean of -22.73±0.72‰ (1σ), in the range expected for C_3 plant-derived material. Carbon isotope values of different parts within the same specimen are very homogeneous, as shown for SJU5, SJU6 and SJU8 samples (Tab 2.2).

Tab. 2.3: wood, leaves and amber analyzed for the $\partial^{13}C$, botanical affinity, geological age and sampled sections.

Sample	*Section*	*Geological Age*	*Plant*	*$\partial^{13}C$ (‰)*	*Tissue*
AN 15	Prà della Vacca	Pelsonian (Anisian)	Lycophytes	-24	leaf
AN 04	Prà della Vacca	Pelsonian (Anisian)	Lycophytes	-23.89	leaf
AN 02	Prà della Vacca	Pelsonian (Anisian)	Lycophytes	-26.34	leaf
AN 01	Prà della Vacca	Pelsonian (Anisian)	Lycophytes	-25.83	leaf
AN 03	Prà della Vacca	Pelsonian (Anisian)	Lycophytes	-23.52	leaf
AN 14	Prà della Vacca	Pelsonian (Anisian)	Seed Ferns	-25.7	leaf
AN 12	Prà della Vacca	Pelsonian (Anisian)	Seed Ferns	-24.94	leaf
AN 11	Prà della Vacca	Pelsonian (Anisian)	Seed Ferns	-25	leaf
AN 10	Prà della Vacca	Pelsonian (Anisian)	Seed Ferns	-25.82	leaf
AN 13	Prà della Vacca	Pelsonian (Anisian)	Seed Ferns	-25.09	leaf
AN 08	Prà della Vacca	Pelsonian (Anisian)	Conifers	-24.12	leaf
AN 06	Prà della Vacca	Pelsonian (Anisian)	Conifers	-24.75	leaf
AN 07	Prà della Vacca	Pelsonian (Anisian)	Conifers	-24.58	leaf
AN 09	Prà della Vacca	Pelsonian (Anisian)	Conifers	-24.33	leaf
AN 05	Prà della Vacca	Pelsonian (Anisian)	Conifers	-25.88	leaf
SAVI 101	Savinér	upper Ladinian	Indet.	-26.06	leaf
SAVI 102	Savinér	upper Ladinian	Indet.	-25.01	wood
SAVI 103/1	Savinér	upper Ladinian	Indet.	-25.7	wood
SAVI 103/2	Savinér	upper Ladinian	Indet.	-25.93	wood
SAVI 104	Savinér	upper Ladinian	Indet.	-25.28	wood
SAVI 105	Savinér	upper Ladinian	Indet.	-25.3	leaf
SAVI 106	Savinér	upper Ladinian	Indet.	-26.08	wood
SAVI 107	Savinér	upper Ladinian	Indet.	-26.06	wood
SAVI 108	Savinér	upper Ladinian	Indet.	-25.73	leaf
SAVI 110	Savinér	upper Ladinian	Indet.	-26.64	wood
CHIUT 58 a-9	Dogna	Julian (Carnian)	Conifer	-22.77	leaf

CHIUT 105-1	Dogna	Julian (Carnian)	Conifer	-23.75	leaf
CHIUT 105-2	Dogna	Julian (Carnian)	Conifer	-23.33	leaf
CHIUT 119-13	Dogna	Julian (Carnian)	Conifer	-22.24	leaf
CHIUT 58 a-8	Dogna	Julian (Carnian)	Seed Ferns	-22.93	leaf
CHIUT 62-7	Dogna	Julian (Carnian)	Conifer	-23.3	leaf
CHIUT 75-6	Dogna	Julian (Carnian)	Conifer	-21.81	leaf
CHIUT 76-11	Dogna	Julian (Carnian)	Conifer	-21.17	leaf
CHIUT 76-12	Dogna	Julian (Carnian)	Conifer	-22.32	leaf
CHIUT 81 a-14	Dogna	Julian (Carnian)	Conifer	-22.07	leaf
CHIUT 93-5	Dogna	Julian (Carnian)	Conifer	-21.41	leaf
CHIUT dt12-3	Dogna	Julian (Carnian)	Conifer	-23.73	leaf
CHIUT dt12-4	Dogna	Julian (Carnian)	Conifer	-23.08	leaf
DB 60/01	Dibona	Julian – Tuvalian (Car.)	Indet.	-22.28	wood
DB 60/02	Dibona	Julian – Tuvalian (Car.)	Indet.	-21.93	wood
DB 60/03	Dibona	Julian – Tuvalian (Car.)	Indet.	-21.16	wood
DB 60/04	Dibona	Julian – Tuvalian (Car.)	Indet.	-20.97	wood
DB 60/05	Dibona	Julian – Tuvalian (Car.)	Indet.	-20.92	wood
DB 60/06	Dibona	Julian – Tuvalian (Car.)	Indet.	-20.59	wood
DB 60/07	Dibona	Julian – Tuvalian (Car.)	Indet.	-22.04	wood
DB 60/08	Dibona	Julian – Tuvalian (Car.)	Indet.	-21.14	wood
DB 60/09	Dibona	Julian – Tuvalian (Car.)	Indet.	-21.36	wood
DB 60/10	Dibona	Julian – Tuvalian (Car.)	Indet.	-21.29	wood
DB 60/11	Dibona	Julian – Tuvalian (Car.)	Indet.	-21.38	wood
DB 60/12	Dibona	Julian – Tuvalian (Car.)	Indet.	-21.88	wood
DB 60/13	Dibona	Julian – Tuvalian (Car.)	Indet.	-22	wood
DB 60/14	Dibona	Julian – Tuvalian (Car.)	Indet.	-22.05	wood
DB 60/15	Dibona	Julian – Tuvalian (Car.)	Indet.	-21.33	wood
DB 60/16	Dibona	Julian – Tuvalian (Car.)	Indet.	-22.02	wood
DB 60/17	Dibona	Julian – Tuvalian (Car.)	Indet.	-22.06	wood
DB 60/18	Dibona	Julian – Tuvalian (Car.)	Indet.	-21.09	wood
DB 60/19	Dibona	Julian – Tuvalian (Car.)	Indet.	-21.25	wood
DB 60/20	Dibona	Julian – Tuvalian (Car.)	Indet.	-21.25	wood
DB 60/21	Dibona	Julian – Tuvalian (Car.)	Indet.	-21.27	wood
DB 60/22	Dibona	Julian – Tuvalian (Car.)	Indet.	-21.98	wood
DB 60/23	Dibona	Julian – Tuvalian (Car.)	Indet.	-22.06	wood
DB 60/24	Dibona	Julian – Tuvalian (Car.)	Indet.	-19.89	wood
DB 60/25	Dibona	Julian – Tuvalian (Car.)	Indet.	-19.96	wood
DB 60/26	Dibona	Julian – Tuvalian (Car.)	Indet.	-21.95	wood
DB 60/27	Dibona	Julian – Tuvalian (Car.)	Indet.	-22.04	wood
DB 60/28	Dibona	Julian – Tuvalian (Car.)	Indet.	-21.19	wood
DB 60/29	Dibona	Julian – Tuvalian (Car.)	Indet.	-22.33	wood
DB 60/30	Dibona	Julian – Tuvalian (Car.)	Indet.	-20.74	wood
NRE 101-2(1)	Dibona	Julian – Tuvalian (Car.)	Indet.	-21.91	wood
NRE 101-2(2)	Dibona	Julian – Tuvalian (Car.)	Indet.	-21.32	wood
NRE 101-2(3)	Dibona	Julian – Tuvalian (Car.)	Indet.	-21	wood
NRE 101-2(4)	Dibona	Julian – Tuvalian (Car.)	Indet.	-21.46	wood
NRE 101-2(5)	Dibona	Julian – Tuvalian (Car.)	Indet.	-21.89	wood
NRE 101-2(6)	Dibona	Julian – Tuvalian (Car.)	Indet.	-21.67	wood
NRE 109/1	Dibona	Julian – Tuvalian (Car.)	Indet	-20.6	wood
NRE 109/2	Dibona	Julian – Tuvalian (Car.)	Indet	-19.5	wood
NRE 109/3	Dibona	Julian – Tuvalian (Car.)	Indet	-21.52	wood
NRE 109/4	Dibona	Julian – Tuvalian (Car.)	Indet	-20.54	wood
NRE 109/5	Dibona	Julian – Tuvalian (Car.)	Indet	-20.39	wood
NRE 109/6	Dibona	Julian – Tuvalian (Car.)	Indet	--20.45	wood
NRE 109/7	Dibona	Julian – Tuvalian (Car.)	Indet	-19.92	wood
NRE 103 50	Dibona	Julian – Tuvalian (Car.)	Seed Ferns	-22.19	wood
NRE 103 51	Dibona	Julian – Tuvalian (Car.)	Seed Ferns	-22.17	wood

NRE 103 51 b	Dibona	Julian – Tuvalian (Car.)	Seed Ferns	-22.19	wood
NRE 103 52 a	Dibona	Julian – Tuvalian (Car.)	Seed Ferns	-21.23	wood
NRE 103 54	Dibona	Julian – Tuvalian (Car.)	Seed Ferns	-21.62	wood
NRE 103 54 b	Dibona	Julian – Tuvalian (Car.)	Seed Ferns	-22.75	wood
NRE 103 54 c	Dibona	Julian – Tuvalian (Car.)	Seed Ferns	-21.45	wood
NRE 103 60	Dibona	Julian – Tuvalian (Car.)	Conifer	-22.32	wood
NRE 103 60 b	Dibona	Julian – Tuvalian (Car.)	Conifer	-23.2	wood
NRE 103 60 c	Dibona	Julian – Tuvalian (Car.)	Conifer	-22.11	wood
NRE 103 61	Dibona	Julian – Tuvalian (Car.)	Conifer	-22.51	wood
NRE 103 61 b	Dibona	Julian – Tuvalian (Car.)	Conifer	-22.56	wood
NRE 103 A 01	Dibona	Julian – Tuvalian (Car.)	Conifer	-19.55	amber
NRE 103 A 02	Dibona	Julian – Tuvalian (Car.)	Conifer	-21.29	amber
NRE 103 A 03	Dibona	Julian – Tuvalian (Car.)	Conifer	-21.72	amber
NRE 103 A 04	Dibona	Julian – Tuvalian (Car.)	Conifer	-19.52	amber
NRE 103 A 05	Dibona	Julian – Tuvalian (Car.)	Conifer	-19.63	amber
NRE 103 A 06	Dibona	Julian – Tuvalian (Car.)	Conifer	-23.48	amber
NRE 103 A 07	Dibona	Julian – Tuvalian (Car.)	Conifer	-21.73	amber
NRE 103 A 08	Dibona	Julian – Tuvalian (Car.)	Conifer	-20.91	amber
NRE 103 A 09	Dibona	Julian – Tuvalian (Car.)	Conifer	-21.09	amber
NRE 103 A 10	Dibona	Julian – Tuvalian (Car.)	Conifer	-18.77	amber
NRE 103 A 11	Dibona	Julian – Tuvalian (Car.)	Conifer	-20.54	amber
NRE 103 A 12	Dibona	Julian – Tuvalian (Car.)	Conifer	-22.05	amber
NRE 103 A 13	Dibona	Julian – Tuvalian (Car.)	Conifer	-18.49	amber
NRE 103 A 14	Dibona	Julian – Tuvalian (Car.)	Conifer	-19.82	amber
NRE 103 A 15	Dibona	Julian – Tuvalian (Car.)	Conifer	-18.29	amber
NRE 103 A 16	Dibona	Julian – Tuvalian (Car.)	Conifer	-21.37	amber
NRE 103 A 17	Dibona	Julian – Tuvalian (Car.)	Conifer	-21.67	amber
NRE 103 A 18	Dibona	Julian – Tuvalian (Car.)	Conifer	-19.75	amber
NRE 103 A 19	Dibona	Julian – Tuvalian (Car.)	Conifer	-20.41	amber
NRE 103 A 20	Dibona	Julian – Tuvalian (Car.)	Conifer	-18.29	amber
NRE 103 A 21	Dibona	Julian – Tuvalian (Car.)	Conifer	-21.21	amber
NRE 103 A 22	Dibona	Julian – Tuvalian (Car.)	Conifer	-18.85	amber

Moreover, $\partial^{13}C$ analyses performed on the external altered portion and on the fresh nucleus of single specimens (SJU6 and SJU8) show no significant differences in the carbon-isotope signature (Fig 2.7).

2.4.3 C) First set: Cretaceous Amber - all other localities

All results are summarized in Tab 2.2 and Fig 2.5. $\partial^{13}C_{amber}$ ranges from -17‰ to -24‰ and spans the heaviest part of the C_3 plant range. $\partial^{13}C$ data of amber with no overlapping ages (see Fig 2.12, red points) and already published $\partial^{13}C$ data of cretaceous amber (see origin and references in Tab 2.4) were plotted to build an amber-based C-isotope curve for the Cretaceous. Data were fitted using a Stineman (1980) function: the output is a geometric weigh applied to the given datapoint and ±10% of the data range in order to obtain a smooth curve. The smoothed curve shows an ~1‰ positive trend during the Valanginian-Aptian interval and a two-steps ~5‰ negative

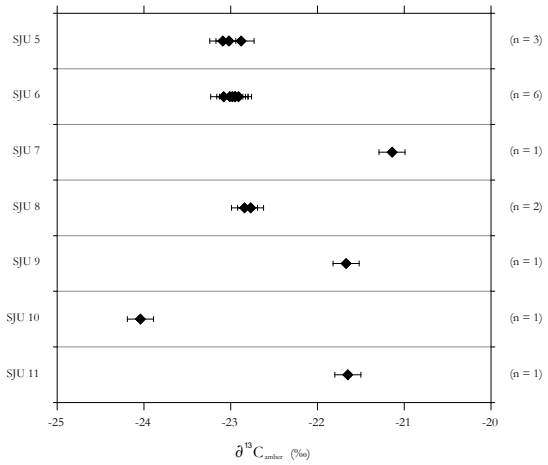

Fig 2.7: stable carbon isotope values of different amber drops from the San Just deposit. Note that multiple analyses of different parts of the same fossil resin show no significant differences (e.g. SJU6).

shift from the early Albian to the Maastrichtian. During the Albian stage and in the Santonian-Campanian interval, $\partial^{13}C_{amber}$ shows two big negative steps. Early Albian amber has a mean $\partial^{13}C$ value enriched in ^{13}C by 3-4‰ with respect to mid Albian fossil resins and Santonian amber is enriched by ~3‰ than Maastrichtian one.

2.4.4 Second set: Triassic Wood

All the results are shown if Fig. 2.8 and Tab 2.5. 130 coalified/charcoalified wood fragments have been analyzed for C-isotopes. All $\partial^{13}C$ are in the range expected for C_3 plants. Coalified wood $\partial^{13}C$ vary within the same stratigraphic beds in a range of 0.94‰ (DJ22) to 3.4‰ (STU104) (mean range: 1.63‰) (standard deviations: 0.33-0.87‰). Charcoal $\partial^{13}C$ from 3 stratigraphic levels has ranges between 1 to 3.3‰. Charcoalified and coalified wood from STU104 bed are offset by 1.5‰, being mean $\partial^{13}C_{coal}$ depleted with respect to mean $\partial^{13}C_{charcoal}$. Charcoal and coal from DJ4 bed doesn't show any sensible difference (Fig 2.8).

2.5 Discussion

2.5.1 C-isotope variability of amber, wood and leaves

Triassic amber $\partial^{13}C$ is enriched with respect to that of leaves and wood, with values in a wide range (~5‰), spanning the heaviest part of the range expected for living C_3 plants. Few authors have explored the amber carbon-isotope variability within a set of samples of the same age. McKellar et al. (2008) reported similar large ranges for Upper Cretaceous Cedar Lake and Grassy Lake ambers

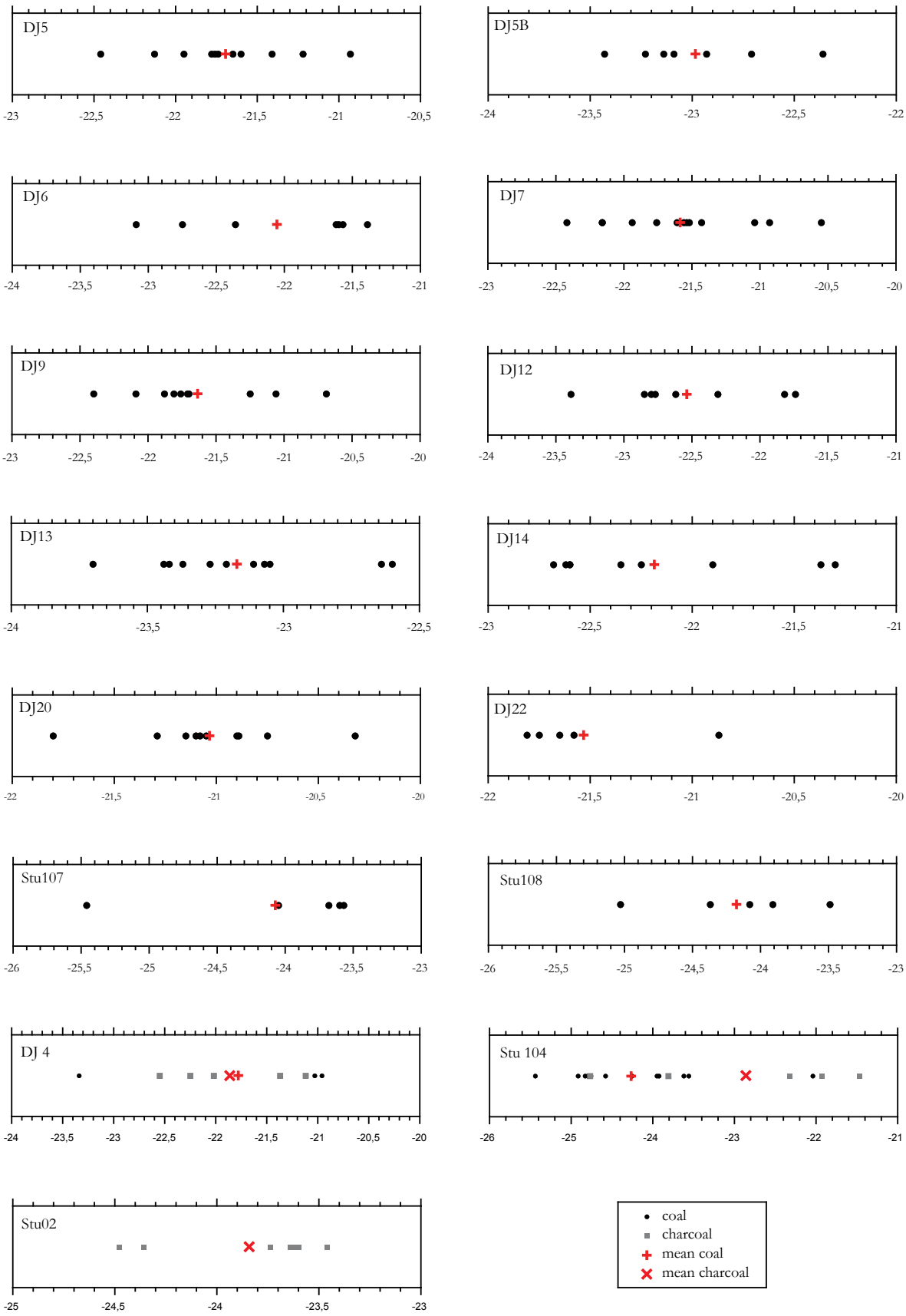

Fig 2.8: stable carbon isotope values and mean values (red cross) of coalified and charcoalified wood form the Ladinian-Carnian Stuores Wiesen section (STU samples) and Carnian Dibona-Milieres section (DJ).

Sample	*$\partial^{13}C$ max (‰)*	*$\partial^{13}C$ min (‰)*	*Range (‰)*	*StDev (‰)*	*N*	*Preservation*
SAVI	-25.01	-26.64	1.63	0.54	7	Coal
STU 107	-23.57	-25.46	1.89	0.80	5	Coal
STU 108	-23.49	-25.03	1.54	0.57	5	Coal
STU 104	-22.04	-25.44	3.40	0.87	13	Coal
DJ 5	-20.93	-22.46	1.53	0.41	10	Coal
DJ 5B	-22.36	-23.43	1.07	0.36	7	Coal
DJ 6	-21.39	-23.09	1.70	0.67	7	Coal
DJ 7	-20.55	-22.42	1.87	0.53	13	Coal
DJ 9	-20.69	-22.40	1.71	0.50	10	Coal
DJ 12	-21.74	-23.39	1.65	0.56	8	Coal
DJ 13	-22.60	-23.70	1.10	0.33	11	Coal
DJ 14	-21.30	-22.68	1.38	0.54	9	Coal
DJ 20	-20.32	-21.80	1.48	0.38	10	Coal
DJ 22	-20.87	-21.81	0.94	0.38	5	Coal
NRE 101	-19.89	-22.33	2.44	0.60	36	Coal
NRE 103	-21.23	-23.20	1.97	0.56	12	Coal
NRE 109	-19.50	-21.52	2.02	0.63	7	Coal
STU 104	-21.47	-24.77	3.30	1.38	5	Charcoal
STU 02	-23.46	-24.48	1.02	0.40	7	Charcoal
DJ 4	-21.12	-22.55	1.43	0.60	5	Charcoal

Tab. 2.5: $\partial^{13}C$ minimum, $\partial^{13}C$ maximum, ranges, standard deviation, number of wood fragments analyzed (N) and preservation of Ladinian-Carnian analyzed wood.

(Tab 2.4). The data of Nissenbaum and Yakir (1995) show much narrower ranges: 1.1‰ for the Lower Cretaceous Mt. Hermon amber (n=5) and 2.5‰ for Cedar Lake amber (n=5). These narrow ranges, however, need confirmation, due to the small number of specimens analyzed (McKellar et al., 2008). With regard to living plants, $\partial^{13}C$ data from conifer resins from the Sydney Botanical Gardens (Australia) have a range of 4.2‰ with a standard deviation of 1.5‰ (Murray et al., 1998). Stern et al. (2008) analyzed recent *Pinus* resins collected from different localities in the UK over a range of altitudes, finding high resin $\partial^{13}C$ variability within the same tree, between trees sampled at the same and different locations and between different plant species, with the higher dispersion for resins belonging to different species growing in the same locality (Tab 2.6). Recent resins show also a general decrease of ^{13}C with increasing altitude, which is in contrast with the shift to higher values with increasing altitude and latitude observed for leaves (e.g.: Körner et al., 1991, Stern et al., 2008), and their $\partial^{13}C$ range becomes more and more large if we consider together different localities sampled at different altitudes in the same area or different *Pinus* species (Stern et al., 2008). Such a pattern could be reasonably linked to the effect that very local environmental conditions have in plant carbon-isotope signature.

Rif. Dibona $\partial^{13}C_{amber}$ variability refers to amber drops produced by a resin-producing plant species belonging to the extinct Cheirolepidiaceae conifer family, as it has been shown by physico-chemical

Age	*∂13C (‰) StDev*	*N*	*Provenance*	*References*
Carnian	1.26	39	Dibona Amber (Southern Alps, Italy)	This study
Campanian	1.35	28	Grassy Lake Amber (Canada)	McKellar *et al.*, 2008
Campanian	1.31	12	Cedar Lake Amber (Canada)	McKellar *et al.*, 2008
Recent	0.40	8	Single tree (*Pinus silvestris*): resin collected over one year	Stern *et al.*, 2008
Recent	1.51	7	Various conifers from Sydney Botanical Gardens (Austalia)	Murray *et al.*, 1998
Recent	1.10	8	*Pinus silvestris* resin from the same location (UK)	Stern *et al.*, 2008
Recent	2.10/2.30	5	Different *Pinus* species resin from tha same location (UK)	Stern *et al.*, 2008
Recent	1.40	10	*Pinus nigra* resin from different locations (UK)	Stern *et al.*, 2008
Recent	1.50	16	*Pinus silvestris* resin from different locations (UK)	Stern *et al.*, 2008

Tab. 2.6: ∂13C standard deviations, number of specimens analyzed and provenance of fossil and recent resins data from literature and this study. Note: standard deviations of published data were calculated here if not already estimated.

analyses and palaeobotanical/palynological studies (Ragazzi et al., 2003; Roghi et al., 2006; Breda et al., 2009). The variability of $\partial^{13}C_{amber}$ can be compared with that of recent *Pinus sylvestris* and *Pinus nigra* resins (Stern et al., 2008) (Tab. 2.6). The 1.26‰ standard deviation of our data compares well also to that of Grassy Lake (Cretaceous; McKellar et al., 2008) derived from a similar number of amber drops (Tab 2.6).

Carnian amber has $\partial^{13}C$ ~2.5‰ heavier than conifer wood fragments within the same bed. A similar offset was observed for Upper Cretaceous gymnosperm-derived coals and associated resinites (+2.6‰) (Murray et al., 1998). Carbon-isotope analyses of Tertiary coal deposits show that diterpenoids and sesquiterpenoids, major components of gymnosperm fossil resin, are enriched by 1-2‰ compared with bulk coals, whereas triterpenoids coming from plant epicuticular waxes are depleted by 1-2‰ compared with the same bulk coals (Schoell et al., 1994), suggesting that some fractionation process also takes place during the biosynthesis of resin terpenoids, causing a ^{13}C enrichment. The observed offset could be also amplified by the taphonomical processes that shift $\partial^{13}C$ of bulk wood to relatively more depleted values, as discussed above (van Bergen and Poole 2002; Poole et al., 2006).

Variability of Middle and lower Upper Triassic wood and leaf $\partial^{13}C$ within the same beds is narrower than that of amber. Coalified wood $\partial^{13}C$ ranges are within ~0.9-3.4‰ (mean 1.6‰). Leaves, excluding the three Ladinian samples, have ranges of ~2.5-2.8‰. Bulk coalified wood $\partial^{13}C$ values have a standard deviation of 0.3-0.8‰ within any single analyzed layer (Tab 2.5), and the Anisian and Carnian leaves have a standard deviation of 0.8‰, both smaller than Triassic amber (1.3‰). Charcoalified wood have ranges of 1-3.3‰ and standard deviations of 0.4-1.4‰. Ranges for wood are in agreement with other data from Mesozoic sediments that show differences in the

$\partial^{13}C$ between wood fragments from the same beds up to 2‰ (Hesselbo et al., 2007 and references therein). New analyses on wood from a Cretaceous alluvial-plain deposit, however, exhibit $\partial^{13}C_{wood}$ range of variability reaching 7.3‰ with a standard deviation of 1.4‰ (Yans et al., 2010). This higher variability has been explained by taxonomic variations, type of preservation of woody fragments (charcoal and coal) and reworking of the analyzed material (Yans et al., 2010).

Carbon-isotope variability of Triassic wood and leaves is narrower than it would be expected from observation of recent plant tissues. Some Carnian wood from Rifugio Dibona was found in paleosols that should have collected plant remains that experienced only short transport, i.e. plants growing in a restricted area within the same environmental conditions (samples NRE101, NRE103, NRE109). In contrast, material from the others beds at Dibona, Dogna, Prati di Stuores, Saviner and Monte Prà della Vacca presumably derived from a larger hinterland and reflects heterogeneous plant communities growing in different environments or ecosystems. Modern plant tissues present highly variable carbon-isotope signatures within the same individual, between different individuals of the same species, and between different species living in the same or different environmental conditions: e.g., $\partial^{13}C$ values of the evergreen conifer *Pinus monticola*, measured on branch wood and leaves and sampled at different heights in the crown, lie in a range of 4-5‰ (Cernusak et al., 2009). The reduced variability of Triassic fossil wood and leaves could be explained by selective degradation of plant OM during fossilization. Taphonomical processes narrow the carbon-isotope variability of bulk plant tissues and move to more depleted values their $\partial^{13}C$ due to the selective removal of plant compounds that have a different $\partial^{13}C$ signature (see Fig. 1 in van Bergen and Poole (2002) for a schematic representation of this process). The $\partial^{13}C$ variability of wood and leaves could also reflect a pristine narrow carbon-isotope variability of the studied Triassic plant community. However, amber $\partial^{13}C$ range of values, larger than that of the associated wood, testify for an original high variability, as that observed in recent material. This is possible due to a less diagenetic overprint of amber. Resin starts to lose water and monoterpene hydrocarbons after plant exudation, whereas non-volatile terpene components polymerize very rapidly, within hours or days, entrapping also non-polymerizable molecules. Structural changes do occur during the (not yet fully understood) resin maturation process (Lambert et al., 2008), but we can reasonably hypothesize that amber maturation does not affect the carbon-isotope composition of bulk resin,

because the carbon pool in which these molecular changes take place remains constant with no selective removal of compounds, i.e., the system becomes closed for carbon soon after exudation. Though, whatever is the diagenetic effect on amber chemistry, large range of $\partial^{13}C_{amber}$ values seems to reflect a pristine high variability as observed in recent material and thus Carnian amber of Rif. Dibona should faithfully retain their original carbon-isotope signature. Furthermore, the C-isotope composition of separated pieces of the same Cretaceous amber drop (San Just deposit)

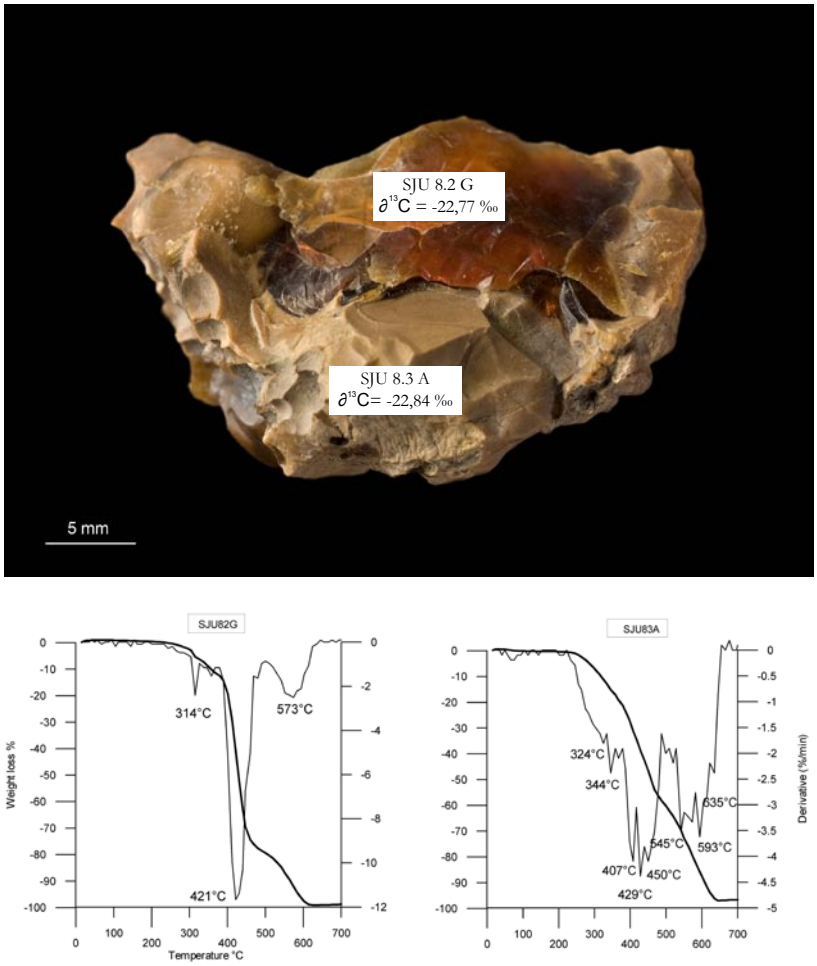

Fig 2.9: stable carbon isotope values and thermogravimetric profiles of the altered and fresh portions of SJU8 amber drop from San Just deposit.

is very homogeneous, both between fresh fragments and fresh and altered parts (Fig 2.7 and Tab 2.2). Thermogravimetric profiles of altered and fresh portions of the same amber (Fig 2.9) show that alteration caused important transformations of the main components (E. Ragazzi and A. Giaretta personal communication). These deep transformations however didn't affect the carbon-isotope composition of analyzed amber as there are no significant differences in the $\partial^{13}C$ signature

of altered and fresh portions of the same amber specimen (Tab 2.2), suggesting that during the alteration process the system is closed for carbon. Cretaceous San Just Amber C-isotope data coupled with thermogravimetric analyses strongly support the hypothesis that fossil resin has a high attitude to retain its carbon-isotope signature even if altered.

Effects of charcoalification on modern wood $\partial^{13}C$ have been extensively studied in charring lab experiments (Jones and Chaloner, 1991; Czimczik et al., 2002; Ferrio et al., 2006; Hall et al., 2008). A general ^{13}C-enrichment of bulk wood at low temperatures (150-300 °C), probably linked to the loss of more depleted lipids (Czimczik et al., 2002), and a ^{13}C-depletion at higher temperatures (<300 °C), mainly due to the loss of the isotopically heavier cellulose and a relative enrichment in lignin, that has more depleted $\partial^{13}C$ values, have been observed. Despite these changes, charcoal seems to retain the original C-isotope signal and thus can be successfully used as chemostratigraphic proxy (Hesselbo et al. 2000; Gröcke 2002; Hesselbo et al., 2003). The +1,5‰ offset between the C-isotope signature of Triassic Stu104 charcoalified and coalified wood is hard to explain by only differences in preservation. The processes that change the C-isotope signature of wood during charring are substantially equal to the taphonomical processes that take place during the burial of wood, i.e., selective removal of compounds. The result is a wood more and more enriched in lignin-derived carbon. Moreover, Triassic charcoal must have experienced the same diagenetic history as coalified wood, since they were found mixed in the same stratigraphic bed. Diagenesis can thus have obliterated the differences in the $\partial^{13}C$ of charred and non-charred wood before coalification. DJ4 wood (Fig 2.8) and other Mesozoic published data (e.g.: Yans et al., 2010) show a similar average $\partial^{13}C$ for charcoal and coal. Stu104 charcoal vs coal offset could be explained as a pristine signal. Maybe charcoal was transported to the depositional environment from an area that experienced fires and was different from the source area of associated wood preserved as coal. Local environmental conditions of the distinct source areas could have determined changes in C-isotope fractionation during the photosynthesis that resulted in a different average $\partial^{13}C_{plant}$ signature.

2.5.2 The Middle – early Late Triassic $\partial^{13}C_{plant}$ trend

Plant $\partial^{13}C$ data register a shift of the organic carbon isotopes of about +3-5‰ between the Middle

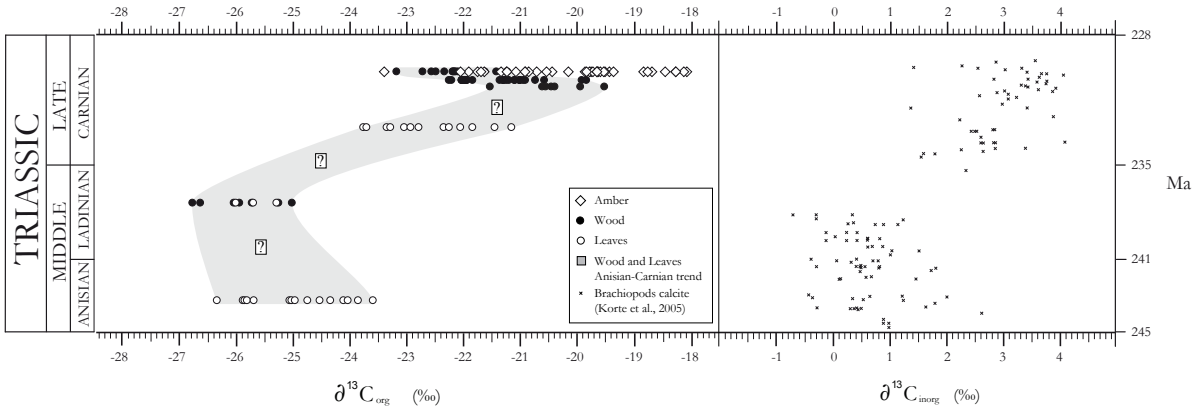

Fig. 2.10: Middle-early Late Triassic carbon isotope trend. On the left, $\partial^{13}C_{org}$ values of wood, leaves and amber; on the right, $\partial^{13}C_{inorg}$ measured on brachiopods calcite by Korte et al. (2005). Absolute ages according to Walker and Geissman (2009).

and the lower Upper Triassic (Fig. 2.10 and Fig 2.11). Julian leaves are enriched by +2-3‰ with respect to Middle Triassic material (Fig 2.10) and at the Julian/Tuvalian boundary wood is shifted by +4-5‰ with respect to the more depleted Ladinian wood (Fig 2.10 and 2.11). Terrestrial plant organic $\partial^{13}C$ data illustrate a positive trend during Anisian-Julian/Tuvalian time that is consistent with inorganic carbonate carbon-isotope data from brachiopods and whole-rock, that shows a rise of 3.5‰ from the late-Middle Triassic to the Carnian (Korte et al., 2005) (Fig. 2.10). This secular shift has been interpreted as due to the re-emergence of coal-swamps and peatlands, and increasing organic-carbon burial after the Permo-Triassic crisis and the early Triassic carbon-cycle instability (Korte et al., 2005). Despite the $\partial^{13}C$ variability within a set of samples of the same age, Triassic wood and leaf $\partial^{13}C$ manifestly record secular carbon-isotope variations in the ocean-atmosphere system. Moreover, this parallel trend suggests that Triassic brachiopod calcite and marine carbonates faithfully registered the secular carbon-isotope evolution of the ocean–atmosphere system.

2.5.3 $\partial^{13}C_{amber}$ trends in the Cretaceous

Building an amber-based C-isotope curve requires to overcome some problems. The first problem is the scarcity of amber throughout the geological record. Often, if not always, amber is localized in one or very few stratigraphic beds within a single section (e.g. Triassic amber of the Dolomites, see chapter 3.1.1.1). For this reason, the resolution of $\partial^{13}C_{amber}$ data would be very poor or it couldn't be possible to build any $\partial^{13}C$ time series for a single section. The second problem is the age of amber deposits. Amber-bearing sediments are mostly coal seams and swamp deposits that

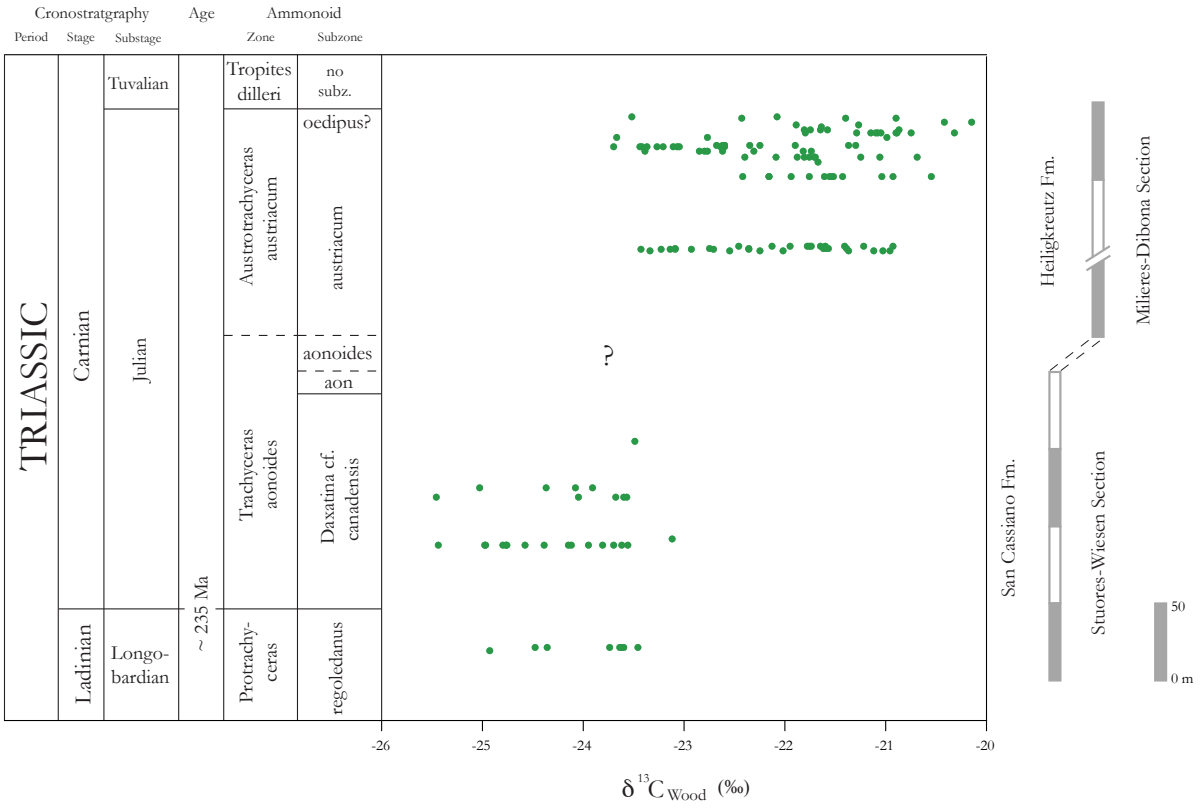

Fig. 2.11: Ladinian-Carnian $\partial^{13}C_{wood}$ trend.

are roughly dated, sometimes with an age uncertainty of several millions of years (see Tab 2.2 and Fig 2.5).

Taking these problems into account, I tried to build a $\partial^{13}C_{amber}$ curve for the Cretaceous analyzing the C-isotope composition of amber coming from several Cretaceous deposits and using existing published data. Amber deposits with age overlaps were excluded to minimize the biases introduced by age uncertainty on curve fitting.

Comparing our data with a composite $\partial^{13}C$ carbonate curve redrawn after Föllmi et al. (2006) and Jarvis et al. (2006) (Fig 2.12) the $\partial^{13}C_{amber}$ fitting curve parallels well the positive secular trend of the inorganic C-isotope from the Valanginian-Hauterivian to the latest Aptian, the ^{13}C depletion during the Albian after the Oceanic Anoxic Event 1b (OAE 1b) and the $\partial^{13}C$ decrease from the Santonian to the Maastrichtian. $\partial^{13}C_{amber}$ data resolution do not allow to detect the numerous OAEs shifts throughout the Cretaceous and to compare the magnitude of $\partial^{13}C_{amber}$ secular shifts *versus* carbonate C-isotopes shifts.

Despite the described great problems, amber can register the major global C-isotope trends in the

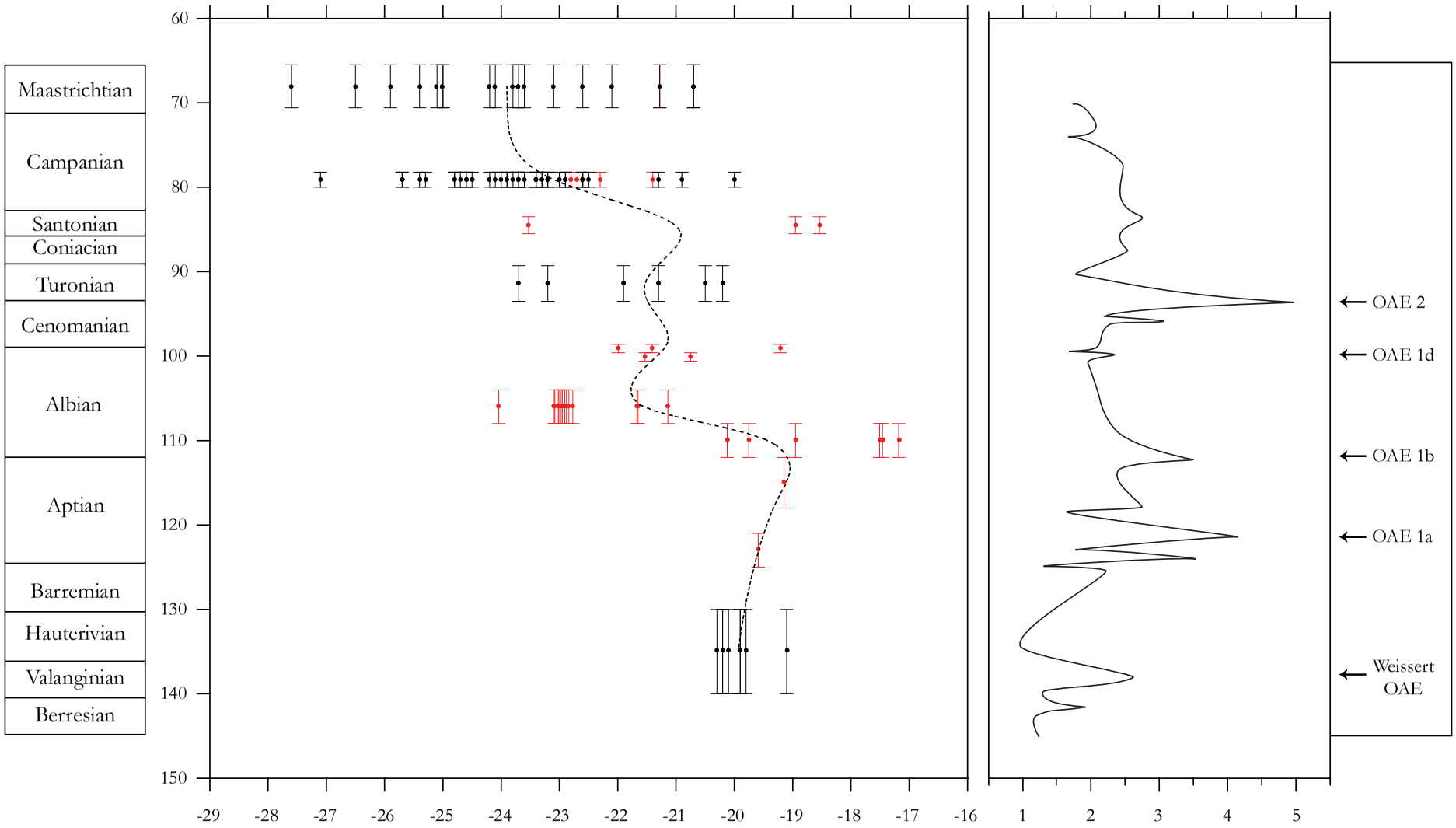

Fig. 2.12: Cretaceous ∂13Camber trend compare to ∂13Cinorg composite curve redrawn after Jarvis et al. (2006) and Föllmi et al. (2006).

ocean/atmosphere system. However, better constrain the age of Cretaceous amber-bearing deposits is the first priority to make amber a factual and useful proxy for chemostratigraphic studies.

2.6 Conclusions

Triassic amber, wood and leaf $\partial^{13}C$ values lie in a large range within the same beds (~ 2-5‰). Carnian ambers have $\partial^{13}C$ values similar to the associated wood but with a larger range of variability than wood and leaves. These restricted wood and leaf $\partial^{13}C$ ranges can be explained by selective degradation of plant OM during the fossilization processes. Despite the high variability, wood and leaf $\partial^{13}C$ values register a positive trend between the Middle and early Late Triassic that is consistent with existing marine inorganic carbon-isotope data from skeletal calcite. This parallel trend suggests that Triassic brachiopod calcite and marine carbonates faithfully registered the secular carbon-isotope evolution of the ocean–atmosphere system.

The range of values in Triassic amber $\partial^{13}C$ is comparable with that obtained for recent resins. Thermogravimetric analyses coupled with C-isotope measurements show that alteration processes doesn't change the $\partial^{13}C$ of amber even if it caused important transformations of the main components. Data suggest that the pristine carbon-isotope signature is not altered by resin maturation during diagenesis, unlike other plant-derived materials as wood and leaves.

Cretaceous $\partial^{13}C_{amber}$ data register secular trends consistent with inorganic carbonate C-isotopes data. Our results show that amber is potentially a very solid tool for C-isotopes – based studies with palaeoenvironmental, palaeoclimatic and stratigraphic purposes. However, the age of amber deposits must be better constrained than it is currently done.

3. BIOMARKER ANALYSES

3.1 ∂^{13}C of plant-derived n-alkanes

Biomarker analyses have become more and more common in a number of geoscience studies, from deep Precambrian time to Holocene, and their isotope study, namely the compound-specific isotope analysis (CSIA), is a relatively new frontier with an high potential for palaeoecology and palaeoclimatology. CSIA allows to study the C-isotope composition of single compounds dispersed into the sediments as they elute from a Gas-Chrometographer (GC). This technique is obviously crucial to overcome problems concerning the source of analyzed material. Bulk OM isotope analysis has a number of problems due to the uncertainty upon its composition (i.e. marine vs terrestrial content, terrestrial and marine OM composition, etc...). As described in chapter 2, it has been shown that changes in OM composition of analyzed samples can explain some negative and positive ∂^{13}C shifts in the geological record (e.g. van de Schootbrugge et al. 2008) deeply biasing global C-cycle and climate studies. CSIA permits to have a higher control on what it is measured for C-isotope and to support bulk OM ∂^{13}C data.

N-alkanes (normal alkanes) are straight-chain saturated hydrocarbons (Fig 3.1). Short chain n-alkanes (n-C_{15} – n-C_{19}) are mostly synthesized by marine algae, whereas normal alkanes with chain

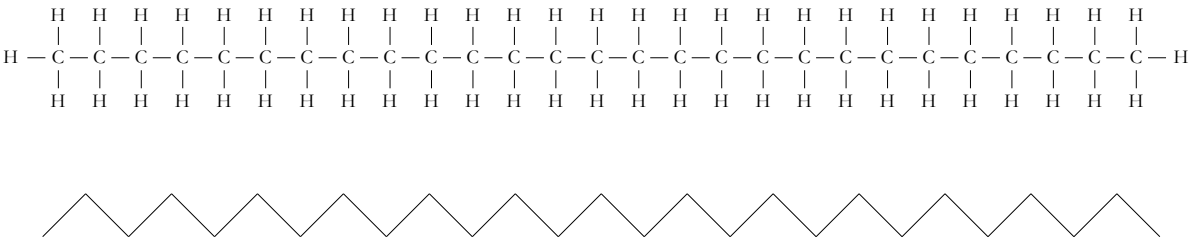

Fig. 3.1: C_{27} n-alkane molecular formulas.

lengths of n-C_{25} - n-C_{35} and odd-over-even carbon-number distribution derive from epicuticular waxes of terrestrial higher plants (Peters et al., 2005). These lipids are common in both marine and continental sediments and relatively resistant to diagenesis (Pancost and Boot, 2004). Their C isotope signature has been successfully used to study $\partial^{13}C$ shifts associated with major events such as the P/T mass extinction (Xie et al., 2007) or the Paleocene/Eocene Thermal Maximum (Pagani et al., 2006; Smith et al., 2007; Handley et al., 2008); to determine the advent of the C4 photosynthetic pathway (Freeman and Colarusso, 2001; Tipple and Pagani, 2007); or to study the relative proportions of C3 and C4 plant material in sediments (Pancost & Boot, 2004, and references therein). $\partial^{13}C$ analysis of n-alkanes partially overcomes issues associated with the large $\partial^{13}C$ range in plants (see chapter 2) as they pool together the contribution of numerous individual plants. Thus, higher plant n-alkanes can be the perfect substrate to infer atmospheric CO_2 C-isotope composition and changes.

We studied the C-isotope signature of n-alkanes extracted from rock samples collected from three sections of Southern Alps in order to build a biomarker-based $\partial^{13}C$ curve for the Ladinian – Carnian interval (Middle-Late Triassic). The $\partial^{13}C$ of n-alkanes has been compared with that of total organic carbon (TOC).

3.2 Sampled Sections

Location of the studied sections is given in Fig. 2.2. All the collected samples are shales without carbonaceous inclusions and any evidence of superficial alteration. Samples were taken 50 centimeters below the exposed surface in order to minimize the possible contamination by recent organic compounds.

Prati di Stuores section is located in the Dolomites (Southern Alps) and it is the GSSP type section for the base of the Carnian (Mietto et al., 2007; 2008). The section encompasses a series of hemipelagites and thin turbidite beds belonging to the San Cassiano Formation and deposited in a rapidly infilling basin under some hundreds of meter of water depth. The section was very well dated by ammonoids, conodonts and palynomorphs.

Milieres-Dibona section lies within the *A. austriacum* ammonoid biochronozone (uppermost lower Carnian) and encompasses a succession of marls, limestone and sandstone belonging to the

Heiligkreuz Formation and deposited in a prodelta - coastal to paralic environment.

3.3 Methods

3.3.1 Samples preparation

Biomarker analysis was performed at the School of Chemistry (University of Bristol) in collaboration with Prof. Richard Pancost (Organic Geochemistry Group).

Sediments were carefully cleaned to remove superficial impurities, and oven-dried. Then clean nuclei of rock samples were ground using a pestle and mortar. The sediments were then extracted using a Soxhlet apparatus (2:1 DCM:MeOH) followed by solid-phase extraction in a rotary evaporator. The resultant total lipid extract was fractionated (into neutral and acid residues) using aminopropyl bond-elut columns (solvents: DCM/iPA 2:1, MeOH and 2% acetic acid in ether). Neutral dry residues were fractionated in a Pasteur pipette packed with alumina and n-hexane/DCM 9:1 and DCM/MeOH 1:2 as eluents.

The obtained apolar and polar fractions in hexane and DCM:MeOH, respectively, were analysed by GC and GC-MS, with the polar fraction undergoing Trimethylsilyl (TMS) derivatisation prior to GC and GC-MS analysis. The acid fraction underwent saponification, acidification and TMS methylation prior to GC and GC-MS analysis.

The apolar fraction was then analyzed for carbon isotopes with an GC-IRMS.

The carbon isotope signature of TOC was analyzed at the Stable Isotope Laboratory, University of Leeds, in collaboration with Dr. Robert Newton and Prof. Paul Wignall. Rock powders were first acid-washed in 10% HCl overnight to remove carbonates, then washed in distilled water and oven-dried. Obtained powder was weighted into tin cups. Organic carbon isotopic analyses were performed on a Micromass Isoprime continous flow mass spectrometer coupled to a Eurovector Elemental Analyser.

3.3.2 Maturity parameters

Maturity biomarker and non-biomarker parameters have been calculated for all the analyzed samples.

Non-biomarker maturity parameter, namely the carbon preference index (CPI), was calculated

from the TIC (Total Ion Current) (Fig 3.2). Biomarker maturity parameters, C_{27} Ts/(Ts+Tm), C_{31} 22S/(22S+22R) homopane and C_{30} moretane/hopane (C30 βα/αβ) ratios, were calculated using m/z 191 chromatograms (Fig 3.2).

The carbon preference index (CPI) was calculated for n-C_{25} – n-C_{31} n-alkanes following the equation:

$$CPI = [((C_{25}+C_{27}+C_{29})/(C_{26}+C_{28}+C_{30}))+((C_{27}+C_{29}+C_{31})/(C_{26}+C_{28}+C_{30}))]/2$$

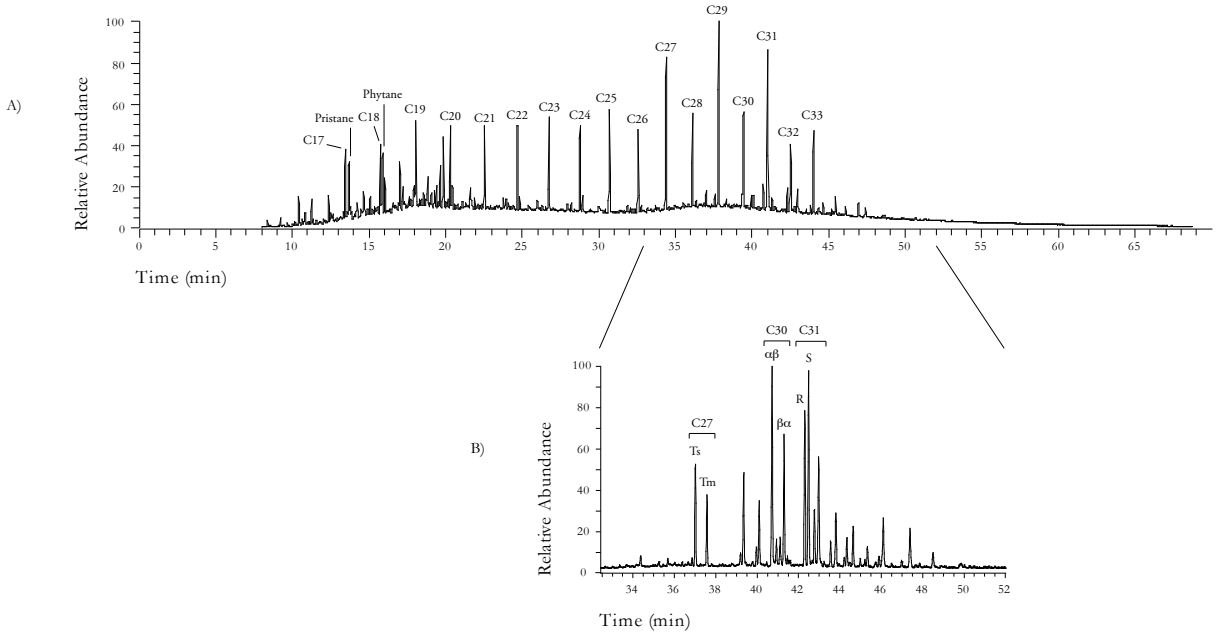

Fig. 3.2: mass chromatogram of the TIC (total ion current) (A) and m/z 191 (B).

3.4 Results and discussion

3.4.1 GC-MS and diagnostic biomarker and non-biomarker ratios

A typical gas chromatograph trace of TIC of the analyzed samples is shown on Fig 3.2 (see Appendix for all the chromatographs traces). In general, n-alkanes range from n-C_{17} to n-C_{33}. High molecular weight (HMW) n-alkanes dominate and show an odd-over-even carbon number distribution for n-C_{25} – n-C_{33} homologues, typical of an higher plant source. Isoprenoids, namely pristane and phytane, are present in very low concentration.

Results of maturity biomarker and non-biomarker parameters are summarized in Fig 3.3 and Tab 3.1.

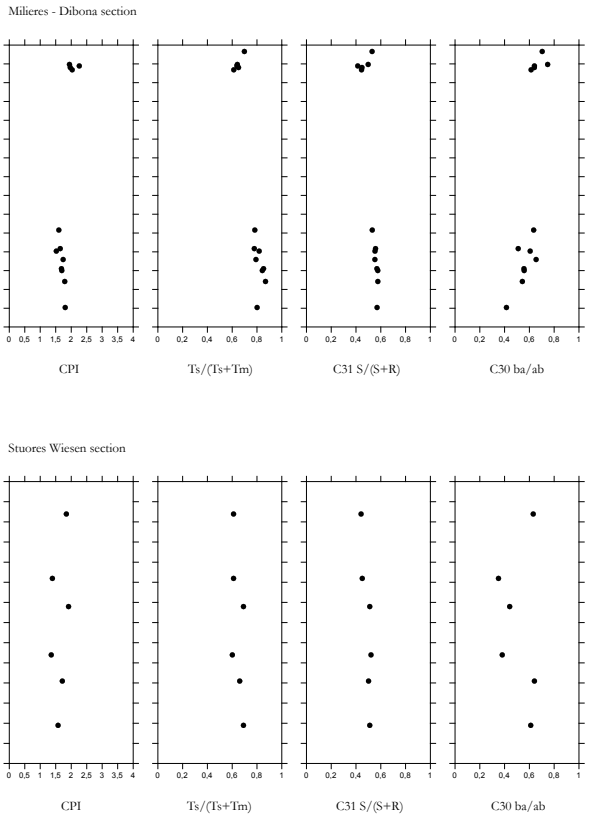

Fig. 3.3: Carbon preference index (CPI) and biomarker maturity parameters of Prati di Stuores section and Milieres-Dibona section.

The CPI and maturity-related biomarker ratios are rather constant throughout both Prati di Stuores and Milieres-Dibona sections, suggesting that analyzed samples have experienced the same uniform thermal maturity. CPI values are dependent on both thermal maturity and source of OM. CPI equal to 1 suggest that the rock extract is thermally mature; CPI values significantly below or above 1 indicate low thermal maturity. CPI below 1 (even-over-odd predominance) indicates mostly a marine origin for n-alkanes, whereas CPI above 1 (odd-over-even predominance) indicates an higher plant origin. Carnian samples' CPI values are consistent with a moderate thermal maturity and mostly an higher plant origin for n-C_{25} – n-C_{33} n-alkanes.

The 17β,21α(H)-moretane and 17α21β(H)-hopane are the product of the conversion of the 17β,21β(H)-hopane biological configuration of hopanoids. As the moretanes are less stable than the hopanes, the C_{30} βα/αβ (moretane/hopane) ratio decreases with thermal maturity. Analyzed samples extracts have C_{30} moretane/hopane values that indicate a low to quite low thermal maturity in agreement with the CPI. However, moretane/hopane ratio can depend also on the source of OM. It has been observed that C_{30} βα/αβ can increase with increasing terrigenous higher plant input (Peters et al., 2005). Samples coming from the Milieres-Dibona section show an increase of

the C_{30} βα/αβ from the basal samples to the uppermost ones (from 0.5 to 0.7) that is in agreement to a slightly increase of the DJ samples' CPI (Fig 3.3 and Tab 3.1). This parallel trend of both moretane/hopane and CPI can testify for a little relative increase of higher-plant input that is consistent with the gradual facies change from the prodelta shales at the base of the section to the paralic/coastal sandstones and palaeosols in the uppermost part of the Heiligkreutz Formation. Equally, the C_{30} βα/αβ decrease from 0.6 to 0.3-0.4 in the middle part of the Stuores Wiesen section (Fig 3.3) agrees with a little decrease of the CPI that can testify for a little decrease in higher plant input.

Milieres – Dibona Section

	TOC	*CPI*	*Ts/(Ts+Tm)*	*C30 βα/αβ*	*C31 S/(S+R)*
MIR 1	0.68	1.80	0.80	0.41	0.57
MIR 5	1.07	1.79	0.87	0.54	0.58
MIR 6	0.77	1.69	0.84	0.56	0.57
MIR 7	0.88	1.68	0.85	0.56	0.57
MIR 9	0.92	1.74	0.79	0.65	0.55
MIR 10	0.85	1.51	0.82	0.61	0.55
MIR 11	0.72	1.64	0.78	0.51	0.56
MIR 16	0.94	1.60	0.78	0.63	0.53
DJ 16	0.62	2.03	0.61	0.61	0.44
DJ 18	0.43	1.96	0.65	0.64	0.45
DJ 19	1.22	2.26	0.64	0.64	0.41
DJ 21	0.84	1.94	0.64	0.75	0.50
DJ 27	0.55		0.70	0.70	0.53

Stuores Wiesen Section

	TOC	*CPI*	*Ts/(Ts+Tm)*	*C30 βα/αβ*	*C31 S/(S+R)*
STU 00	0.31	1.57	0.69	0.61	0.51
STU 5	0.16	1.71	0.66	0.64	0.50
STU 12	0.71	1.35	0.60	0.38	0.52
STU 102	0.27	1.91	0.69	0.44	0.51
STU 105	0.68	1.39	0.61	0.35	0.45
STU 108	0.49	1.84	0.61	0.63	0.44

Tab 3.1: values of carbon preference index (CPI) and biomarker maturity parameters of Prati di Stuores section and Milieres-Dibona section.

C_{31} biological 22R hopane is converted to a mixture of 22R and 22S diastereomers with thermal maturity until they reach the equilibrium (22S/(22S+22R) = 0.57-0.62). C_{31} homohopane 22S/(22S+22R) values range from 0.41 to 0.58 at Milieres-Dibona section and from 0.44 to 0.52 at Stuores Wiesen section, meaning that our samples at most barely entered oil generation (>0.57,

Peters et al., 2005).

Ts/(Ts+Tm) increases with increasing thermal maturity, as C_{27} 17α-trisnorhopane (Tm) is less stable than C_{27} 18α-trisnorhopane (Ts). High Ts/(Ts+Tm) values for both Milieres-Dibona and Stuores Wiesen section are typical of a mature organic matter, in contrast to the above discussed data. However, Ts/(Ts+Tm) is strongly dependent to the source of OM, depositional environment and lithology (Moldowan et al., 1986; Peters et al., 2005): clay minerals of the analyzed shales could have catalyzed the structural rearrangement of the Tm to the Ts isomer (Peters et al., 2005) resulting in an higher Ts/(Ts+Tm).

Summarizing, data show a moderate thermal maturity for our rock extracts, little below the oil window, and mostly an higher plant origin for long chain n-alkanes.

3.4.2 $\partial^{13}C_{n\text{-alkanes}}$

It was not possible to analyze the C-isotope signature of all extracted n-alkanes of each sample because of their low abundance and sporadic co-elution with other compounds.

$\partial^{13}C$ values of all extracted n-alkanes range from -21.08‰ to -30.97‰ (Fig 3.4 and Tab 3.2). The $\partial^{13}C$ of n-C_{17} n-C_{33} n-alkanes vary in a range of 2-3‰ within the same sample with no obvious correlation to the carbon number. In some samples, odd n-alkanes are enriched with respect of the even ones (e.g.: MIR 16, Fig 3.4). This "zigzag pattern" has been observed in recent leaf waxes n-alkanes isolated from single C_3, C_4 and CAM plants (Collister et al., 1994; O'Malley et al., 1997; Chikaraishi and Naraoka, 2003; Bi et al., 2005), but its explanation is still unclear.

Odd n-C_{25} – n-C_{31} n-alkanes are always abundant and no co-eluted in every samples, so it was easy to measure their C-isotope signature. $\partial^{13}C$ values of odd n-C_{25} – n-C_{31} n-alkanes range from -22.02‰ to -30.93‰, in the range expected for C_3 plants. They are generally depleted by 2-4‰ with respect to wood coming from the same stratigraphic segments (Fig BOH) in agreement with data of recent plant-derived n-alkanes that have more depleted values than bulk plant tissue because of further C-isotope fractionation during their biosynthesis (e.g.: Chikaraishi and Naraoka, 2003).

Odd n-C_{25} – n-C_{31} n-alkanes C-isotope signature is also depleted by 1-8‰ than TOC $\partial^{13}C$. Plots in Fig 3.5 show a good correlation between the $\partial^{13}C$ of n-$C_{25\text{-}29}$ n-alkanes and the $\partial^{13}C_{TOC}$ (R^2 = 0.7-0.8) and a less obvious correlation between n-C_{31} and TOC $\partial^{13}C$ (R^2 = 0.55). The offset between

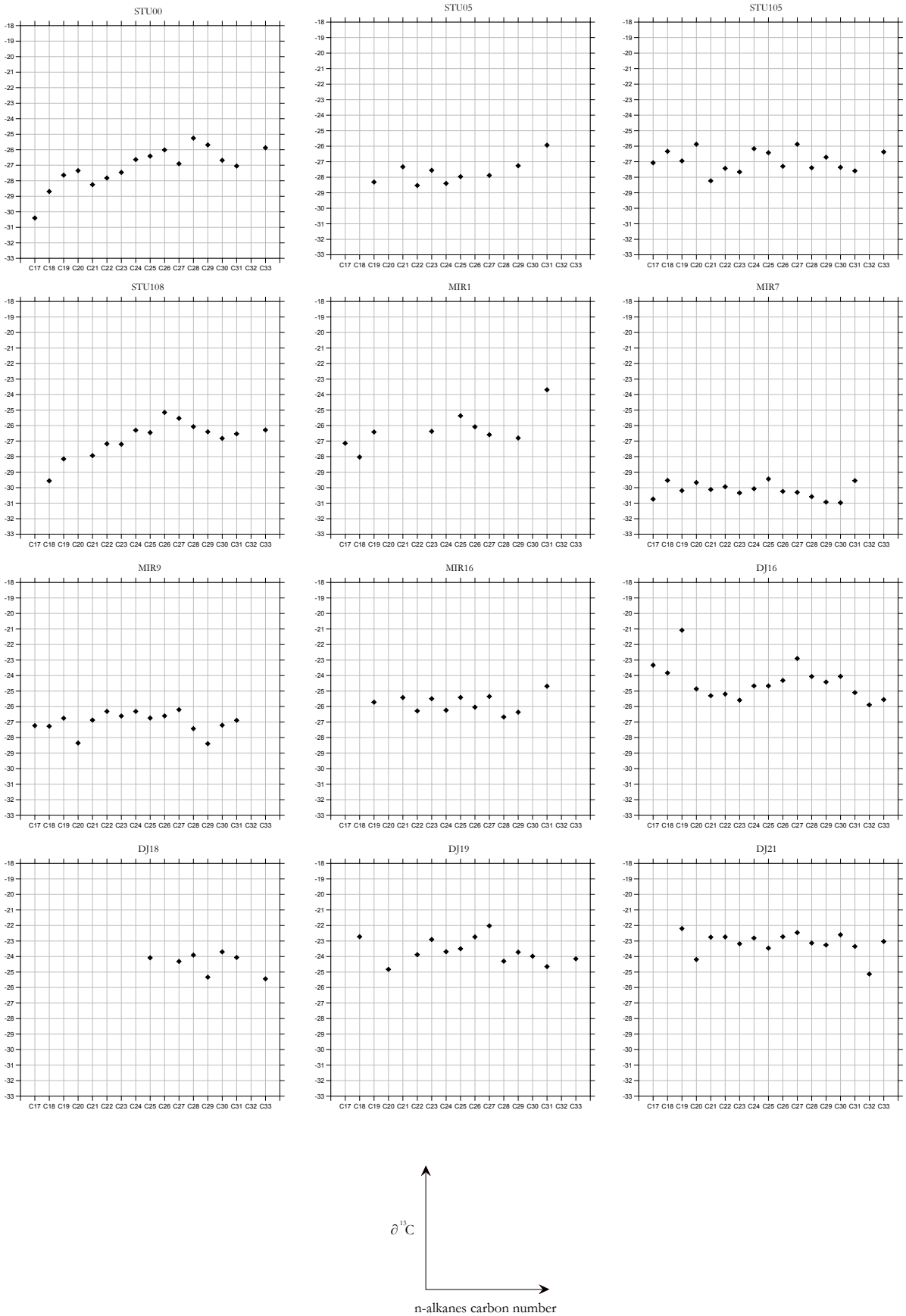

Fig. 3.4: carbon isotope signature of extracted n-alkanes.

STU00			STU05			STU105		
n-alkanes	$\partial^{13}C$	StDev	n-alkanes	$\partial^{13}C$	StDev	n-alkanes	$\partial^{13}C$	StDev
C17	-30.40	0.66	C17			C17	-27.07	0.15
C18	-28.69	0.80	C18			C18	-26.33	0.57
C19	-27.64	0.50	C19	-28.31	0.33	C19	-26.95	1.45
C20	-27.35	0.33	C20			C20	-25.87	0.63
C21	-28.25	0.92	C21	-27.33	0.04	C21	-28.23	1.09
C22	-27.82	0.81	C22	-28.53	0.84	C22	-27.43	0.27
C23	-27.46	0.15	C23	-27.55	1.28	C23	-27.66	0.71
C24	-26.63	0.74	C24	-28.40	0.87	C24	-26.16	0.64
C25	-26.41	0.91	C25	-27.96	0.11	C25	-26.42	0.81
C26	-26.01	0.15	C26			C26	-27.30	0.92
C27	-26.90	0.07	C27	-27.88	1.58	C27	-25.87	0.01
C28	-25.25	0.18	C28			C28	-27.39	0.06
C29	-25.69	0.19	C29	-27.26	0.34	C29	-26.71	0.54
C30	-26.68	0.88	C30			C30	-27.36	0.99
C31	-27.05	0.51	C31	-25.93	0.84	C31	-27.59	0.57
C32			C32			C32		
C33	-25.87	0.22	C33			C33	-26.37	1.01
Phytane	-29.69	0.47	Phytane			Phytane		
Pristane	-31.28	0.29	Pristane			Pristane	-29.19	0.00
STU108			MIR1			MIR7		
n-alkanes	$\partial^{13}C$	StDev	n-alkanes	$\partial^{13}C$	StDev	n-alkanes	$\partial^{13}C$	StDev
C17			C17	-27.14	0.15	C17	-30.74	0.16
C18	-29.56	4.17	C18	-28.03	0.83	C18	-29.53	0.26
C19	-28.15	0.56	C19	-26.41	0.10	C19	-30.19	0.47
C20			C20			C20	-29.67	0.70
C21	-27.93	0.77	C21			C21	-30.12	0.27
C22	-27.17	0.40	C22			C22	-29.94	0.85
C23	-27.20	0.44	C23	-26.37	0.03	C23	-30.34	0.03
C24	-26.30	1.71	C24			C24	-30.07	0.09
C25	-26.45	0.20	C25	-25.37	0.43	C25	-29.44	0.03
C26	-25.15	0.45	C26	-26.08	0.94	C26	-30.24	0.52
C27	-25.53	0.11	C27	-26.59	0.57	C27	-30.30	0.15
C28	-26.07	0.16	C28			C28	-30.58	0.19
C29	-26.40	0.03	C29	-26.80	1.15	C29	-30.93	0.07
C30	-26.82	0.01	C30			C30	-30.97	0.20
C31	-26.53	0.00	C31	-23.69	0.75	C31	-29.55	0.83
C32			C32			C32		
C33	-26.28	1.44	C33			C33		
Phytane			Phytane	-29.27	2.35	Phytane	-30.65	1.38
Pristane			Pristane			Pristane	-33.47	0.49

Tab. 3.2: $\partial^{13}C$ values of extracted n-alkanes, phytane and pristane. Standard deviation based on duplicate analyses.

MIR9			MIR16			DJ16		
n-alkanes	∂13C	StDev	n-alkanes	∂13C	StDev	n-alkanes	∂13C	StDev
C17	-27.23	0.63	C17			C17	-23.33	0.16
C18	-27.27	1.06	C18			C18	-23.83	0.88
C19	-26.75	0.84	C19	-25.72	0.42	C19	-21.08	1.08
C20	-28.35	1.83	C20			C20	-24.86	0.39
C21	-26.87	0.21	C21	-25.42	0.13	C21	-25.30	0.68
C22	-26.31	0.12	C22	-26.28	0.62	C22	-25.19	0.35
C23	-26.61	0.64	C23	-25.49	0.66	C23	-25.59	0.16
C24	-26.31	0.24	C24	-26.24	0.33	C24	-24.67	0.33
C25	-26.74	0.59	C25	-25.41	0.29	C25	-24.67	0.71
C26	-26.60	0.37	C26	-26.04	0.03	C26	-24.32	0.38
C27	-26.20	0.35	C27	-25.35	0.09	C27	-22.90	0.36
C28	-27.42	0.28	C28	-26.67	0.23	C28	-24.06	0.14
C29	-28.39	0.25	C29	-26.36	0.57	C29	-24.42	0.03
C30	-27.20	0.13	C30			C30	-24.05	0.46
C31	-26.89	0.11	C31	-24.69	0.93	C31	-25.10	0.12
C32			C32			C32	-25.89	0.10
C33			C33			C33	-25.55	1.79
Phytane	-29.88	0.00	Phytane			Phytane	-23.17	0.53
Pristane	-27.49	0.23	Pristane	-25.80	0.13	Pristane	-26.36	1.57
DJ18			DJ19			DJ21		
n-alkanes	∂13C	StDev	n-alkanes	∂13C	StDev	n-alkanes	∂13C	StDev
C17			C17			C17		
C18			C18	-22.72	0.00	C18		
C19			C19			C19	-22.20	0.01
C20			C20	-24.83	0.31	C20	-24.19	0.81
C21			C21			C21	-22.75	0.25
C22			C22	-23.88	1.34	C22	-22.74	0.62
C23			C23	-22.90	0.01	C23	-23.18	0.03
C24			C24	-23.69	0.57	C24	-22.81	0.30
C25	-24.08	0.84	C25	-23.50	0.72	C25	-23.46	0.32
C26			C26	-22.74	0.03	C26	-22.72	0.55
C27	-24.32	0.97	C27	-22.02	0.19	C27	-22.46	0.18
C28	-23.91	0.03	C28	-24.30	1.16	C28	-23.13	0.34
C29	-25.33	0.10	C29	-23.72	0.58	C29	-23.26	0.08
C30	-23.70	0.67	C30	-23.98	0.64	C30	-22.60	0.29
C31	-24.06	0.91	C31	-24.65	0.31	C31	-23.35	0.02
C32			C32			C32	-25.13	0.20
C33	-25.44	1.13	C33	-24.15	0.27	C33	-23.03	0.65
Phytane			Phytane			Phytane		
Pristane			Pristane			Pristane		

Tab. 3.2: (continuation)

$\partial^{13}C_{n\text{-alkane}}$ and $\partial^{13}C_{TOC}$ increases as values become more depleted (see chapter 4, for a possible interpretation of this result).

3.4.3 ∂^{13}C of other compounds

In some samples it has been possible to measure the ∂^{13}C of acyclic isoprenoids, namely pristane and phytane. These compounds are mostly the product of the oxidation (pristane) or reduction (phytane) of phytol, an important part of chlorophyll, but phytane can derive also from methanogenic or halopytic bacteria and pristane from unsaturated isoprenoids in zooplankton or tocopherols (Killops and Killops, 2005; Peters et al., 2005) . $\partial^{13}C_{pristane}$ ranges from -33.5‰ to -25.8‰ and $\partial^{13}C_{phytane}$ range from -30.65‰ to -23.17‰ (Fig 3.6). The offset between the C-isotope composition of pristane and phytane in samples where both have been measured, is between 1,59‰ and 3,19‰, with $\partial^{13}C_{pristane}$ depleted with respect to $\partial^{13}C_{phytane}$ in all samples except one where $\partial^{13}C_{pristane}$ is enriched with respect to $\partial^{13}C_{phytane}$ by 2.39‰. In general, pristane and phytane do not differ more than ±0.3‰ if they share a common source (Peters et al., 2005), thus, higher differences in the C-isotope signature can be ascribed to a different source. However, the analytical

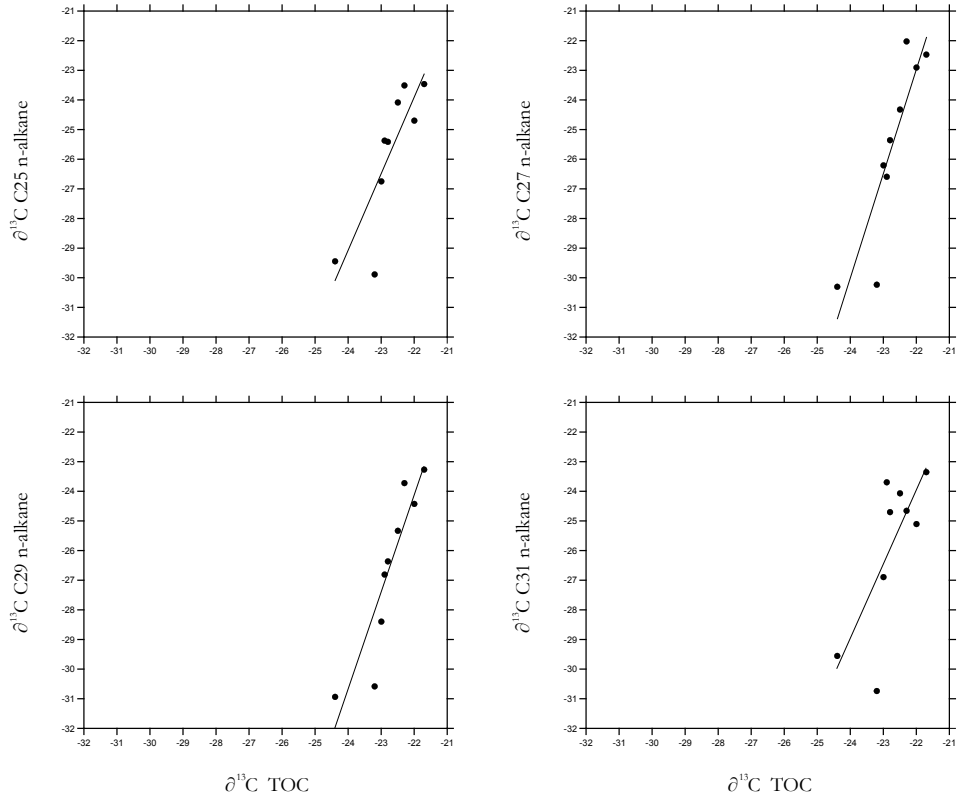

Fig. 3.5: the carbon isotope signature of odd long chain n-alkanes vs the carbon isotope signature of total organic carbon (TOC).

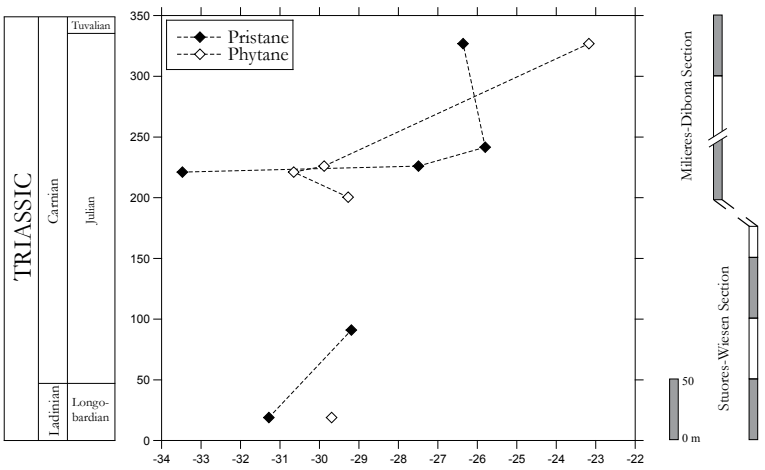

Fig. 3.6: $\partial^{13}C$ values of pristane and phytane vs age.

error based on duplicate analyses reaches ±1.57‰ (1? σ) (Tab 3.2) due to the very low abundance of these compounds and could have amplified the $\partial^{13}C$ divergences.

3.5 An early Carnian molecular $\partial^{13}C$ curve

N-alkanes $\partial^{13}C$ show a positive shift from the latest Ladinian to the end of the Julian (early Carnian) (Fig 3.7). The magnitude of this positive shift is ~4-5‰ for n-$C_{17\text{-}19}$ alkanes and ~3‰ for n-alkanes with longer chain (>n-C_{20}). Pristane and phytane $\partial^{13}C$ values at the Ladinian/Carnian boundary are lower than those at the end of the Julian (Fig 3.6) and parallel well the n-alkanes trend. As described in chapter 2 for wood C-isotope data (Fig 2.10 and Fig 2.11), also n-alkanes and isoprenoids draw a secular positive shift that is consistent with marine existing $\partial^{13}C$ records based on bulk carbonates and brachiopod calcitic shells (Korte et al., 2005; Preto et al., 2010).

Within this positive trend, in the first 50 meters of the Milieres-Dibona section corresponding to a portion of the *Austrotrachyceras austriacum* ammonoid subzone, both long-chain and short-chain n-alkanes show an abrupt negative carbon isotope excursion (CIE) of ~3-5‰ and a sudden positive rebound to "normal" values. $\partial^{13}C_{phytane}$ draw a ~-2‰ shift that parallels that of n-alkanes data and $\partial^{13}C_{pristane}$ show a ~+5‰ shift corresponding to the final rebound of the negative CIE (Fig 3.7).

The very good environmental-control on the analyzed molecules, i.e. the attribution of n-alkanes to a terrestrial and/or marine source, allows to infer CIEs in the superficial C reservoirs. Thus,

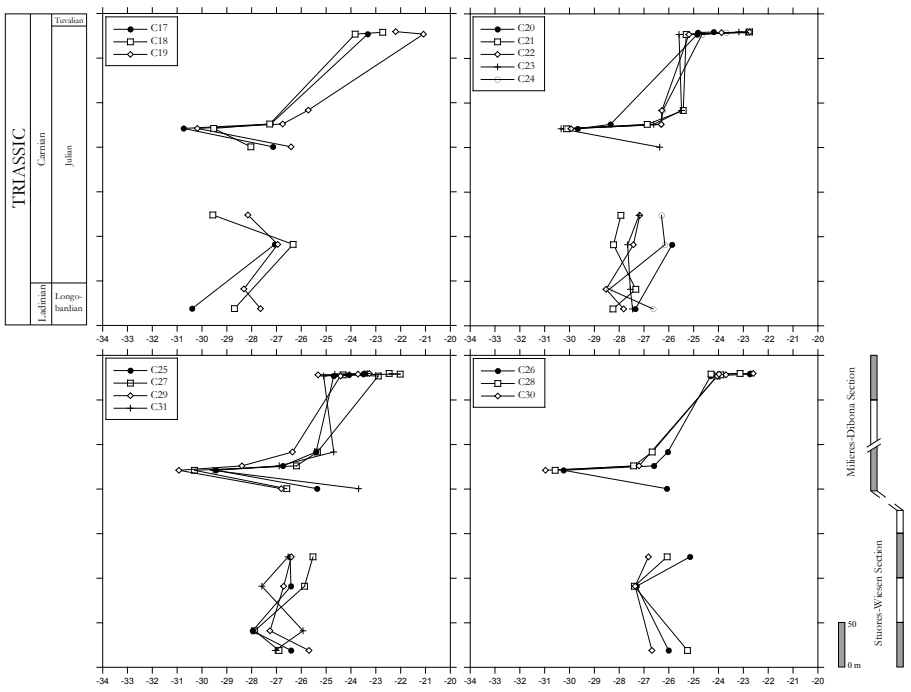

Fig. 3.7: $\partial^{13}C_{n\text{-}alkanes}$ curves.

these new molecular C-isotope data testify for a sudden negative $\partial^{13}C$ shift of the exchangeable C-isotope reservoirs of the active C-cycle (atmosphere-land-ocean).

3.6 Conclusions

- Biomarker and non-biomarker maturity parameters show that extracted lipids have experienced a moderate thermal maturation and that the source of OM was mostly terrestrial. Long chain n-alkanes (n-$C_{25\text{-}33}$) show an odd-over-even distribution that is typical of an higher-plant source.
- N-alkanes have $\partial^{13}C$ values ranging from -21.08‰ to -30.97‰. Odd n-$C_{25\text{-}33}$ n-alkanes have C-isotope values in the range expected for C_3 plant and are more depleted in ^{13}C than bulk wood coming from the same stratigraphic layers, in agreement with $\partial^{13}C$ measurements of Recent material. $\partial^{13}C$ of n-$C_{25\text{-}33}$ is also more depleted than $\partial^{13}C_{TOC}$. The C-isotope offset of n-alkenes vs TOC increases as values become more depleted.
- Isoprenoids $\partial^{13}C$ range from -23.17‰ to -33.5‰. Difference between the C-isotope signature of pristane and phytane can be explained by different sources.
- N-alkanes and isoprenoids draw a positive secular C-isotope shift during the latest Ladinian - early Carnian interval that is consistent with $\partial^{13}C_{wood}$ and marine carbonates.

– An abrupt negative $\partial^{13}C$ shift is registered by all extracted n-alkanes and isoprenoids within the *A. austriacum* ammonoid subzone.

4. THE C-ISOTOPE SINGNATURE OF THE CARNIAN PLUVIAL EVENT (CPE)

4.1 Abstract

Major climate changes and mass extinctions are associated to C-isotope anomalies in the atmosphere-ocean system that have been linked to the onset of large igneous provinces (LIPs) and associated emissions of greenhouse gases and aerosols (Courtillot & Renne, 2003; Rampino, 2010). However, climatic and biological consequences of the eruption of some of the known LIPs are not yet explored. During the Carnian (Late Triassic), large volumes of flood basalts were erupted to form the so-called Wrangellia LIP (western North America). This huge volcanic province is similar in age to a major climatic and biotic change (Furin et al., 2006), namely the Carnian Pluvial Event (CPE) (Simms & Ruffell, 1989), but no evidences of a causal relationship exist other than timing. Here it is reported a sharp negative $\partial^{13}C$ excursion at the onset of the CPE recorded in organic matter. A ~-4‰ abrupt C isotope excursion is present in leaf waxes n-alkanes, whereas total organic carbon (TOC) records show a ~-2‰ shift. It is proposed that this C isotope negative shift was caused by a rapid injection of light C in the atmosphere-ocean system linked to the eruption of Wrangellia flood basalts.

4.2 Introduction

As described in chapter 1, the Upper Triassic relative stability was interrupted only by an episode of more humid conditions, known as the Carnian Pluvial Event (CPE) (Preto et al., 2010 and references therein). The CPE is marked by increased input of coarse siliciclastics and the shut-down of carbonate production and sedimentation across the Tethyan realm (Rigo et al., 2007; Schlager and Schöllnberger, 1974), high extinction rates of several groups (e.g. ammonoids, crinoids,

bryozoa) (Simms & Ruffell, 1989), a floral change to more hygrophytic forms (Roghi, 2004; Roghi et al., 2010) and a dramatic increase of conifer resin exudation (Roghi et al., 2006). On a longer time scale, a increase in organic carbon burial is evidenced by a positive shift in the $\partial^{13}C$ of marine carbonate (Korte et al, 2005) that took place from the Anisian to the Late Carnian. Compared to the big five mass extinctions, overall Carnian extinction rates are low (Rohde & Muller 2005), but the CPE coincides with the origin and/or radiation of some of several important groups (Fig. 4.1): The first known dinosaurs and calcareous nannoplankton occur in the Carnian (Rogers et al., 1993; Furin et al., 2006; Erba, 2006) and the radiation of modern-like conifers was in the Late Triassic (Taylor et al, 2009). The CPE also coincides with the eruption of the Wrangellia oceanic flood basalt province, suggesting that a causal relationship might exist between the two events (Furin et al. 2006). The onset of large igneous province eruptions (LIPs) is often associated with major negative C-isotope excursions (CIEs), (e.g.; Magaritz et al, 1988; Marzoli et al., 2004; Wignall et al., 2009) and mass extinctions, but no C-isotope perturbations during the CPE are known.

4.3 Materials and Methods

In order to better define the poorly-resolved carbon cycle perturbations associated with the CPE, the $\partial^{13}C$ of plant-derived long-chain C_{25}-C_{31} n-alkanes, bulk wood, pristane, phytane and bulk TOC from marine sediments have been measured (for analytical procedures see methods sections in chapters 2 and 3). Pristane and phytane derive from phytol by carboxilation and reduction respectively, phytol being an important part of phytoplankton chlorophyll and thus representing a marine C-isotope signal. $\partial^{13}C$ analyses of TOC were included to improve C-isotope data resolution around the CPE. Samples were collected from two sections in Dolomites (Southern Alps, Italy), Stuores Wiesen and Milieres-Dibona. Stuores Wiesen is the GSSP type section for the base of the Carnian (Mietto et al., 2007; 2008) and consists of a series of hemipelagites and thin turbidite beds, deposited in a rapidly infilling basin in hundreds of meter of water depth. It encompasses the Frankites regoledanus, Daxatina canadensis and Trachyceras aon ammonoid biochronozones. The Milieres-Dibona section lies within the Austrotrachyceras austriacum ammonoid subzone (uppermost lower Carnian) and is a succession of marls, limestone and sandstone deposited in a prodelta - coastal to paralic environment. Fossil wood is present as dispersed coalified fragments

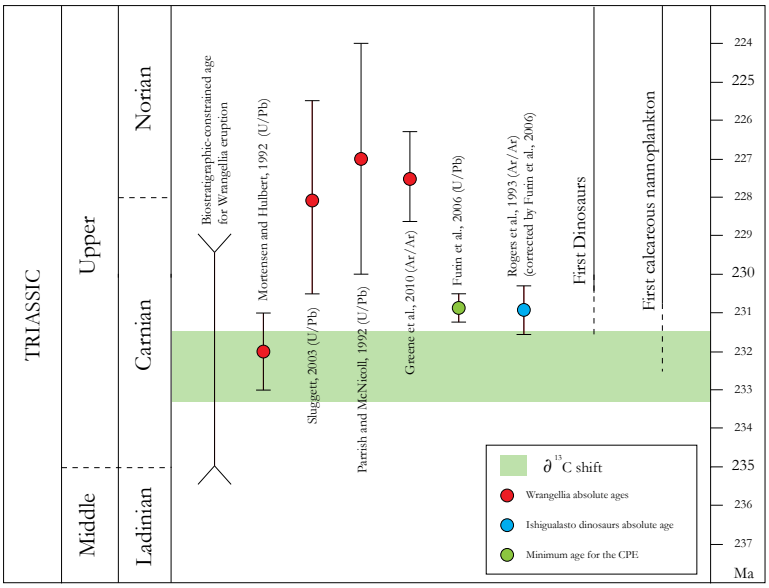

Fig. 4.1: U/Pb absolute ages available for the Wrangellia LIP, U/Pb minimum absolute age for the CPE, Ar/Ar absolute age of the first dinosaurs, the emergence of calcareous nannoplankton and age of the negative C-isotope excursion associated to the CPE.

throughout both sections.

4.4 Results

$\partial^{13}C_{wood}$ data lie in the range expected for C_3 plants, from -20.15‰ to 25.46‰. Values of wood fragments do not exceed a range of 2.4‰ within the same stratigraphic bed. Extracted C_{25}-C_{31} long chain n-alkanes show an odd-over-even carbon number predominance that suggests derivation from higher plant epicuticular waxes (the carbon preference index (CPI) calculated for C_{25}-C_{31} n-alkanes has values from 1.5 to 2.3). Odd C_{25}-C_{31} n-alkanes $\partial^{13}C$ values range from -22.02‰ to -30.93‰ and are slightly depleted (1-2‰) with respect to bulk wood and TOC. TOC content varies between 0.43% and 1.34% and $\partial^{13}C_{TOC}$ values range from -21.7‰ to -25.5‰.

4.5 Discussion

As described in chapter 2 and 3, a composite record of C_{25}-C_{31} n-alkanes and wood $\partial^{13}C$ show a +3‰ secular trend during the Carnian that mirrors TOC $\partial^{13}C$ data (Fig. 4.2) and published marine inorganic C isotopes from brachiopod calcite and bulk carbonates (Korte et al. 2005). This positive shift in marine dissolved inorganic carbon $\partial^{13}C$ was attributed by Korte and colleagues to the re-establishment of coal swamps and increase in C burial after early Triassic C-cycle instability. Within this positive trend, higher plant C_{25}-C_{31} n-alkanes and TOC $\partial^{13}C$ values reveal a sudden and pronounced negative shift of ~-4‰ and ~-2‰ respectively, in the lower part of the Heiligkreutz

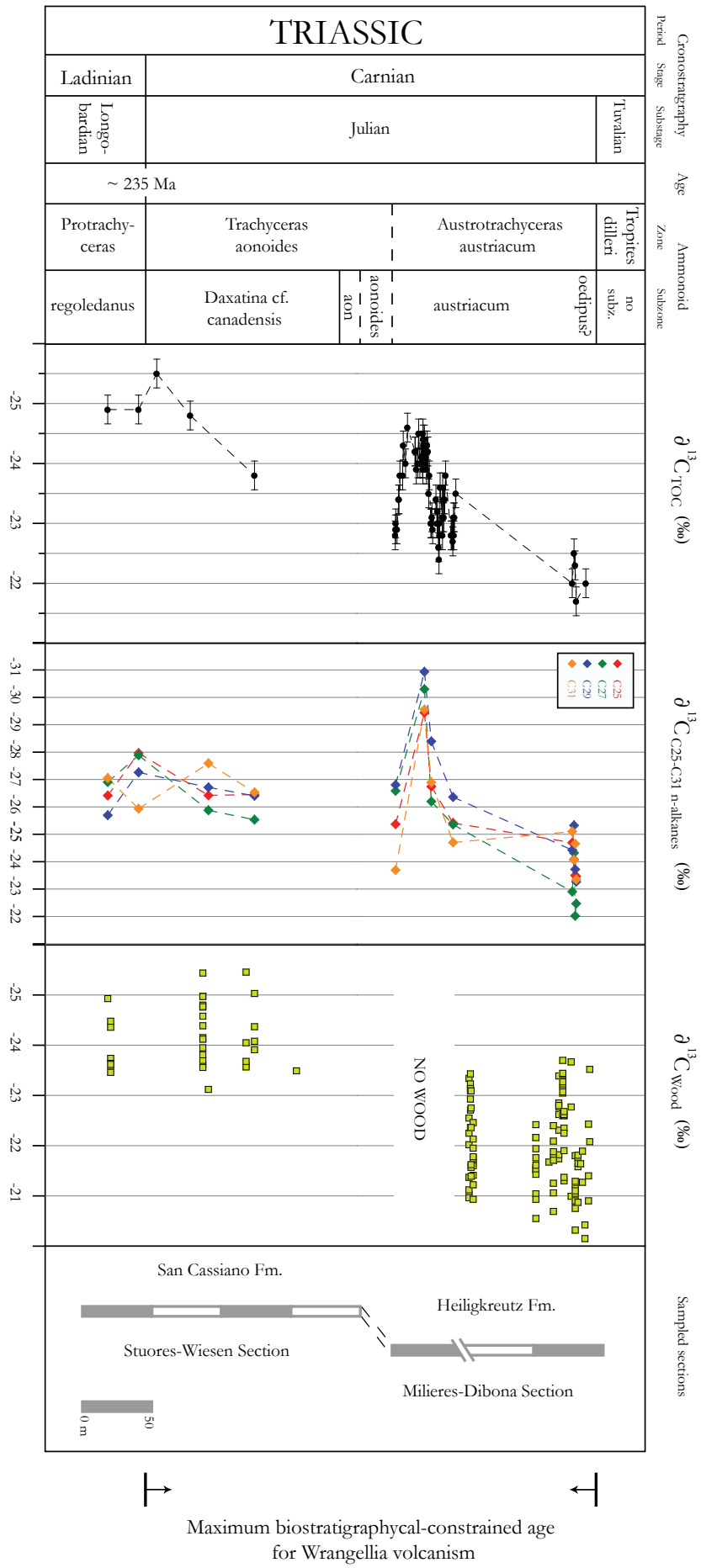

Fig. 4.2: $\partial^{13}C_{TOC}$, $\partial^{13}C_{n\text{-alkanes}}$ and $\partial^{13}C_{wood}$ curves.

Formation corresponding to the lower *Austrotrachyceras austricum* ammonoid biochronozone (uppermost lower Carnian) (Fig. 4.2, Fig. 4.3). This CIE does not coincide with any sedimentological, lithological or paleoenvironmental changes in the Milieres section (Fig 4.3). The $\partial^{13}C_{phytane}$ record shows a ~-2‰ shift that parallels that of n-alkanes and TOC data and $\partial^{13}C_{pristane}$ show a ~+5‰ shift corresponding to the final rebound of the negative CIE. The wider excursion recorded by n-alkanes as compared to TOC (Fig. 4.3) can be explained by increasing efficiency in the water use by plants under the higher humidity conditions during the CPE, testified by hygrophitic palynological assemblages and paleosols typical of humid climate, that cause an increase in ^{13}C-discrimination (Bowen et al., 2004), i.e. stomata are more opened and the pi/pa ratio of the Fahrquar et al. (1989) equation (see chapter 2.1, equation 2.1) increases.

These new C-isotope data clearly show that during the CPE, CO_2 enriched in ^{12}C was injected into the exchangeable reservoirs of the active C-cycle (atmosphere-ocean-land). One possibility for this is CO_2 release by the coeval Wrangellia LIP, either by direct injection of magmatic CO_2 or by triggering additional CO_2 release from other light carbon reservoirs as, e.g., methane chlathrate deposits on continental shelves. Key to this association is the timing of Wrangellia eruption: biostratigraphic data constrain Wrangellia volcanism to the late Ladinian – late Carnian. Sediments underlying basalts contain Ladinian bivalves belonging to the genus Daonella (Greene et al., 2010) and overlying sediments present a lower Tuvalian (upper Carnian) ammonoid association with Tropites dilleri (Tozer et al., 1994). Most of the existing absolute Ar/Ar ages of Wrangellia basalts are reset to ages younger than that of deposition (see ref. Greene et al., 2010 and references therein). Some U/Pb age however agree with Wrangellia basalts biostratigraphic constrains (Greene et al., 2010) and are very similar to the existing absolute minimum age for the CPE (Furin et al., 2006) (Fig. 4.1). Absolute ages, biostratigraphic and megnetostratigraphic constrains indicate that the eruption of Wrangellia basalts lasted for at most 2 Myrs (Greene et al., 2010). For at least one LIP the injection of ^{12}C is demonstrated to occur at the very onset of basalt eruption (Wignall et al., 2009).

Despite pioneer C-isotope analyses on some LIP basalts (namely, Kerguelen, Deccan Traps, East Greenland and the Faeroes) suggest that the $\partial^{13}C$ of volcanic CO_2 could have been as low as -23‰, and thus could have determined short-time C-isotope shifts (Hansen 2006), it is generally

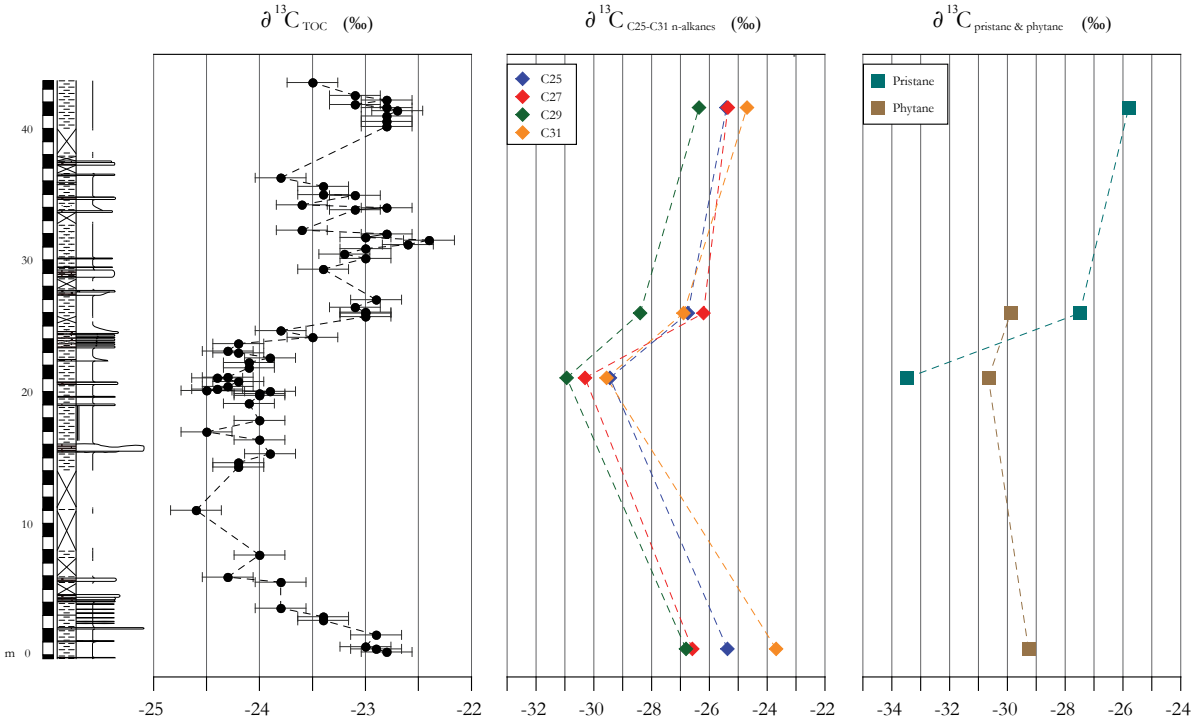

Fig. 4.3: particular of $\partial^{13}C_{TOC}$, $\partial^{13}C_{n\text{-}alkanes}$, $\partial^{13}C_{pristane}$ and $\partial^{13}C_{phytane}$ curves around the C-isotope negative shift at Milieres-Dibona section.

accepted that CO_2 release from a volcanic source is not sufficient to explain large and rapid $\partial^{13}C$ shifts as those at mass extinctions or some oceanic anoxic events (Wignall, 2001), because the C-isotope composition of recent hawaiian volcanic CO_2 is too heavy ($\partial^{13}C$=-7‰). Greene et al. (2010) estimated the volume of erupted Wrangellia basalts is up to $140x10^3$ Km^3, although previous estimates indicate larger volumes of up to $1x10^6$ Km^3 (Lassiter, 1995). The volume of flood basalts erupted could have been much greater because Wrangellia oceanic plateau was accreted in an orogenic wedge in the Late Jurassic – Early Cretaceous (Greene et al., 2010) and thus it is intensely deformed and part of the erupted flood basalts have certainly been subducted. Assuming the larger size given by Lassiter et al. (1995) and that the eruption of 1 Km^3 of modern basalts emits ~$5x10^{12}$ g of C (McCartney et al., 1990), ~$5x10^{18}$ g of C would have been released during the eruption of Wrangellia LIP. Dickens et al. (1995) calculated that to cause a -2 to -3‰ $\partial^{13}C$ shift in the present-day exchangeable C reservoirs, a release of 2.7-6.8$x10^{20}$ g of C is required. This is far more than the most optimistic estimates of the Wrangellia C release. Moreover, data show that $\partial^{13}C_{TOC}$ quickly reach the most negative values in approximately 8 m of the more than 150 m thick Dibona-Milieres section (Fig. 4.3). Considering that the Dibona-Milieres section entirely lies within the A. austriacum ammonoid subzone, one of ten in the 7 Myrs-long Carnian age (Walker and Geissman, 2009), it

is reasonable to hypothesize that the austriacum biochronozone has a duration in the order of 1 Myr or less, and the negative $\partial^{13}C_{TOC}$ shift occurred in a small portion of this time span, i.e., the amount of light C that triggered the C-isotope perturbation must have been transferred into the atmosphere/ocean system in a time span similar or, most probably, shorter than the duration of Wrangellia eruption (~2Myrs) (Greene et al., 2010).

Models show that the venting of greenhouse gases associated to flood basalts eruption initiates a global warming (Jenkyns, 2010). An increase in sea temperatures can destabilize methane clathrate hydrate reservoirs: CH_4 release and oxidation to CO_2 could have provided the amount of light CO_2 necessary to determine the detected ~2‰ negative C-isotope excursion (clathrate CH_4 $\partial^{13}C$=-60‰) (Dickens et al., 1995).

Sedimentological evidence from CPE sections supports the hypothesis of rapid injection of CO_2 into the atmosphere-ocean system: a rapid influx of CO_2 results in the acidification of seawater and has a strong impact on the stability and production of carbonates. A rise of the CCD (Carbonate Compensation Depth) observed in the Lagonegro basin of western Tethys and the crisis of carbonate sedimentation from shallow water to deep water settings at the CPE (Rigo et al., 2007) are best explained by a decrease in the pH of seawater. A rise of the CCD is also associated with events such as the Early Aptian Oceanic Anoxic Event (Erba et al., 2010) and the Paleocene-Eocene Thermal Maximum (Zachos et al., 2005). In contrast to these events however, the CPE occurred during a time of "aragonite seas" (Stanley and Hardie 1998) when seawater chemistry was more similar to Recent than that of the Cretaceous and Paleocene/Eocene "calcite sea" (Hardie 1996; Ries 2010; Hasiuk and Lohmann, 2010).

4.6 Conclusions. I - The CPE C-isotope signature.

The discovery of an intense, rapid negative carbon isotope excursion sheds light on the nature of the CPE and lines it up to the major known climatic perturbations of the Mesozoic and Cenozoic. The hypothesis that the CPE is a consequence of the eruption of Wrangellia LIP finds solid bases and a new tessera is offered to support the link between LIP onset and global climate changes in Earth history. As it occurred in an aragonite sea time, the CPE may constitute a case study for ocean acidification for a seawater chemistry not as far from that of the present as those of better

studied Cretaceous and Paleogene events.

4.7 Conclusions. II - A possible mechanism for massive resin exudation?

Along with CO_2, volcanic eruptions emit SO_2 that is volumetrically significant to have sensible effects on environments. SO_2 is a greenhouse gas that triggers an initial climate warming sudden after the eruption and a climate cooling due to the formation of sulfate aerosols in a longer timescale (Wignall 2001). One consequence of SO_2 release is the formation of acid rains that can severely damage the environments. As testified by last century large forest damage and decline due to industrialization, plants subject to acid rains are more stressed and vulnerable (Schulze 1989). Some plants produce resin in response to wounding, as mechanical injury, fires, pathogens and herbivores attack (Henwood 1993). The exceptional plant resin exudation during the CPE, testified by several coeval amber deposits around the world (Gianolla et al., 1998; Roghi et al., 2006) (Fig 1.2), may be related to the effect of extensive plant stress due to widespread acid rainfalls as consequence of large volcanic SO_2 emissions into the Carnian atmosphere. Unfortunately, there is no evidence for a link between acid rains and increasing resin exudation in modern environments and the poorly dated amber-bearing deposits of the Cretaceous cannot be unequivocally correlated to episodes of intense volcanisms. A number of other climatic or biological mechanisms could have been triggered massive resin exudation, such as wounding due to intense storm and rains, widespread fire episodes, the bloom of new wood boring insects etc. Concerning Carnian amber, another intriguing factor to take into account is that conifers, the group of plants to which Dibona amber was attributed (see chapter 2), appeared and radiated during the Late Triassic so there could be a link between massive resin production and the early stage of conifer evolution. Surely, there is a lack of studies on recent resin exudation mechanisms so it is not possible to disprove none of these hypotheses. However, the link between huge amber deposits and the CPE is unequivocal and a causal relationship must exist.

5. CONCLUSIONS

- Triassic amber, wood and leaf $\partial^{13}C$ values lie in a large range within the same beds (~ 2-5‰). Carnian ambers have $\partial^{13}C$ values similar to the associated wood but with a larger range of variability than wood and leaves. These restricted wood and leaf $\partial^{13}C$ ranges can be explained by selective degradation of plant OM during the fossilization processes.
- Despite the high variability, wood and leaf $\partial^{13}C$ values register a positive trend between the Middle and early Late Triassic that is consistent with existing marine inorganic carbon-isotope data from skeletal calcite. This parallel trend suggests that Triassic brachiopod calcite and marine carbonates faithfully registered the secular carbon-isotope evolution of the ocean–atmosphere system.
- The range of values in Triassic amber $\partial^{13}C$ is comparable with that obtained for recent resins. Thermogravimetric analyses coupled with C-isotope measurements show that alteration processes doesn't change the $\partial^{13}C$ of amber even if it caused important transformations of the main components. Data suggest that the pristine carbon-isotope signature is not altered by resin maturation during diagenesis, unlike other plant-derived materials as wood and leaves.
- Cretaceous $\partial^{13}C_{amber}$ data register secular trends consistent with inorganic carbonate C-isotopes data. Our results show that amber is potentially a very solid tool for C-isotopes – based studies with palaeoenvironmental, palaeoclimatic and stratigraphic purposes. However, the age of amber deposits must be better constrained than it is currently done.
- Biomarker and non-biomarker maturity parameters show that extracted lipids have

experienced a moderate thermal maturation and that the source of OM was mostly terrestrial. Long chain n-alkanes (n-C_{25-33}) show an odd-over-even distribution that is typical of an higher-plant source.

- N-alkanes have $\partial^{13}C$ values ranging from -21.08‰ to -30.97‰. Odd n-C_{25-33} n-alkanes have C-isotope values in the range expected for C_3 plant and are more depleted in ^{13}C than bulk wood coming from the same stratigraphic layers, in agreement with $\partial^{13}C$ measurements of Recent material. $\partial^{13}C$ of n-C_{25-33} is also more depleted than $\partial^{13}C_{TOC}$. The C-isotope offset of n-alkenes vs TOC increases as values become more depleted.
- Isoprenoids $\partial^{13}C$ range from -23.17‰ to -33.5‰. Difference between the C-isotope signature of pristane and phytane can be explained by different sources.
- N-alkanes and isoprenoids draw a positive secular C-isotope shift during the latest Ladinian - early Carnian interval that is consistent with $\partial^{13}C_{wood}$ and marine carbonates.
- An abrupt negative $\partial^{13}C$ shift is registered by all extracted n-alkanes and isoprenoids within the *A. austriacum* ammonoid subzone.
- The discovery of an intense, rapid negative carbon isotope excursion (CIE) sheds light on the nature of the CPE and lines it up to the major known climatic perturbations of the Mesozoic and Cenozoic. This CIE is here linked to the eruption of Wrangellia LIP: new tessera is offered to support the link between LIP onset and global climate changes in Earth history. As it occurred in a aragonite sea time, the CPE may constitute a case study for ocean acidification for a seawater chemistry not as far from that of the present as those of better studied Cretaceous and Paleogene events.
- Massive amber exudation during the CPE could have been triggered by acid rains formed as a consequence of SO_2 release from Wrangellia volcanism. This hypothesis requires more data.

6. REFERENCES

Anderson, K.B., Winans, R.E., Botto, R.E., 1992. The nature and fate of natural resins in the geosphere – II. Identification, classification and nomenclature of resinites. Organic Geochemistry 18, 829-841.

Ansorge J., 2007. Upper Triassic insects and amber from Leshoto (South Africa). IV International Congress FossilX3, 4-9 May, Victoria-Gasteiz, Spain, abstract book, p. 52.

Arens, N.C., Jahren, A.H., 2000. Carbon Isotope Excursion in Atmospheric CO_2 at the Cretaceous-Tertiary Boundary: Evidence from Terrestrial Sediments. Palaios 15, 314-322.

Arens, N.C., Jahren, A.H., Amundson, R., 2000. Can C_3 plants faithfully record the carbon isotopic composition of atmospheric dioxide?. Paleobiology 26, 137-164.

Badeck, F.W., Tcherkez, G., Nogues, S., Piel, C., Ghashghaie, J., 2005. Post-photosynthetic fractionation of stable carbon isotopes between plant organs - a widespread phenomenon. Rapid Communications in Mass Spectrometry 19, 1381-1391.

Barclay, R.S., McElwain, J.C., Sageman, B.B., 2010. Carbon sequestration activated by a volcanic CO_2 pulse during Ocean Anoxic Event 2. Nature Geoscience 3, 205-208.

Bechtel, A., Reinhard Gratzer, R., Sachsenhofer, R.F., Gusterhuber, J., Lücke, A., Püttmann, W., 2008. Biomarker and carbon isotope variation in coal and fossil wood of Central Europe through the Cenozoic. Palaeogeography, Palaeoclimatology, Palaeoecology 262, 166-175.

Beerling, D.J., Jolley, D.W., 1998. Fossil plants record an atmospheric $^{12}CO_2$ and temperature spike across the Palaeocene-Eocene transition in NW Europe. Journal of the Geological Society 155, 591-594.

Benner, R., Fogel, M.L., Sprague, E.K., Hodson, R.E., 1987. Depletion of ^{13}C in lignin and its

implications for stable carbon isotope studies. Nature 329, 708-710.

Bi, X., Sheng, G., Liu, S., Li, C., Fu, J., 2005. Molecular and carbon and hydrogen isotopic composition of n-alkanes in plant leaf waxes. Organic Geochemistry 36, 1405–1417.

Bizzarini, F., Gnoli, M., 1991. Trematoceras elegans (Munster) and other Late Triassic cephalopods from the San Cassiano Formation, Eastern Dolomites (Italy). Bollettino della Società Paleontologica Italiana 30, 109-116.

Bowen, G.J., Beerling, D.J., Koch, P.J., Zachos, J.C., Quattlebaum, T., 2004. A humid climate state during the Palaeocene/Eocene thermal maximum. Nature, 432, 495-498.

Breda, A., Preto, N., Roghi, G., Furin, S., Meneguolo, R., Ragazzi, E., Fedele, P., Gianolla, P., 2009. The Carnian Pluvial Event in the Tofane area (Cortina D'Ampezzo, Dolomites, Italy). Geo.Alp 6, 80-115.

Broglio-Loriga, C., Fugagnoli, A., Van Konijnenburg – van Cittert, J.H.A., Kustatscher, E., Posenato, R., Wachtler, M. 2002. The Anisian Macroflora from the Northern Dolomites (Kühwiesenkopf / Monte Pra della Vacca, Braies): a first report. Rivista Italiana di Paleontologia e Stratigrafia 108 (3), 381-389.

Budai, T., Csasza, R.G., Csillag, G., Dudko, A., Kolosza, R.L., Majoros, G., 1999. A Balaton-Felvidek Földtana. Geological Institute of Hungary, Budapest, 257 p.

Cernusak, L.A, Tcherkez, G., Keitel, C., Cornwell, W.K., Santiago, L.S., Knohl, A., Barbour, M.M., Williams, D.G., Reich, P.B., Ellsworth, D.S., Dawson, T.E., Griffiths, H.G., Farquhar, G.D., Wright, I.J., 2009. Why are non-photosynthetic tissues generally ^{13}C enriched compared with leaves in C_3 plants? Review and synthesis of current hypotheses. Functional Plant Biology 36, 199-213.

Chikaraishi, Y., Naraoka, H., 2003. Compound-specific ∂D–$\partial^{13}C$ analyses of n-alkanes extracted from terrestrial and aquatic plants. Phytochemistry 63, 361–371.

Collister, J.W., Rieley, G., Stern, B., Eglinton, G., Fry, B., 1994. Compound-specific $\partial^{13}C$ analyses of leaf lipids from plants with differing carbon dioxide metabolisms. Organic Geochemistry 21, 619–627.

Colombi, C.A., Parrish, J.T., 2008. Late Triassic environmental evolution in southwestern Pangea: plant taphonomy of the Ischigualasto Formation. Palaios 23,. 778–795.

Courtillot, V.E., Renne, P.R., 2003. On the age of flood basalts events. Comptes Rendus Geoscience,

335, 113-140.

Czimczika, C.I., Prestonb, C.M, Schmidtc, M.W.I., Wernera, R.A., Schulze, E.D., 2002. Effects of charring on mass, organic carbon, and stable carbon isotope composition of wood. Organic Geochemistry 33 (2002) 1207–1223.

Dal Corso, J., Preto, N., Kustatscher, E., Mietto, P., Roghi, G., Jenkyns, H.C., accepted. Carbon-isotope variability of Triassic amber, as compared with wood and leaves (Southern Alps, Italy). Palaeogeography, Palaeoclimatology, Palaeoecology.

Dawson, T.E., Mambelli, S., Plamboeck, A.H., Templer, P.H., Tu, K.P., 2002. Stable Isotopes in Plant Ecology. Annual Review of Ecology and Systematics 33, 507-559.

De Zanche, V., Gianolla, P., Mietto, P., Siorpaes, C., Vail, P.R., 1993. Triassic sequence stratigraphy in the Dolomites (Italy). Memorie di Scienze Geologiche, 45, 1-27.

Delclòs, X., Arillo, A., Penalver, E., Barròn, E., Soriano, C., Del Valle, R.L., Bernàrdez, E., Corral, C., Ortuno, V.M., 2007 Fossiliferous amber deposits from the Cretaceous (Albian) of Spain. C. R. Palevol 6 (2007) 135–149.

Dickens, G.R., O'Neil, J.R., Rea, D.K., Owen, R.M., 1995. Dissociation of oceanic methane hydrates as a cause of the carbon isotope excursion at the end of the Paleocene. Paleoceanography 10, 965-971.

Erba, E., 2006. The first 150 million years history of calcareous nannoplankton: Biosphere–geosphere interactions. Palaeogeography, Palaeoclimatology, Palaeoecology 232, 237–250.

Erba, E., Bottini, C., Weissrt, H., Keller, C.E., 2010. Calcareous Nannoplankton Response to Surface-Water Acidification Around Oceanic Anoxic Event 1a. Science 329, 428-432.

Farquhar, G.D., Ehleringer, J. R., Hubick, K. T., 1989. Carbon isotope discrimination and photosynthesis. Annual Review of Plant Physiology and Plant Molecular Biology, 40, 503-538.

Ferrio, J.P., Alonso, N., Lopez, J.B., Araus, J.L., Voltas, J., 2006. Carbon isotope composition of fossil charcoal reveals aridity changes in the NW Mediterranean Basin. Global Change Biology 12, 1253–1266.

Föllmi et al. (2006) Interactions between environmental change and shallow water carbonate buildup along the northern Tethyan margin and their impact on the Early Cretaceous carbon isotope record. Paleoceanography 21, doi:10.1029/2006PA001313.

Freeman, K.H., Colarusso, L.A., 2001. Molecular and isotopic records of C_4 grassland expansion in the late Miocene. Geochimica et Cosmochimica Acta 65, 1439–1454.

Furin, S., Preto, N., Rigo, M., Roghi, M., Gianolla, P., Crowley, J.L., Bowring, S.A., 2006. High-precision U-Pb zircon age from the Triassic of Italy: Implications for the Triassic time scale and the Carnian origin of calcareous nannoplankton and dinosaurs. Geology 34, 1009-1012.

Gábor, C., and Földvári, M., 2005. Upper Triassic amber fragments from the Balaton Highland, Hungrary. A Magyar Állami Földtani Intézet Évi Jelentése, 2005, 37-46.

Gianolla, P., Ragazzi, E., Roghi, G., 1998. Upper Triassic amber from the Dolomites (northern Italy). A paleoclimatic indicator? Rivista Italiana di Paleontologia e Stratigrafia 104, 381–390.

Greene, A.R., Scoates, J.S., Weis, D., Katvala, E.C., Israel, S., Nixon, G.T., 2010. The architecture of oceanic plateaus revealed by the volcanic stratigraphy of the accreted Wrangellia oceanic plateau. Geosphere 6, 47-73.

Gröcke, D.R., 1998. Carbon-isotope analyses of fossil plants as a chemostratigraphic and palaeoenvironmental tool. Lethaia 31, 1-13.

Gröcke, D.R., 2002. The carbon isotope composition of ancient CO_2 based on higher-plant organic matter. Philosophical Transaction of the Royal Society A 360, 633-658.

Gröcke, D.R., Hesselbo, S.P., Jenkyns, H.C., 1999. Carbon-isotope composition of Lower Cretaceous fossil wood: Ocean-atmosphere chemistry and relation to sea-level change. Geology 27, 155-158.

Guehl, J.M., Domenach, A.M., Bereau, M., Barigah, T.S., Casabianca, H., Ferhi, A., Garbaye, J., 1998. Functional diversity in an Amazonian rainforest of French Guyana: a dual isotope approach (∂^{15}N and ∂^{13}C). Oecologia 116, 316-330.

Hall, G., Woodborne, S., Scholes, M., 2008. Stable carbon isotope ratios from archaeological charcoal as palaeoenvironmental indicators. Chemical Geology 247, 384–400.

Handley, L., Pearson, P.N., McMillan, I.K., Pancost, R.D., 2008. Large terrestrial and marine carbon and hydrogen isotope excursions in a new Paleocene/Eocene boundary section from Tanzania. Earth and Planetary Science Letters 275, 17–25.

Hansen, H.J., 2006. Stable isotopes of carbon from basaltic rocks and their possible relation to atmospheric isotope excursions. Lithos 92, 105–116.

Hardie, L.A., 1996. Secular variation in seawater chemistry: An explanation for the coupled secular

variation in the mineralogies of marine limestones and potash evaporites over the past 600 m.y. Geology 24, 279-283.

Hasiuk, F.J., Lohmann, K.C., 2010. Application of calcite Mg partitioning functions to the reconstruction of paleocean Mg/Ca. Geochimica et Cosmochimica Acta 74, 6751–6763.

Henwood, A., 1993. Recent plant resin and the taphonomy of organisms in amber: a review. Modern Geology 19, 35-59.

Hesselbo, S., Jenkyns, H.C., Duarte, L.V., Oliveira, L.C.V., 2007. Carbon-isotope record of the Early Jurassic (Toarcian) Oceanic Anoxic Event from fossil wood and marine carbonate (Lusitanian Basin, Portugal). Earth and Planetary Science Letters 253, 455-470.

Hesselbo, S.P., Grocke, D.R., Jenkyns, H.C., Bjerrum, C.J., Farrimond, P., Morgans Bell, H.S., Green, O.R., 2000. Massive dissociation of gas hydrate during a Jurassic oceanic anoxic event. Nature 406, 392-395.

Hesselbo, S.P., Morgans-Bell, H.S., McElwain, J.C., Rees, P.M., Robinson, S.A., Ross, C.E., 2003. Carbon-Cycle Perturbation in the Middle Jurassic and Accompanying Changes in the Terrestrial Paleoenvironment. The Journal of Geology 111, 259-276.

Hochuli, P.A., Vigran, J.O., 2010. Climate variations in the Boreal Triassic — Inferred from palynological records from the Barents Sea. Palaeogeography, Palaeoclimatology, Palaeoecology 290, 20–42.

Hornung, T., Brandner, R., 2005. Biochronostratigraphy of the Reingraben Turnover (Hallstatt Facies Belt): Local black shale events controlled by regional tectonics, climatic change and plate tectonics. Facies 51, 460-479.

Jahren, A.H., 2004. The carbon stable isotope composition of pollen. Review of Palaeobotany and Palynology 132, 291-313.

Jahren, A.H., Arens, N.C., 2009. Prediction of atmospheric $\partial^{13}CO_2$ using plant cuticle isolated from fluvial sediment: tests across a gradient in salt content. Palaios 24, 394-401.

Jahren, A.H., Arens, N.C., Harbeson, S.A., 2008. Prediction of atmospheric $\partial^{13}CO_2$ using fossil plant tissues. Review of Geophisics 46, RG1002, doi:10.1029/2006RG000219.

Jahren, A.H., Arens, N.C., Sarmiento, G., Guerrero, J., Amundson, R., 2001. Terrestrial record of methane hydrate dissociation in Early Cretaceous. Geology 29, 159-162.

Jahren, A.H., Byrne, M.C., Graham, H.V., Sternberg, L.S.L., Summons, R.E., 2009. The environmental water of the middle Eocene Arctic: Evidence from ∂D, $\partial^{18}O$ and $\partial^{13}C$ within specific compounds. Palaeogeography, Palaeoclimatology, Palaeoecology 271, 96-103.

Jahren, A.H., Conrad, C.P., Arens, N.C., Mora, G., Lithgow-Bertelloni, C., 2005. A plate tectonic mechanism for methane hydrate release along subduction zones. Earth and Planetary Science Letters 236, 691–704.

Jarvis, I., Mabrouk, A., Moody, R.T.J., de Cabrera, S., 2002. Late Cretaceous (Campanian) carbon isotope events, sea-level change and correlation of the Tethyan and Boreal realms. Palaeogeography, Palaeoclimatology, Palaeoecology 188, 215-248.

Jenkyns, H.C., 2010. Geochemistry of oceanic anoxic events. Geochemistry, Geophysics, Geosystems, 11, Q03004, doi:10.1029/2009GC002788.

Jones, T.P., Chaloner, W.G., 1991. Fossil charcoal, its recognition and palaeoatmospheric significance. alaeogeography, Palaeoclimatology, Palaeoecology 97, 39-50.

Kelber, K.P., Hansch W., 1996. Keuperpflanzen Die Enträtselung einer über 200 Millionen Jahre alten Flora. Museo, 11, 1-157, Heillbronn.

Killops, S., Killops, V., 2005. Introduction to Organic Geochemistry – Second Edition. Blackwell Publishing, 393pp.

Koken, E., 1913. Kenntnis der Schichten von Heiligenkreuz (Abteital, Südtirol): Abhandlungen der Kaiserlich-Königlichen Geologischen Reichsanstalt 16, 1–43.

Körner, C., Farquhar, G.D., Wong, S.C., 1991. Carbon isotope discrimination by plants follows latitudinal and altitudinal trends. Oecologia 88, 30-40.

Korte, C., Kozur, H., Veizer, J., 2005. $\partial^{13}C$ and $\partial^{18}O$ values of Triassic brachiopods and carbonate rocks as proxies for coeval seawater and palaeotemperature. Palaeogeography, Palaeoclimatology, Palaeoecology 226, 287-306.

Kustatscher, E., Manfrin, S., Mietto, P., Posenato, R., Roghi, G., 2006. New biostratigraphic data on Anisian (Middle Triassic) palynomorphs from the Dolomites, Italy. Review of Palaeobotany and Palynology 140, 79-90.

Lambert, J.B., Santiago-Blay, J.A., Anderson, K.B., 2008. Chemical Signatures of Fossilized Resins and Recent Plant Exudates. Angewandte Chemie International Edition 47, 9608-9616.

Lassiter, J.C., DePaolo, D.J., and Mahoney, J.J., 1995. Geochemistry of the Wrangellia flood basalt province: Implications for the role of continental and oceanic lithosphere in flood basalt genesis: Journal of Petrology 36, 983–1009.

Leavitt, S.W., Long, A., 1982. Evidence for $^{13}C/^{12}C$ fractionation between tree leaves and wood. Nature 298, 42-744.

Litwin, R.J., Ash, S.R., 1991. 1st Early Mesozoic amber in the western emisphere. Geology 19, 273-276.

Loader, N.J., Hemming, D.L., 2004. The stable isotope analysis of pollen as an indicator of terrestrial palaeoenvironmental change: a review of progress and recent developments. Quaternary Science Reviews 23, 893-900.

Loader, N.J., Robertson, I., McCarroll, D., 2003. Comparison of stable carbon isotope ratios in the whole wood, cellulose and lignin of oak tree-rings. Palaeogeography, Palaeoclimatology, Palaeoecology 196, 395-407.

Magaritz, M., Bär, R., Baud, A., Holser, W.T., 1988. The carbon-isotope shift at the Permian–Triassic boundary in the southern Alps is gradual. Nature 331, 337–339.

Martinez, R.N., Sereno, P.C., Alcober, O.A., Colombi, C.E., Renne, P.R., Montanez, I.P., Currie, B.S., 2011. A basal dinosaur from the down of the dinosaur era in southwestern Pangea. Science 331, 206-210.

Marzoli, A., Bertrand, H., Knight, K.B., Cirilli, S., Buratti, N., Vérati, C., Nomade, S., Renne, P.R., Youbi, N., Martini, R., Allenbach, K., Neuwerth, R., Rapaille, C., Zaninetti, L., Bellieni, G., 2004. Synchrony of the Central Atlantic magmatic province and the Triassic–Jurassic boundary climatic and biotic crisis. Geology 32, 973–976.

McCartney, K., Huffman, A.R., Tredoux, M., 1990. A paradigm for endogenous causation of mass extinctions. In: Sharpton, V.L., Ward, P.D., Global Catatrophes in Earth history. Geological Society of America, Special Paper 247, 125 – 138.

Mckellar, R.C., Wolfe, A.P., Tappert, R., Muehlenbachs, K., 2008. Correlation of Grassy Lake and Cedar Lake ambers using infrared spectroscopy, stable isotopes, and palaeontomology. Canadian Journal of Earth Sciences 45, 1061-1082.

Mietto, P, Andreetta, R., Broglio Loriga, C., Buratti, N., Cirilli, S., De Zanche, V., Furin, S., Gianolla,

P., Manfrin, S., Muttoni, G., Neri, C., Nicora, A., Posenato, R., Preto, N., Rigo, M., Roghi, G., Spötl C., 2007. A Candidate Of The Global Boundary Stratotype Section And Point For The Base Of The Carnian Stage (Upper Triassic): GSSP at the base of the canadensis Subzone (FAD of Daxatina) in the Prati di Stuores/Stuores Wiesen section (Southern Alps, NE Italy). Albertiana 36, 78-101.

Mietto, P., Manfrin, S., Preto, N., Gianolla, P., 2008. Selected ammonoid fauna from Prati di Stuores/ Stuores Wiesen and related sections across the Ladinian-Carnian boundary (Southern Alps, Italy). Rivista Italiana di Paleontologia e Stratigrafia 114, 377-429.

Mortensen, J.K., and Hulbert, L.J., 1992, A U-Pb zircon age for a Maple Creek gabbro sill, Tatamagouche Creek area, southwestern Yukon Territory, in Radiogenic age and isotopic studies: Report 5: Geological Survey of Canada Paper 91-2, 175–179.

Murray, A.P., Edwards, D., Hope, J.M., Boreham, C.J., Booth, W.E., Alexander, R.A., Summons, R.E., 1998. Carbon isotope biogeochemistry of plant resins and derived hydrocarbons. Organic Geochemistry 29, 1199-1214.

Murray, A.P., Padley, D., McKirdy, D.M., Booth, W.E., Summons, R.E., 1994. Oceanic transport of fossil dammar resin: The chemistry of coastal resinites from South Australia. Geochimica et Cosmochimica Acta 58, 3049-3059.

Nissenbaum, A., Yakir, D., 1995. Stable isotope composition of amber, in Amber, resinite, and fossil resins (eds. K. B. Anderson and J. C. Crelling). ACS Symposium series, American Chemical Society, Washington DC, pp. 32–42.

O'Malley, V.P., Burke, R.A., Schlotzhauer, W.S., 1997. Using GC-MS/Combustion/IRMS to determine the $^{13}C/^{12}C$ ratios of individual hydrocarbons produced from the combustion of biomass materials - application to biomass burning. Organic geochemistry 27, 567-581.

Pagani, M., Caldeira, K., Archer, D., Zachos, J.C., 2006. an ancient carbon mystery. Science 314, 1156-1157.

Pancost, R.D., Boot, C.S., 2004. The palaeoclimatic utility of terrestrial biomarkers in marine sediments. Marine Chemistry 92, 239–261.

Parrish, J.T., 1993. Climate of the supercontinent Pangea. Journal of Geology 101, 215–233.

Parrish, R.R., and McNicoll, V.J., 1992, U-Pb age determinations from the southern Vancouver

Island area, Brit- ish Columbia, in Radiogenic age and isotopic studies, Report 5: Geological Survey of Canada Paper 91-2, 79–86.

Peñalver, E., Delclos, X., Soriano, C., 2007. A new rich amber outcrop with palaeobiological inclusions in the Lower Cretaceous of Spain. Cretaceous Research 28, 791-802.

Peters, K., Walters, C.C., Moldowan, J.M., 2005. The Biomarker Guide – Second Edition. Cambridge University Press, 1155pp.

Pichler, A., 1868, Beiträge zur Geognosie Tirols. XI. Fossiles Harz. Jahrbuch der Kaiserlich-Königlichen Geologischen Reichsanstalt, v. 18, p. 45-52.

Poole, I., Dolezych, M., Kool, J., van der Burgh, J., van Bergen, P.F., 2006. Do stable carbon isotopes of brown coal woods record changes in Lower Miocene palaeoecology? Palaeogeography, Palaeoclimatology, Palaeoecology 236, 345–354.

Preto, N., Hinnov, L., 2003; Unraveling the origin of carbonate platform cyclothems in the Upper Triassic Durrenstein Formation (Dolomites, Italy). Journal of Sedimentary Research 73, 774–789.

Preto, N., Kustatscher, E., Wignall, P.B., 2010. Triassic climates – State of the art and perspectives. Palaeogeography, Palaeoclimatology, Palaeoecology 290, 1–10.

Preto, N., Spötl, C., Guaiumi, C., 2009. Evaluation of bulk carbonate $\partial^{13}C$ data from Triassic hemipelagites and the initial composition of carbonate mud. Sedimentology 56, 1329-1345.

Preto, N., Spötl, C., Mietto, P., Gianolla, P., Riva, A., Manfrin, S., 2005. Aragonite dissolution, sedimentation rates and carbon isotopes in deep-water hemipelagites (Livinallongo Formation, Middle Triassic, northern Italy). Sedimentary Geology 181, 173-194.

Prochnow, S.J., Nordt, L.C., Atchley, S.C., Hudec, M.R., 2006. Multi-proxy paleosol evidence for Middle and Late Triassic climate trends in eastern Utah. Palaeogeography, Palaeoclimatology, Palaeoecology 232, 53–72.

Ragazzi, E., Giaretta, A., Perrichot, V., Neraudeau D., Schmidt, A., Roghi, G., 2009. Thermal analysis of Cretaceous ambers from southern France. Geodiversitas 31, 163-175.

Ragazzi, E., Roghi, G., Giaretta, A., Gianolla, P., 2003. Classification of amber based on thermal analysis. Thermochimica Acta 404, 43-54.

Rampino, M.R., 2010. Mass extinctions of life and catastrophic flood basalt volcanism. Proceedings of the National Academy of Science 107, 6555-6556.

Retallack, G.J., Jahren, H.A., 2008. Methane Release from Igneous Intrusion of Coal during Late Permian Extinction Events. The Journal of Geology 116, 1-20.

Ries, J.B., 2010. Review: geological and experimental evidence for secular variation in seawater Mg/Ca (calcite-aragonite seas) and its effects on marine biological calcification. Biogeosciences 7, 2795–2849.

Rigo, M., Preto, N., Roghi, G., Tateo, F., Mietto, P., 2007. A rise in the Carbonate Compensation Depth of western Tethys in the Carnian (Late Triassic): Deep-water evidence for the Carnian Pluvial Event. Palaeogeography, Palaeoclimatology, Palaeoecology 246, 188–205.

Robinson, S.A., Hesselbo, S.P., 2004. Fossil-wood carbon-isotope stratigraphy of the non-marine Wealden Group (Lower Cretaceous, southern England). Journal of the Geological Society 161, 133-145.

Rogers, R.R., Swisher, C.C., III, Sereno, P.C., Monetta, A.M., Forster, C.A., Martinez, R.N., 1993, The Ischigualasto tetrapod assemblage (Late Triassic, Argentina) and $^{40}Ar/^{39}Ar$ dating of dinosaur origins: Science 260, 794–797.

Roghi, G., Ragazzi, E., Dal Corso, J., Giaretta, A., Jenkyns, H.C., Soriano, C., Delclos, X., in prep. Physico-chemical investigation of Albian (Early Cretaceous) San Just amber (Escucha Formation, Spain).

Roghi, G., 2004. Palynological investigations in the Carnian of the Cave del Predil area (Julian Alps, NE Italy). Review of Palaeobotany and Palynology 132, 1–35.

Roghi, G., Gianolla, P., Minarelli, L., Pilati, C., Preto, N., 2010. Palynological correlation of Carnian humid pulses throughout western Tethys. Palaeogeography, Palaeoclimatology, Palaeoecology 290, 89–106.

Roghi, G., Ragazzi, E., Gianolla, P., 2006. Triassic Amber of the Southern Alps. Palaios 21,143-154.

Rohde, A., Muller, R.A., 2005. Cycles in fossil siversity. Nature 434, 208-210.

Rundgren, M., Loader, N.J., Hammarlund, D., 2003. Stable carbon isotope composition of terrestrial leaves: inter- and intraspecies variability, cellulose and whole-leaf tissue difference, and potential for climate reconstruction. Journal of Quaternary Science 18, 583–590.

Schlager, W., Schöllnberge, W., 1974. Das Prinzip stratigraphischer Wenden in der Schichtfolge der

Nördlichen Kalkalpen. Mitt. Geol. Ges. 66–67, 165–193.

Schoell, M., Simoneit, B.R.T., Wang, T.G., 1994. Organic geochemistry and coal petrology of Tertiary brown coal in Zhoujing mine, Baise Basin, South China – 4. Biomarker sources inferred from stable carbon isotope composition of individual compounds. Organic Geochemistry 21, 713-719.

Schulze, E.D., 1989. Air pollution and forest decline in a Spruce (Picea abies) forest. Science 244, 776-783.

Sigmund, A., 1937. Die Minerale Niederösterreichs. 2nd ed.: Deuticke, Wien-Leipzig, 247 p.

Simms & Ruffell, 1989 Simms, M.J., and Ruffell, A.H., 1989, Synchroneity of climatic change and extinctions in the Late Triassic. Geology 17, 265–268.

Simms, M.J., Ruffel, A.H., Johnson, L.A., 1995. Biotic and climatic changes in the Carnian (Triassic) of Europe and adjacent areas. In: Fraser, N.C., Sues, H.-D. (Eds.), In the Shadow of the Dinosaurs: Early Mesozoic Tetrapods. Cambridge University Press, pp. 352–365.

Simms, M.J., Ruffell, A.H., 1990. Climatic and biotic change in the late Triassic. Journal of the Geological Society of London 147, 321–327.

Sluggett, C.L., 2003, Uranium-lead age and geochemical constraints on Paleozoic and early Mesozoic magma- tism in Wrangellia Terrane, Saltspring Island, British Columbia [B.Sc. thesis]: Vancouver, University of British Columbia, 84 p.

Smith, F.A., Wing, S.L., Freeman, K.H., 2007. Magnitude of the carbon isotope excursion at the Paleocene–Eocene thermal maximum: The role of plant community change. Earth and Planetary Science Letters 262, 50–65.

Soom, M., 1984. Bernstein vom Nordrand der Schweizer Alpen: Stuttgarter Beiträge zur Naturkunde, Serie C 18, 15-20.

Stanley Jr., G.D., 1988. The history of early Mesozoic reef communities: a three-step process. Palaios 3, 170–183.

Stanley Jr., G.D., 2003. The evolution of modern corals and their early history. Earth-Sci. Rev. 60, 195–225.

Stanley, S.M., Hardie, L.A., 1998. Secular oscillations in the carbonate mineralogy of reef-building and sediment-producing organisms driven by tectonically forced shifts in seawater chemistry

Palaeogeography, Palaeoclimatology, Palaeoecology 144, 3-19.

Stefani, M., Furin, S., Gianolla, P., 2010. The changing climate framework and depositional dynamics of Triassic carbonate platforms from the Dolomites. Palaeogeography, Palaeoclimatology, Palaeoecology 290, 43–57.

Stern, B., Lampert Moore, C.D., Heron, C., Pollard, A.M., 2008. Bulk stable light isotopic ratios in recent and archaeological resins: towards detecting the transport of resins in antiquity? Archaeometry 50, 351-370.

Taylor, T.N., Taylor, E.L., Krings, M., 2009. Paleobotany - The Biology and Evolution of Fossil Plants, Second Edition. Academic Press, Elsevier, 1230p.

Tipple, B.J., Pagani, M., 2007. The early origin of terrestrial C_4 photosynthesis. Annual Review of Earth and Planetary Sciences 35, 435-461.

Tipple, B.J., Pagani, M., 2007. The early origins of Terrestrial C_4 Photosynthesis. Annual Review of Earthand Planetary Science 35, 435-461.

Tozer, E.T., 1994. Canadian Triassic ammonoid faunas. Geological Survey of Canada, Bulletin 467.

van Bergen, P.F., Poole, I., 2002. Stable carbon isotopes of wood: a clue to palaeoclimate? Palaeogeography, Palaeoclimatology, Palaeoecology 182, 31-45.

van de Schootbrugge, B., Payne, J. L., Tomasovych, A., Pross, J., Fiebig, J., Benbrahim, M., Foellmi, K. B., Quan, T. M., 2008. Carbon cycle perturbation and stabilization in the wake of the Triassic-Jurassic boundary mass-extinction event. Geochemistry, Geophysics Geosystems 9, Q04028, doi:10.1029/2007GC001914.

Vávra, N., 1984. "Reich an armen Fundstellen": Übersicht über die fossilen Harze Österreichs. Stuttgarter Beiträge zur Naturkunde, Serie C, v. 18, pp. 9-14.

Walker, J.D., Geissman, J.W., compilers, 2009, Geologic Time Scale: Geological Society of America, doi: 10.1130/2009.CTS004R2C. ©2009 The Geological Society of America.

Whiteside, J.H., Olsen, P.E., Eglinton, T., Brookfield, M.E., Sambrotto, R.N., 2010. Compound-specific carbon isotopes from Earth's largest flood basalt eruptions directly linked to end-Triassic mass extinction. Proceedings of the National Academy of Science 107, 6721-6725.

Wignall, P.B., 2001. Large igneous provinces and mass extinctions. Earth-Science Reviews 53, 1–

33.

Wignall, P.B., Sun, Y., Bond, D.P.G, Izon, G., Newton, R.J., Védrine, S., Widdowson, M., Ali, J.R., Lai, X., Jiang, H., Cope, H., Bottrell, S.H., 2009. Volcanism, Mass Extinction, and Carbon Isotope Fluctuations in the Middle Permian of China. Science 324, 1179-1182.

Xie, S., Pancost, R.D., Huang, X., Jiao, D., Lu, L., Huang, J., Yang, F., Evershed, R.P., 2007. Molecular and isotopic evidence for episodic environmental change across the Permo/Triassic boundary at Meishan in South China. Global and Planetary Change 55, 56–65.

Yans, J., Gerards, T., Gerrienne, P., Spagna, P., Dejax, J., Schnyder, J., Storme, J., Keppens, E., 2010. Carbon-isotope analysis of fossil wood and dispersed organic matter from the terrestrial Wealden facies of Hautrage (Mons Basin, Belgium), Palaeogeography, Palaeoclimatology, Palaeoecology 291, 85-105.

Zachos, J.C., Rohl, U., Schellenberg, S.A., Sluijs, A., Hodell, D.A., Kelly, D.C., Thomas, E., Nicolo, M., Raffi, I., Lourens, L.J., McCarren, Dick Kroon, D., 2005. Rapid Acidification of the Ocean During the Paleocene-Eocene Thermal Maximum. Science 308, 1611-1615.

APPENDIX

STU00

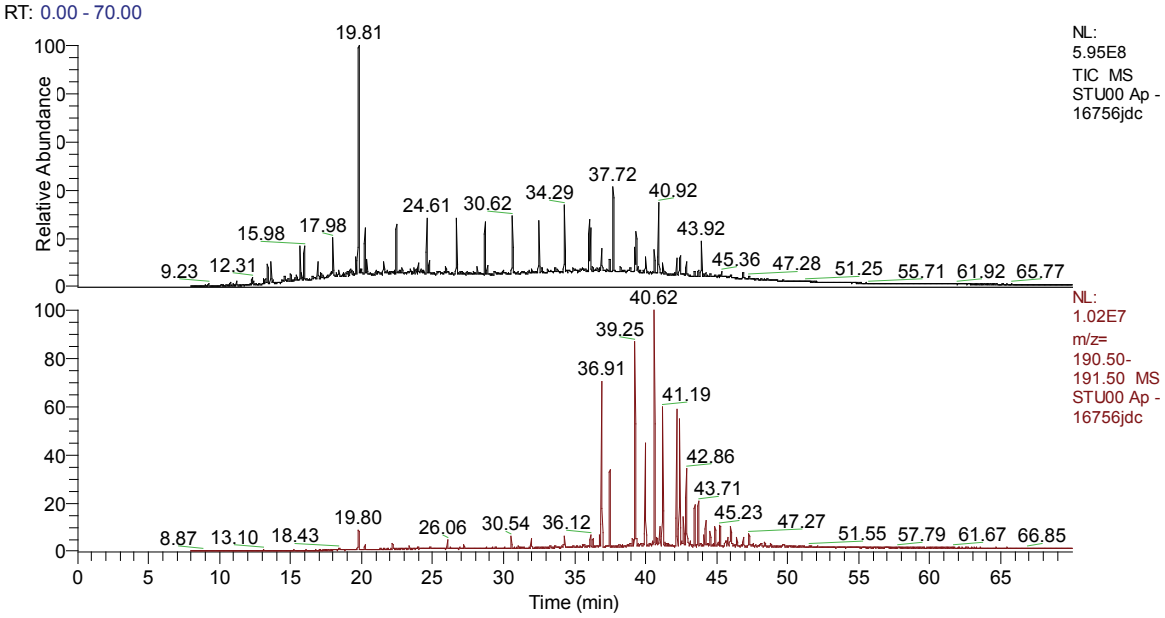
RT: 0.00 - 70.00
Relative Abundance
Time (min)
NL:
5.95E8
TIC MS
STU00 Ap -
16756jdc
NL:
1.02E7
m/z=
190.50-
191.50 MS
STU00 Ap -
16756jdc
19.81
15.98
17.98
24.61
30.62
34.29
37.72
40.92
43.92
9.23
12.31
45.36
47.28
51.25
55.71
61.92
65.77
40.62
39.25
36.91
41.19
42.86
43.71
45.23
47.27
8.87
13.10
18.43
19.80
26.06
30.54
36.12
51.55
57.79
61.67
66.85

STU05

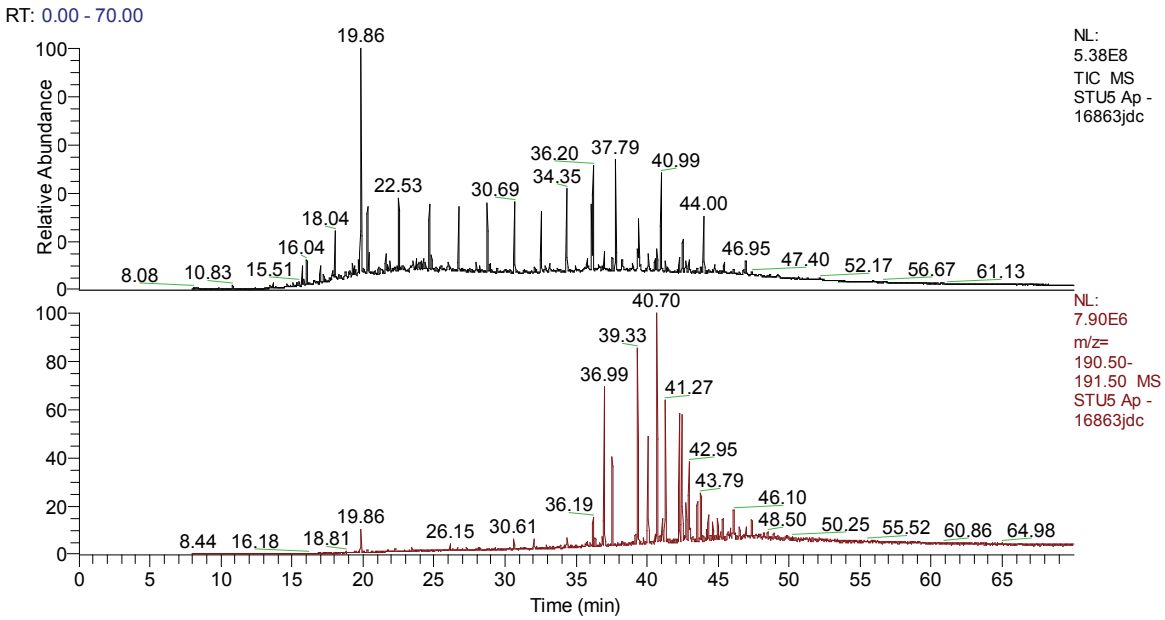
RT: 0.00 - 70.00
Relative Abundance
Time (min)
NL:
5.38E8
TIC MS
STU5 Ap -
16863jdc
NL:
7.90E6
m/z=
190.50-
191.50 MS
STU5 Ap -
16863jdc
19.86
22.53
30.69
36.20
37.79
34.35
40.99
44.00
18.04
16.04
15.51
8.08
10.83
46.95
47.40
52.17
56.67
61.13
40.70
39.33
36.99
41.27
42.95
43.79
46.10
48.50
36.19
19.86
18.81
26.15
30.61
8.44
16.18
50.25
55.52
60.86
64.98

STU12

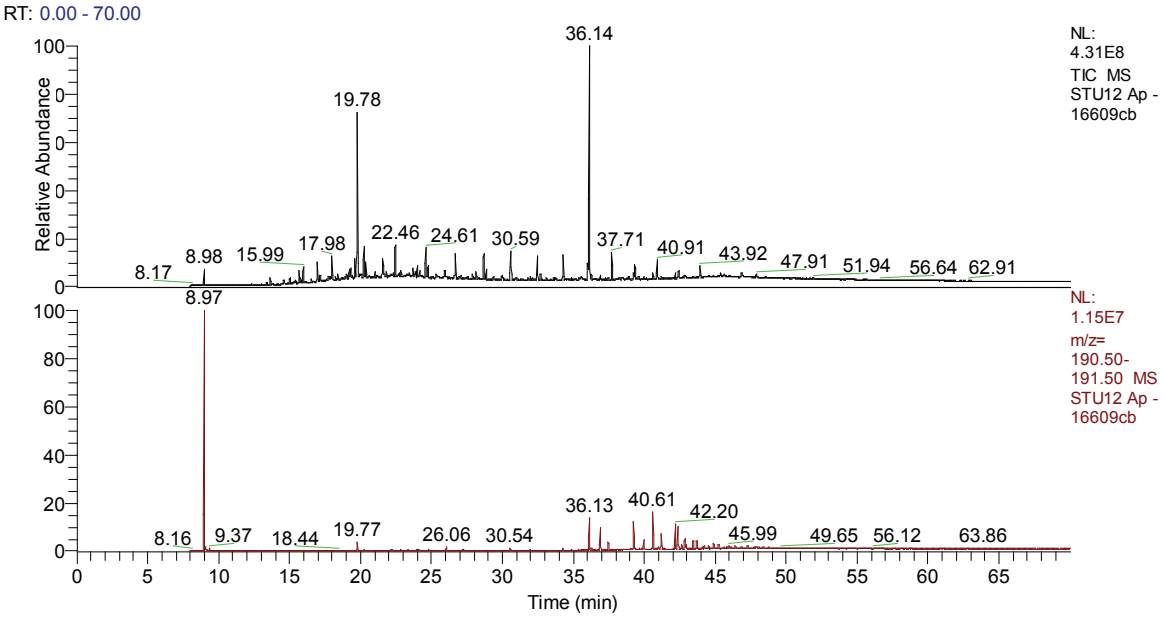

STU102

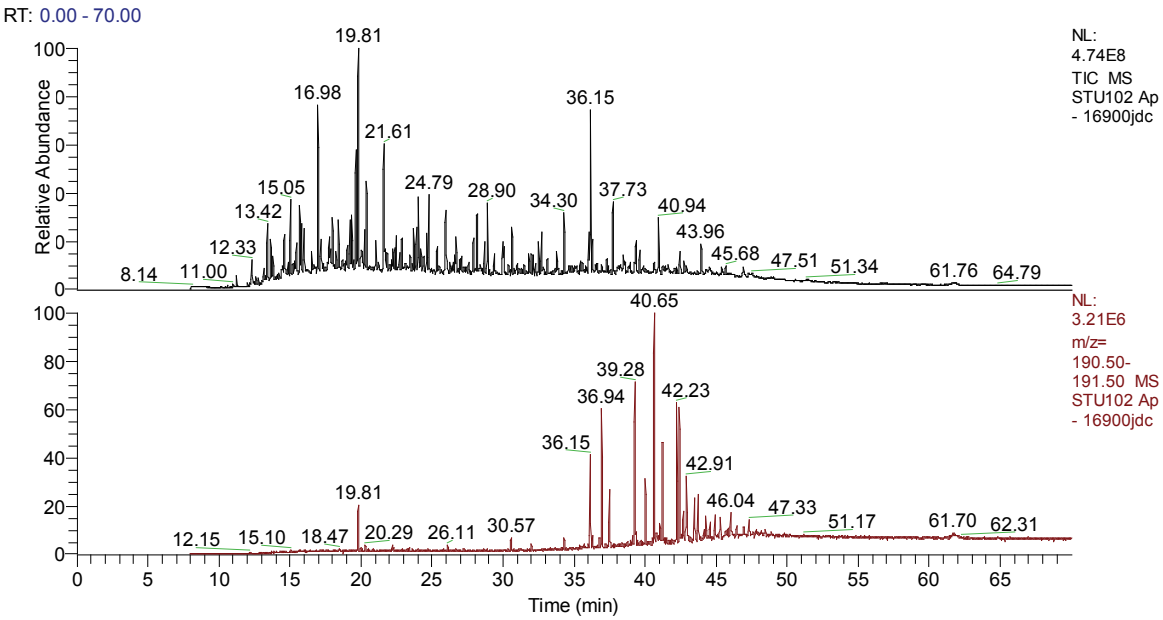

STU105

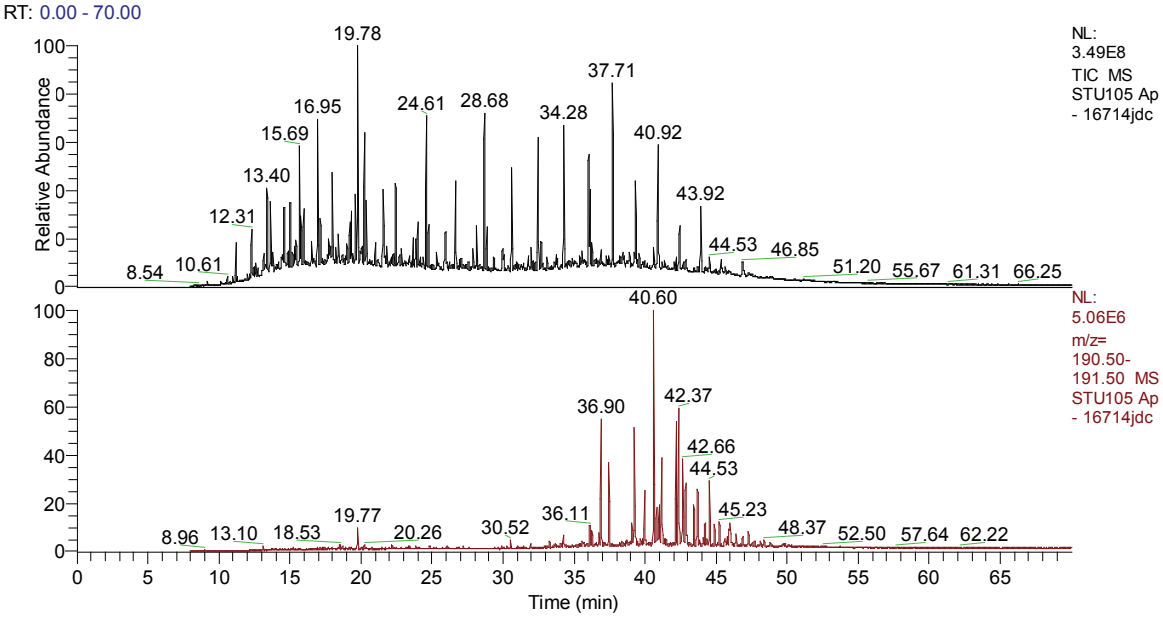

STU108

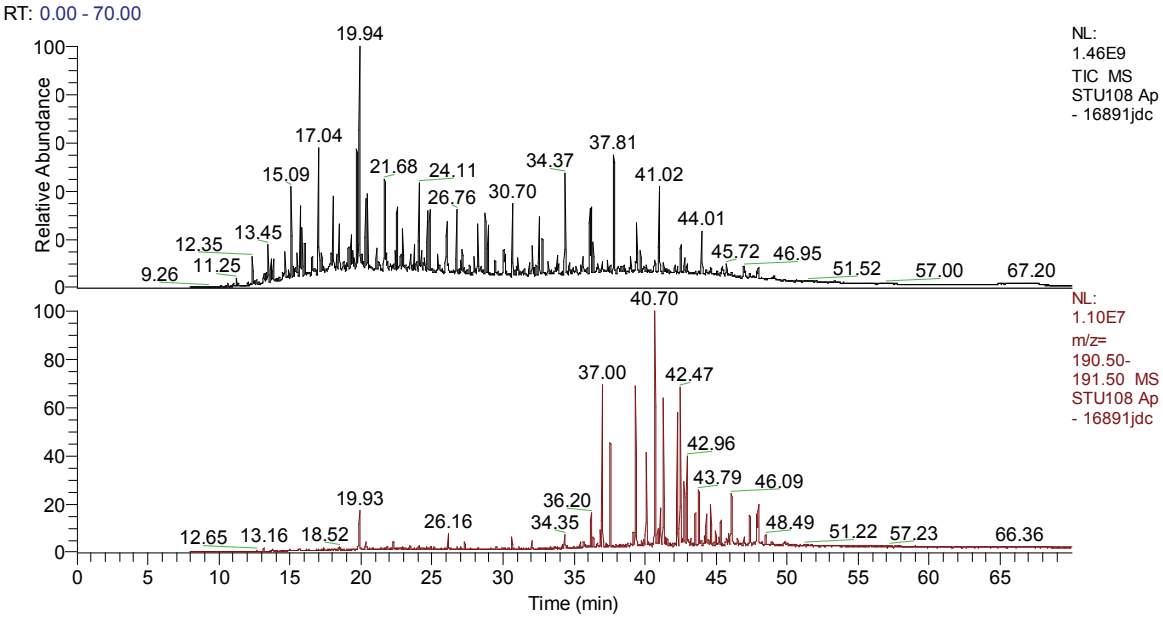

MIR01

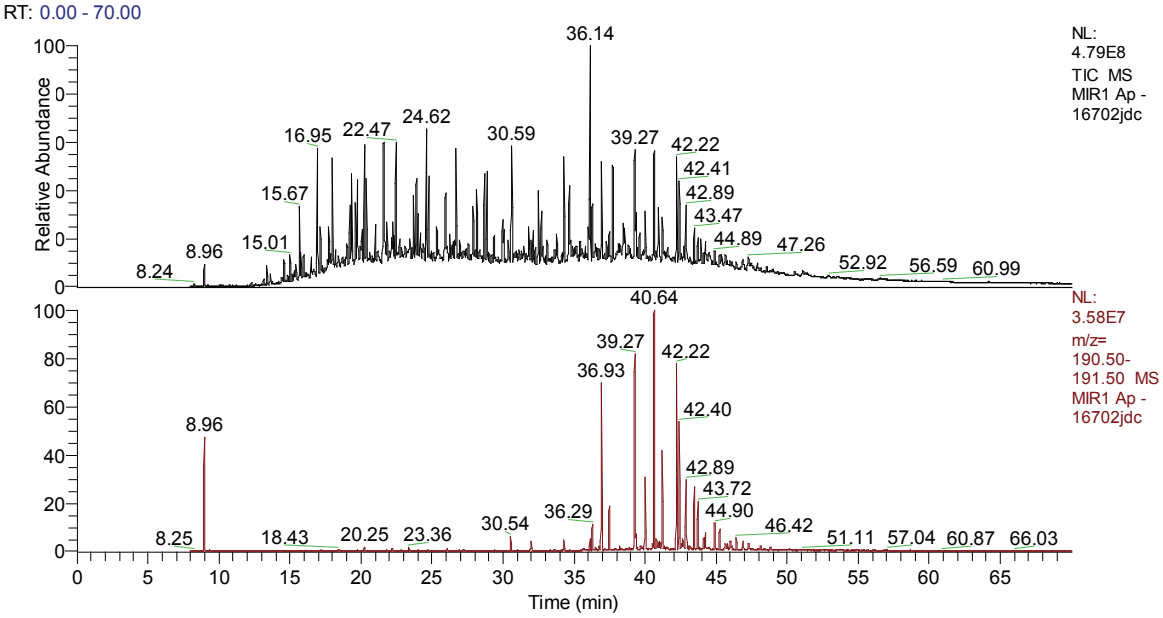
RT: 0.00 - 70.00
Relative Abundance
Time (min)
NL:
4.79E8
TIC MS
MIR1 Ap -
16702jdc
NL:
3.58E7
m/z=
190.50-
191.50 MS
MIR1 Ap -
16702jdc

MIR05

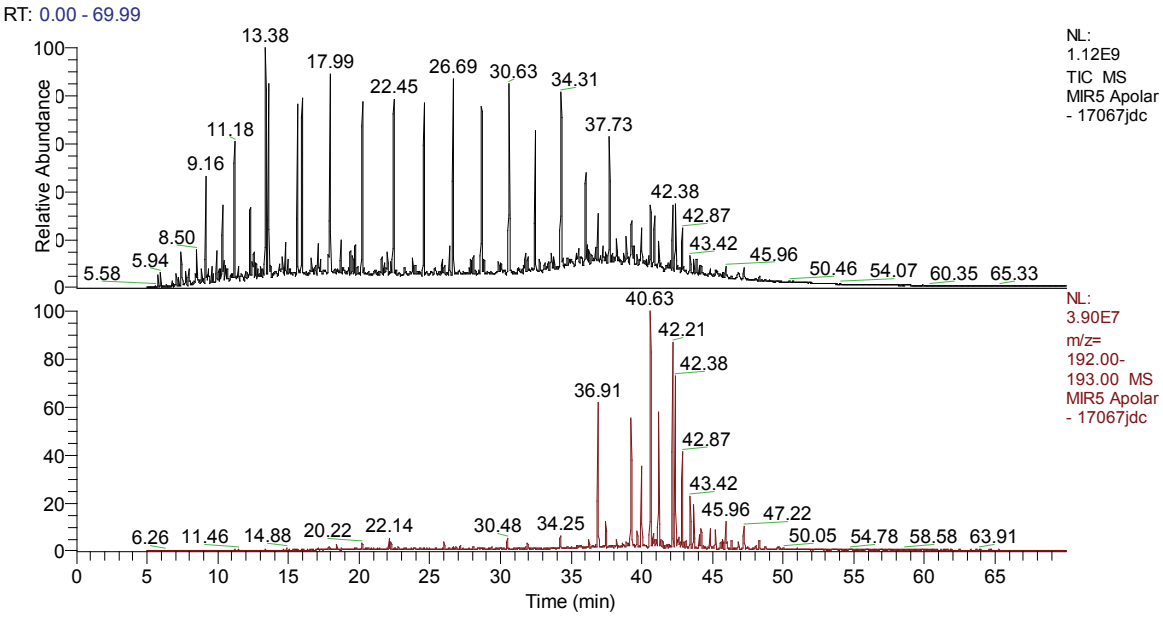
RT: 0.00 - 69.99
Relative Abundance
Time (min)
NL:
1.12E9
TIC MS
MIR5 Apolar
- 17067jdc
NL:
3.90E7
m/z=
192.00-
193.00 MS
MIR5 Apolar
- 17067jdc

MIR06

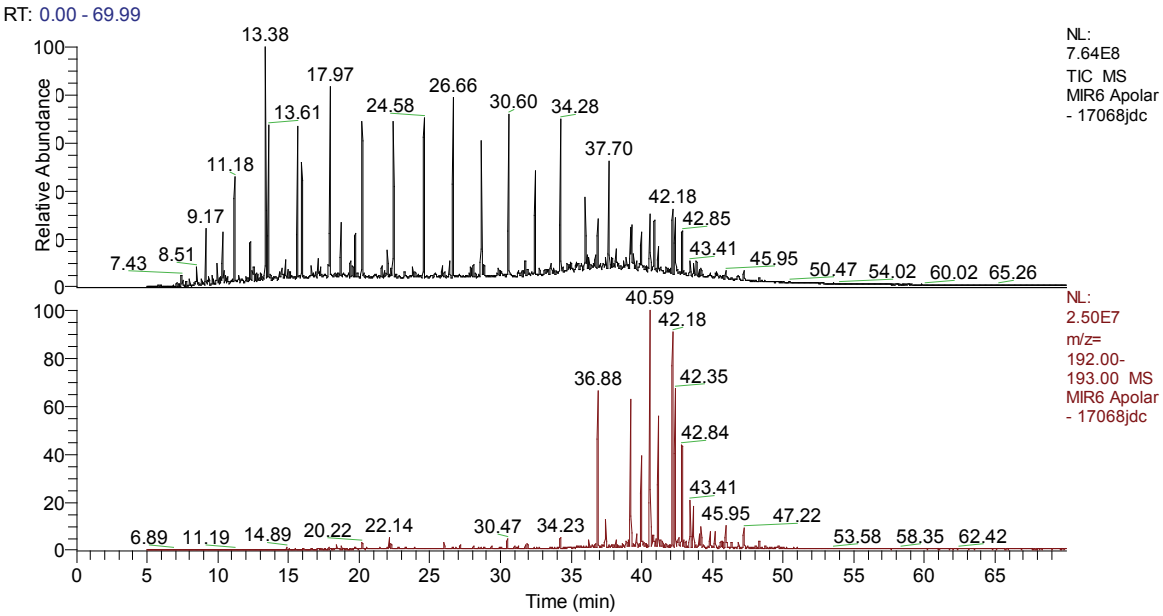
RT: 0.00 - 69.99
Relative Abundance
Time (min)
NL:
7.64E8
TIC MS
MIR6 Apolar
- 17068jdc
NL:
2.50E7
m/z=
192.00-
193.00 MS
MIR6 Apolar
- 17068jdc

MIR07

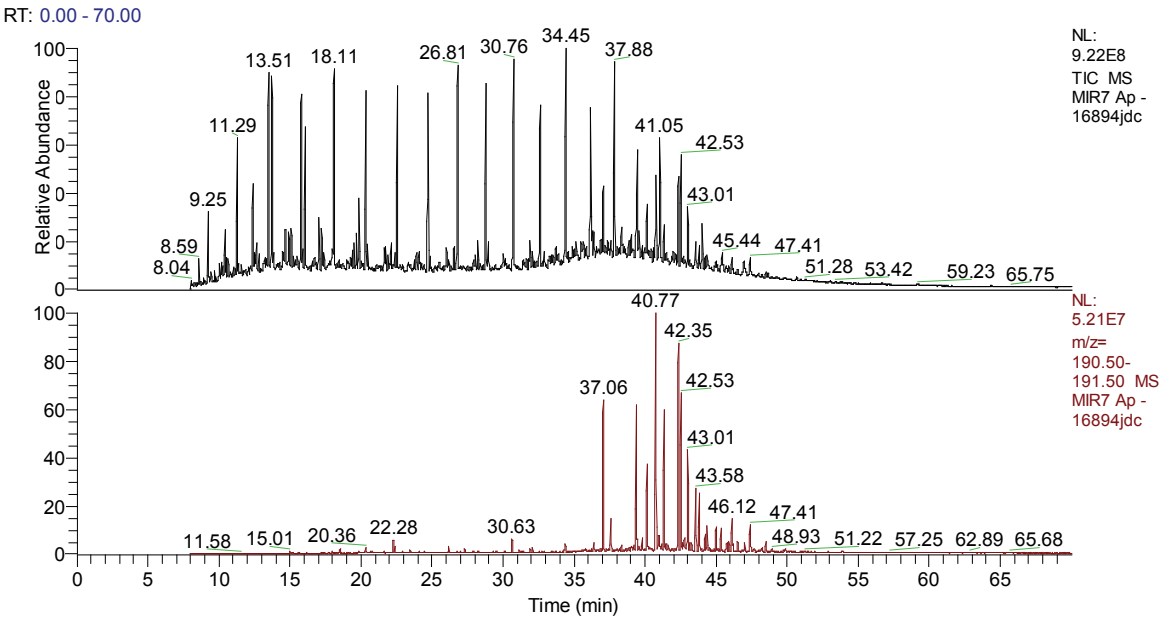
RT: 0.00 - 70.00
Relative Abundance
Time (min)
NL:
9.22E8
TIC MS
MIR7 Ap -
16894jdc
NL:
5.21E7
m/z=
190.50-
191.50 MS
MIR7 Ap -
16894jdc

MIR09

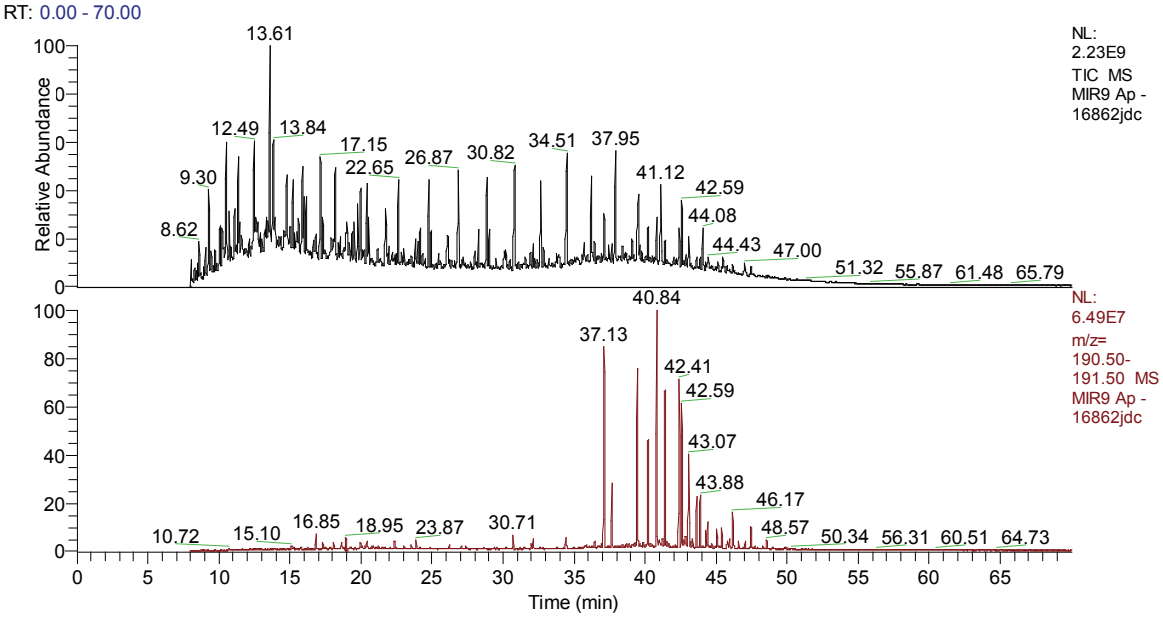
RT: 0.00 - 70.00
Relative Abundance
Time (min)
NL:
2.23E9
TIC MS
MIR9 Ap -
16862jdc
NL:
6.49E7
m/z=
190.50-
191.50 MS
MIR9 Ap -
16862jdc

MIR10

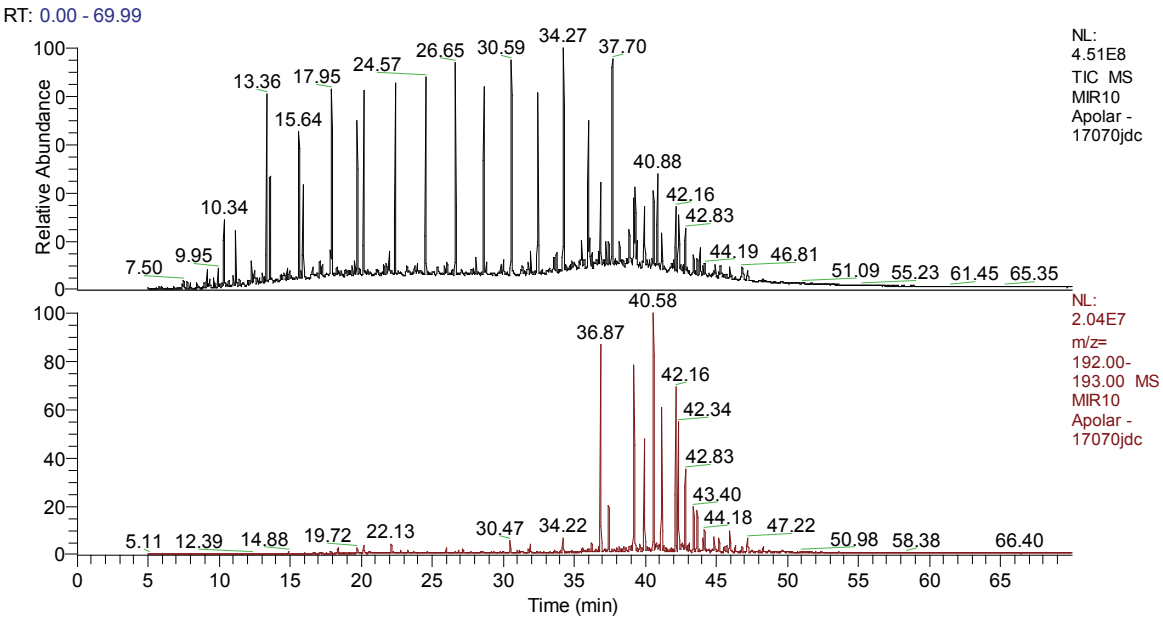
RT: 0.00 - 69.99
Relative Abundance
Time (min)
NL:
4.51E8
TIC MS
MIR10
Apolar -
17070jdc
NL:
2.04E7
m/z=
192.00-
193.00 MS
MIR10
Apolar -
17070jdc

MIR11

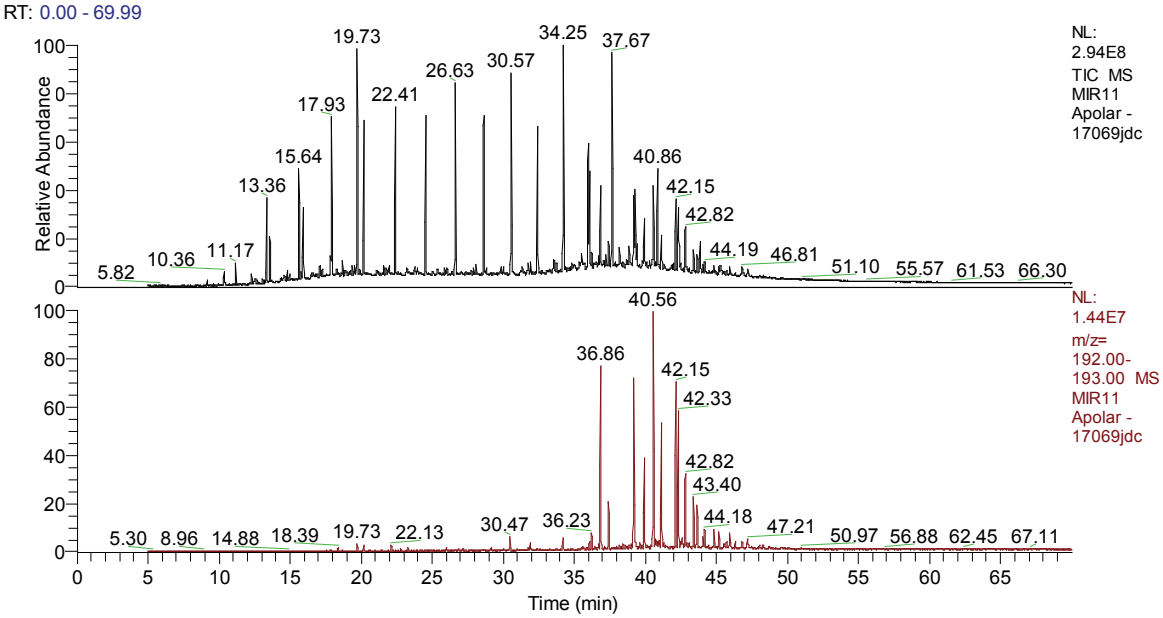
RT: 0.00 - 69.99
Relative Abundance
Time (min)
NL:
2.94E8
TIC MS
MIR11
Apolar -
17069jdc
NL:
1.44E7
m/z=
192.00-
193.00 MS
MIR11
Apolar -
17069jdc

MIR16

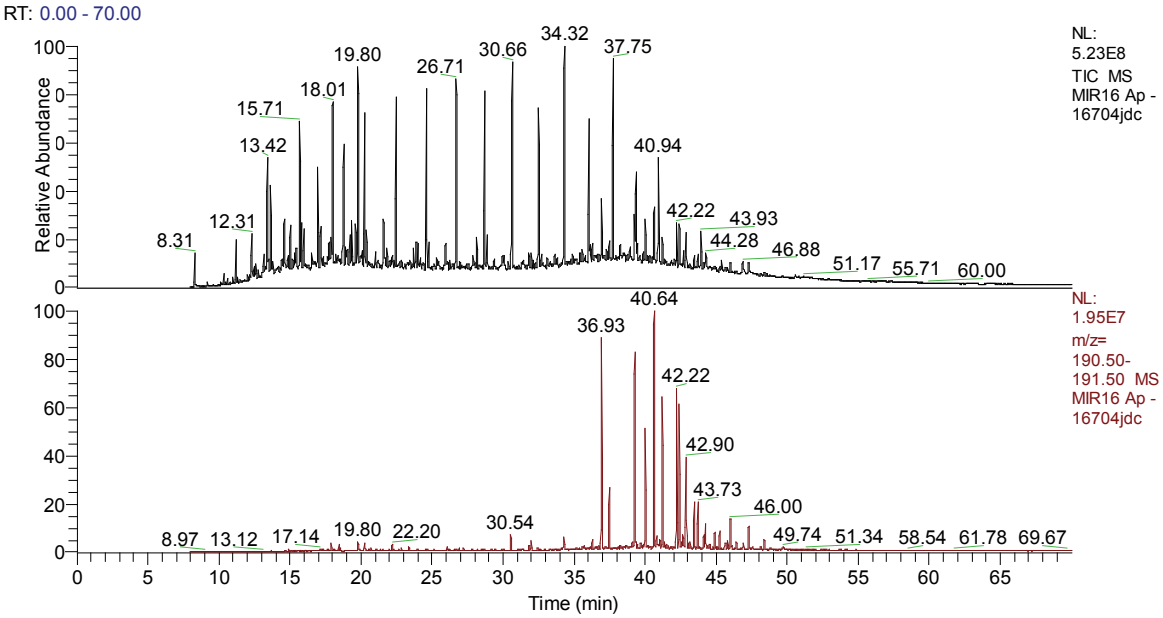
RT: 0.00 - 70.00
Relative Abundance
Time (min)
NL:
5.23E8
TIC MS
MIR16 Ap -
16704jdc
NL:
1.95E7
m/z=
190.50-
191.50 MS
MIR16 Ap -
16704jdc

DJ16

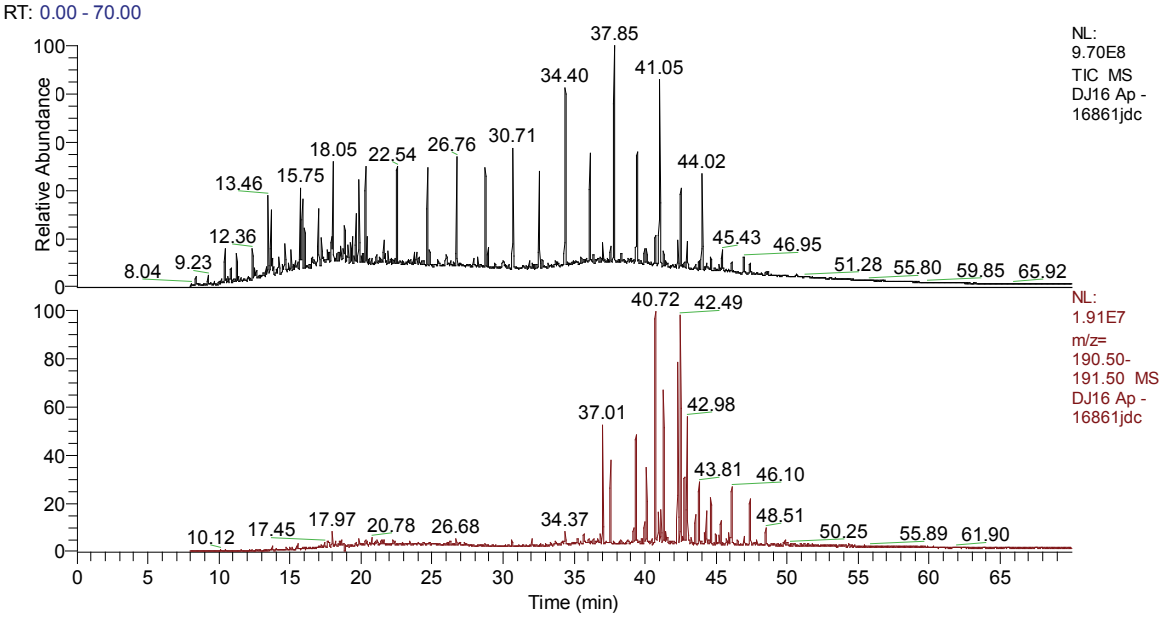
RT: 0.00 - 70.00
Relative Abundance
Time (min)
NL:
9.70E8
TIC MS
DJ16 Ap -
16861jdc
NL:
1.91E7
m/z=
190.50-
191.50 MS
DJ16 Ap -
16861jdc

DJ18

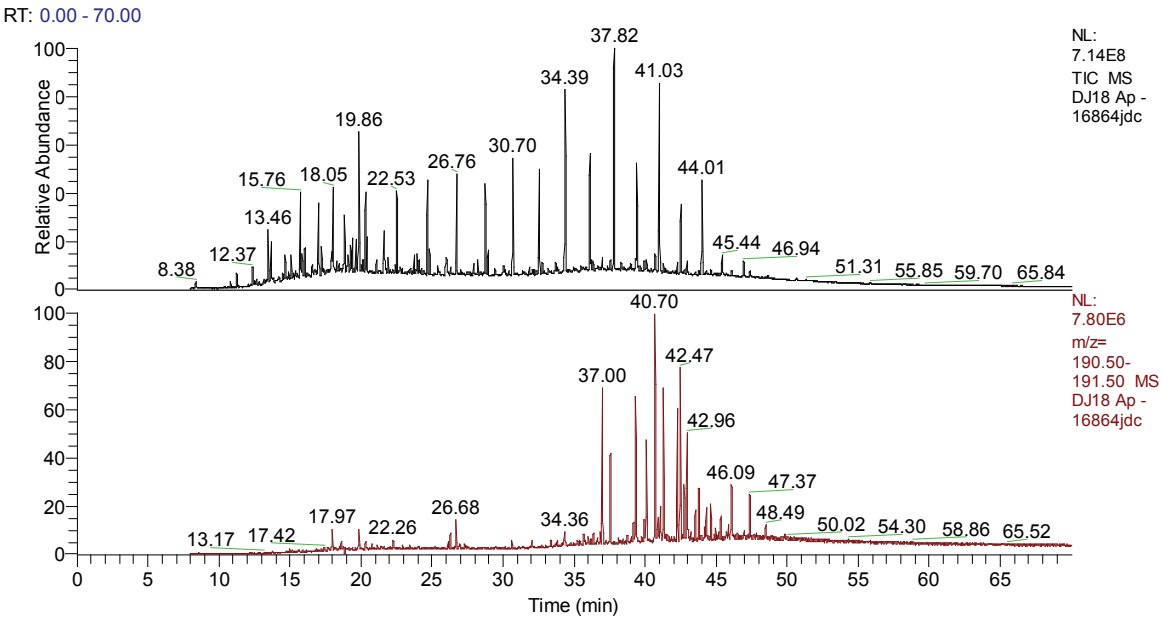
RT: 0.00 - 70.00
Relative Abundance
Time (min)
NL:
7.14E8
TIC MS
DJ18 Ap -
16864jdc
NL:
7.80E6
m/z=
190.50-
191.50 MS
DJ18 Ap -
16864jdc

DJ19

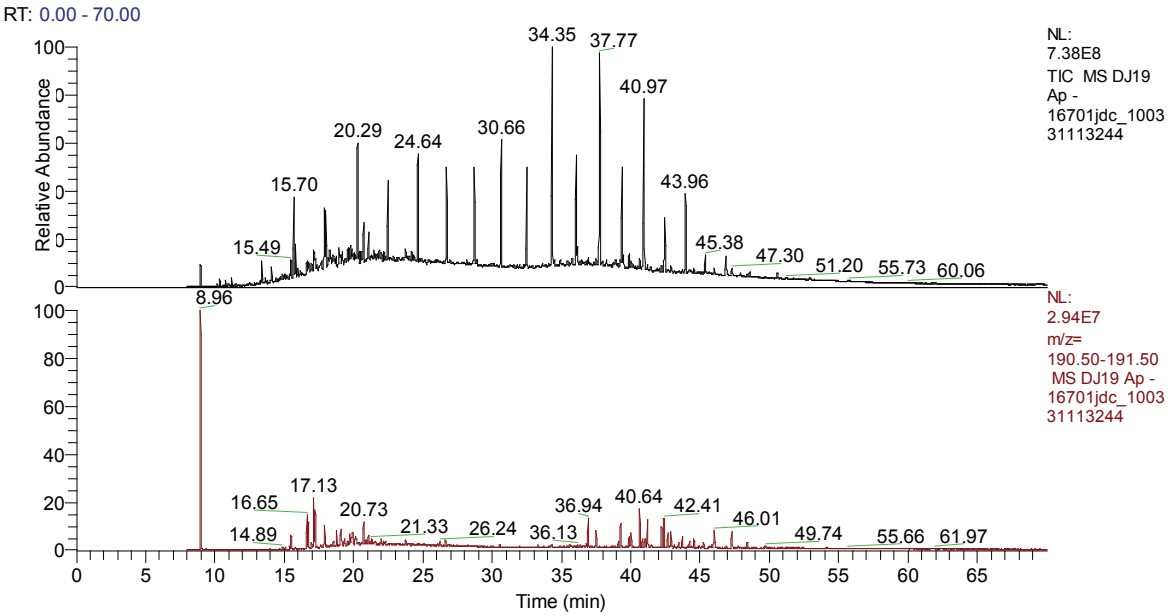
RT: 0.00 - 70.00
Relative Abundance
Time (min)
NL:
7.38E8
TIC MS DJ19
Ap -
16701jdc_1003
31113244
34.35
37.77
40.97
20.29
24.64
30.66
15.70
43.96
15.49
45.38
47.30
51.20
55.73
60.06
NL:
2.94E7
m/z=
190.50-191.50
MS DJ19 Ap -
16701jdc_1003
31113244
8.96
17.13
16.65
20.73
21.33
26.24
36.13
36.94
40.64
42.41
46.01
14.89
49.74
55.66
61.97

DJ21

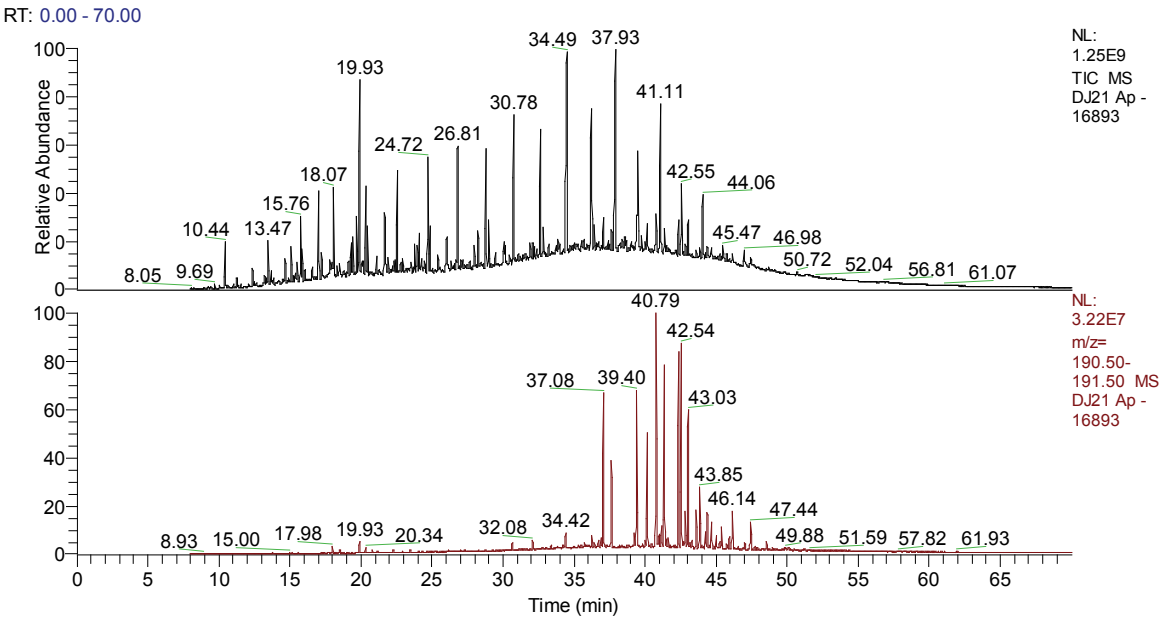
RT: 0.00 - 70.00
Relative Abundance
Time (min)
NL:
1.25E9
TIC MS
DJ21 Ap -
16893
34.49
37.93
19.93
41.11
30.78
24.72
26.81
18.07
42.55
44.06
15.76
10.44
13.47
45.47
46.98
50.72
52.04
56.81
61.07
8.05
9.69
NL:
3.22E7
m/z=
190.50-
191.50 MS
DJ21 Ap -
16893
40.79
42.54
37.08
39.40
43.03
43.85
46.14
47.44
8.93
15.00
17.98
19.93
20.34
32.08
34.42
49.88
51.59
57.82
61.93

DJ27

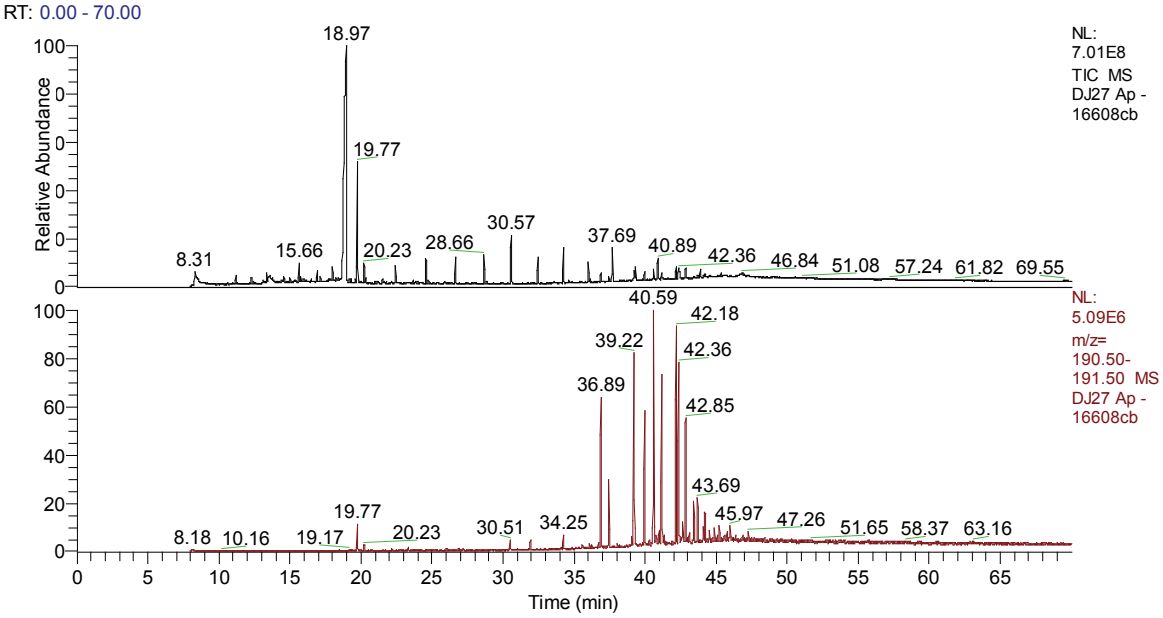
RT: 0.00 - 70.00
Relative Abundance
18.97
19.77
8.31
15.66
20.23
28.66
30.57
37.69
40.89
42.36
46.84
51.08
57.24
61.82
69.55
NL:
7.01E8
TIC MS
DJ27 Ap -
16608cb
40.59
42.18
39.22
42.36
36.89
42.85
43.69
19.77
45.97
47.26
8.18
10.16
19.17
20.23
30.51
34.25
51.65
58.37
63.16
NL:
5.09E6
m/z=
190.50-
191.50 MS
DJ27 Ap -
16608cb
Time (min)